UNDERSTANDING AND CONTROLLING DEFECTS IN QUANTUM CONFINED SEMICONDUCTOR SYSTEMS

by

HONGFU LUO

B.S., Tianjin University of Technology, 2011

AN ABSTRACT OF A DISSERTATION

submitted in partial fulfillment of the requirements for the degree

DOCTOR OF PHILOSOPHY

Department of Chemistry
College of Arts and Sciences

KANSAS STATE UNIVERSITY
Manhattan, Kansas

2016

Abstract

Semiconducting nanoparticles have emerged in the past few decades as an interesting material with great potential in various interdisciplinary applications such as light-emitting devices, solar cells and field-effect transistors, mostly notably for their size-dependent electronic structure and properties. Manipulation of their electronic-optical characters through defects control is one of the most important approaches towards realization of these applications.

This thesis focuses on understanding the role of defects, including their impact on carrier density and conductivity at both room and elevated temperature, their impact on growth kinetics of colloidal nanoparticles and new opportunities for dopant control. To achieve these goals, colloidal CdSe quantum dots are doped with gallium atoms and important changes in electronic and optical properties of the material are reported, which shows a significant impact on the growth kinetics of quantum dots, and reveals clues about the mechanism of the gallium dopant incorporation into the CdSe. It is shown that the gallium doping significantly impacts the conductivity of CdSe thin film made of the quantum dots as well as the photoluminescence and chemical reactivity of the quantum dots, in agreement with the expected n-type character. P3HT/CdSe hybrid cells are constructed with Ga-, In- and Sn-doped CdSe QDs, demonstrating high conductivity and stronger electronic coupling which leads to enhanced charge separation and transport efficiency, both essential for hybrid inorganic-organic solar cells.

This work also demonstrates a novel heating method that can drastically improve size distribution control of colloidal nanoparticle synthesis. Sub-2-nm ultra-small CdSe QDs are prepared with the induction (magnetic) heating and show excellent agreement of its emission profile compared with natural sunlight. The impact of extreme high heating rate on the development of more accurate nucleation and growth theories are also discussed.

Finally, this study also investigates the stabilization of charges from intrinsic defects by looking for altered blinking behaviors of CdSe nanorods (NRs) under different polar environments. TMOS-PTMOS gradient films are prepared with infusion withdrawal dip-coating technique. Although no significant differences are observed of the fluorescence statistics of these NRs, permanent bleaching induced by exciting laser light is discovered, which significantly lowers raw blinking spot count and increases the “off” time of these fluorophores.

UNDERSTANDING AND CONTROLLING DEFECTS IN QUANTUM CONFINED SEMICONDUCTOR SYSTEMS

by

HONGFU LUO

B.S., Tianjin University of Technology, 2011

A DISSERTATION

submitted in partial fulfillment of the requirements for the degree

DOCTOR OF PHILOSOPHY

Department of Chemistry
College of Arts and Sciences

KANSAS STATE UNIVERSITY
Manhattan, Kansas

2016

Approved by:

Major Professor
Viktor Chikan

Copyright

Abstract

Semiconducting nanoparticles have emerged in the past few decades as an interesting material with great potential in various interdisciplinary applications such as light-emitting devices, solar cells and field-effect transistors, mostly notably for their size-dependent electronic structure and properties. Manipulation of their electronic-optical characters through defects control is one of the most important approaches towards realization of these applications.

This thesis focuses on understanding the role of defects, including their impact on carrier density and conductivity at both room and elevated temperature, their impact on growth kinetics of colloidal nanoparticles and new opportunities for dopant control. To achieve these goals, colloidal CdSe quantum dots are doped with gallium atoms and important changes in electronic and optical properties of the material are reported, which shows a significant impact on the growth kinetics of quantum dots, and reveals clues about the mechanism of the gallium dopant incorporation into the CdSe. It is shown that the gallium doping significantly impacts the conductivity of CdSe thin film made of the quantum dots as well as the photoluminescence and chemical reactivity of the quantum dots, in agreement with the expected n-type character. P3HT/CdSe hybrid cells are constructed with Ga-, In- and Sn-doped CdSe QDs, demonstrating high conductivity and stronger electronic coupling which leads to enhanced charge separation and transport efficiency, both essential for hybrid inorganic-organic solar cells.

This work also demonstrates a novel heating method that can drastically improve size distribution control of colloidal nanoparticle synthesis. Sub-2-nm ultra-small CdSe QDs are prepared with the induction (magnetic) heating and show excellent agreement of its emission profile compared with natural sunlight. The impact of extreme high heating rate on the development of more accurate nucleation and growth theories are also discussed.

Finally, this study also investigates the stabilization of charges from intrinsic defects by looking for altered blinking behaviors of CdSe nanorods (NRs) under different polar environments. TMOS-PTMOS gradient films are prepared with infusion withdrawal dip-coating technique. Although no significant differences are observed of the fluorescence statistics of these NRs, permanent bleaching induced by exciting laser light is discovered, which significantly lowers raw blinking spot count and increases the “off” time of these fluorophores.

Table of Contents

List of Figures

List of Tables

Acknowledgements

I would like to express my sincere gratitude toward all the people that guided and assisted me throughout this work.

I thank my advisor Prof. Viktor Chikan for his dedicated support and guidance in the past five years of my research and completion of my degree. From inspiration of new ideas to carrying through challenges during my studies, his mentorship has contributed immensely toward my entire Ph.D. program.

My thanks also go to Prof. Daniel Higgins for his assistance of my blinking studies projects and providing access to experimental instruments during my over-half-a-year stay at his lab. I thank Dr. Dipak Giri for training me on the fluorescence spectroscope and dip coating. I thank Prof. Christine Aikens and Dr. Emilie Guidez for providing the DFT calculations in the CdSe doping project, and former group members and collaborators including Dr. Santanu Roy, Dr. Christopher Tuinenga, Christopher Lewis, Joshua Shipman, and KU microscopy staff for their tremendous contribution in this project. I thank Prof. Shenqiang Ren and his team, including Randall Scott, Dr. Alec Kirkeminde, Dr. Maogang Gong and Jennifer Totleben for their work in the solar cell project. I thank Prof. Emily McLaurin and Bemnet Kebede for their work in the induction and microwave syntheses project, which would not be possible without their invaluable input.

I would like to also express my appreciation toward Prof. Jun Li, Prof. Placidus Amama and Prof. Ruth Miller for being on my graduate committee, attending my oral proposition and final defense, revising my thesis and giving helpful advices. I'd like to thank Michael Hinton, Earline Dikeman and Dr. Tingting Liu for their help with fulfilling my teaching duties. I'd like to thank the staff at the Chemistry Department, especially Jim Hodgson, Ron Jackson, Tobe Eggers, Mary Dooley, and Kimberly Ross, for their technical and administrative assistance.

I acknowledge American Chemical Society for Grant ACS PRF No. 49320-DNI10, National Science Foundation for Grant EPS-0903806, Department of Energy for award DESC0005448, University of Kansas for startup and new faculty general research fund (NFGRF), Camille and Henry Dreyfus Foundation for the Camille Dreyfus Teacher-Scholar Award (2011-2016), and Kansas State University for funding the research projects and my Ph.D. program.

Finally, I thank my former group members who are not yet mentioned above, including Dr. Raj Kumar Dani, Matthew Taw, my good friend George Podaru, as well as all of my friends at the Chemistry Department especially Dr. Yiqun Yang and Dr. Hao Xu, for their friendship and support have made my life in Manhattan in the past five years a truly memorable experience.

Chapter 1 - Introduction

1. Background

Semiconducting nanoparticles have a great variety of unique properties that are different from their bulk material because of the quantum size effect and large surface to volume ratio. These properties give them interesting application potential in areas such as solar cells[1], bio-imaging[2], catalysis[3] and data storage[4]. Due to the strong dependence of these properties on their crystalline size, controlling the size of these particles is crucial to tuning these characteristics[5]. CdSe quantum dots (QDs) have been studied extensively as a model system of such particles. The ability to manufacture mono-dispersed CdSe quantum dots in bulk is of critical interest since their photoelectronic properties are closely related to their size and low-cost fabrication makes them desirable in applications compared to conventional silicon-based solar cells. In order to study these properties with respect to size variation, it is of great importance to be able to produce highly homogeneous, mono-dispersed nanoparticles in a bench-top synthetic route, with potential of scaling up to industrial production, which should also provide control over their surface chemistry, crystalline structure and shape[5]. Although current synthetic methods provide some level of control of these parameters, there's plenty more to be desired. Doping nanoparticles introduces interesting electronic, optical, and chemical changes. Solving issues related to doping quantum dots such as self-purification, and investigating their effects are also of great research interests in this field.

2. Unique Properties of Quantum Dots and Rationale for CdSe Quantum Dots

Surface to Volume Ratio

Quantum dots have large surface-to-volume ratios due to their small sizes. A quantum dot can be treated approximately as a spherical particle, whose surface-to-volume ratio R then can be expressed as

$$R = \frac{6}{D}$$

where D is the diameter of the sphere. The large surface to volume ratio is an attractive feature as various functions, including chemical and biological sensors and catalysis for instance, utilize the surface of the particle for their electronic, optical and chemical properties. A particle with larger surface-to-volume ratio is more effective at providing features resulting from these properties per unit volume of the material. A quantum dot with 5 nm diameter would have the surface-to-volume-ratio 1000 times that of a particle with 5 μm diameter, and therefore be 1000 times more efficient at providing the aforementioned functions. In addition, the large surface area promotes formation of surface defects, a unique challenge that has significant impact on the optical, physical, chemical properties of these QDs.

Quantum Confinement Effect

An electron-hole pair generated inside a quantum dot can be treated in a way similar to that of an electron-proton pair and defined as an exciton, where the most probable distance of the pair is accordingly defined as the Bohr exciton radius. When the size of the particle is close to or smaller than the Bohr exciton radius, the quantum dot serves as a three-dimensional potential well, resulting in significantly different electronic and optical properties. In bulk material, the exciton behaves like a free particle where it has continuous energy states. When the size of the particle reduces to below its Bohr radius, its energies become discreet, and its bandgap becomes size-dependent. A quantum mechanical treatment similar to the particle-in-a-box problem indicates a blueshift of its photoluminescence when its size decreases, which is in accordance with experimental observations. The relation of its energy levels and dimension spacing could be expressed with the following equations:

$$\psi_{n_x,n_y,n_z} = \sqrt{\frac{8}{L_x L_y L_z}} \sin\left(\frac{n_x \pi x}{L_x}\right) \sin\left(\frac{n_y \pi x}{L_y}\right) \sin\left(\frac{n_z \pi x}{L_z}\right)$$

$$E_{n_x,n_y,n_z} = \frac{\hbar^2 \pi^2}{2m}\left[\left(\frac{n_x}{L_x}\right)^2 + \left(\frac{n_y}{L_y}\right)^2 + \left(\frac{n_z}{L_z}\right)^2\right]$$

As a result, shown in Figure 1.1[6], in semiconducting quantum dots the Fermi level lies between the bandedge and therefore the bandedge, or its size, becomes the deciding factor in its optical and electrical properties. For comparison, the Fermi level in bulk metal lies within the band and the energy level spacing are so small that its optical and electrical properties appear

continuous. For CdSe quantum dots, Figure 1.2[7] shows a comparison of their bandedge energies (a) and absorption spectra (b). For practical calculation and prediction of CdSe QDs sizes and excitation energies, Yu *et al.*[8] have attempted an experimental approach in determining the two relations and reported an empirical function as follows:

$$\text{CdSe: } D = (1.6122 \times 10^{-9})\lambda^4 - (2.6575 \times 10^{-6})\lambda^3 + (1.6242 \times 10^{-3})\lambda^2 - (0.4277)\lambda + (41.57)$$

where D is the diameter of the particle and λ is the wavelength of the absorption peak.

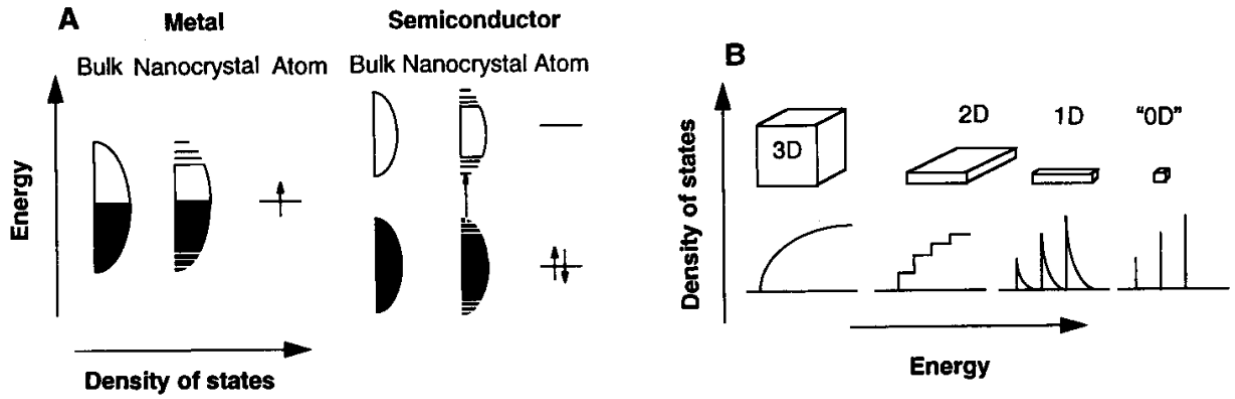

Figure 1.1[6] A: Comparison of density of states in bulk metal and semiconductor nanocrystals. B: Comparison of density of states of quantum dots with other quantum confined structures. (Reprinted with permission from ref. 6. Copyright © 1996 AAAS.)

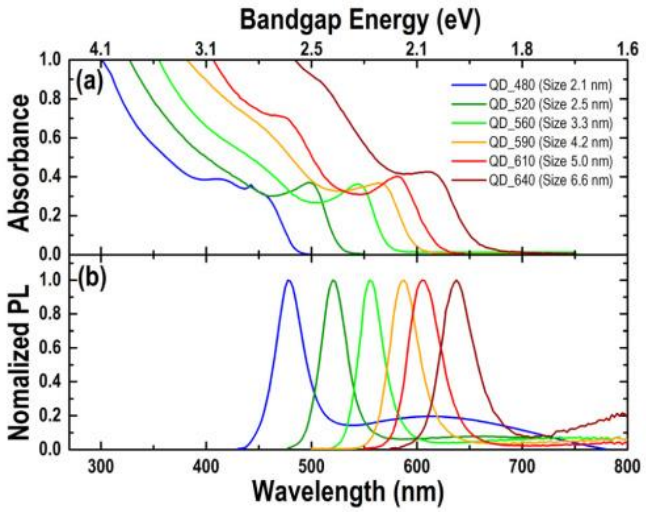

Figure 1.2[7] (a)Bandgap of CdSe QDs of different sizes (b) their absorption spectra. (Reprinted with permission from ref. 7. Copyright © 2013 Optical Society of America.)

Defects and Doping

Roles of defects and reasons of doping in semiconducting nanoparticles

Defects in crystalline materials arise for various reasons and from various sources. In the case of quantum dots, defects could be produced during high temperature synthesis through lack of annealing, from chemical etching, or by introducing dopant atoms into the crystal structure. In high temperature syntheses, the quantum dot could go through different crystalline phases driven by chemical potential, shifting from a phase with higher chemical potential at high temperatures to one with lower potential while it cools. However if the cooling was fast enough that the particle does not have enough time to fully complete the phase shift, defects are created at the boundary of different phases. Chemical etching agents could also be applied to the particle, which removes certain atoms on the surface of the particle, destroying its crystalline structure. Therefore defects created by this method are mostly on the surface. A foreign atom of similar size to the host crystal atom could be introduced to replace the host atom creating a doped particle.

By introducing different dopant atoms, p-type or n-type semiconductors could be achieved, a method commonly used in semiconducting material manufacturing. Generally, defects could be undesirable as they reduce conductivity and mechanical integrity of the crystalline material. In semiconducting nanoparticles, defects could potentially lower their

photoluminescent efficiency by creating trap states that do not result in light emission at desired wavelength. However it may also induce chemical, electrochemical and spectroscopic changes that could be beneficial to various applications, as will be discussed in Chapter 3. In this thesis, the doping aspect of introducing defects in colloidal quantum dots will be discussed extensively.

In matters of application, although it is well known that undoped nanocrystals are already highly photoluminescent strongly dependent on sizes, Klimov *et al.*[9] have pointed out that such emisisons are rather inefficient in lasers and that instead carriers introduced by dopant could drastically increase its emission efficiency. For instance, Wang *et al.*[10] have demonstrated that by doping CdSe quantum dots, the lasing threshold could be reduced to three times lower than that of the undoped crystals. In the field of bioimaging, Pradhan *et al.*[11] have successfully doped ZnSe nanoparticles for superior emitting characteristics to replace the toxic CdSe based emitters, and have shown its lower susceptibility to temperature and other environmental variations which is critical to its application in real world external conditions. The authors also reported reduced photo-oxidation under prolonged illumination of doped nanocrystals through faster transfer of photons to the dopants thus decreasing probability of unintended chemical reactions, a property of extreme importance for such type of material's application in solar cells.

Challenges and issues of doping

There are several challenges towards successful incorporation of dopant atoms into the host particle in a desired manner. Tchebotareva *et al.*[12] have pointed out that the probability of dopants contained in a nanocrystal can be expressed as follows:

$$P(k) = \frac{e^{-V_{nc}n}(V_{nc}n^{k})}{k!}$$

where the volume of the nanocrystal is V_{nc}, the number of dopants is k, and the concentration of dopants is n. Such relation indicates the random nature of Poissonian distribution of the doping process. The variation of dopant concentration with respect to sizes of the particles and the uncertainty of the distribution of dopant atoms into particles could pose a challenge to producing uniformly doped particles. Therefore a fine control of the density of dopants in particles is very desirable. In this thesis, various aspects of control including reducing size distribution of colloidal quantum dots will be discussed at length.

Another challenge of doping is impurities in these QDs from different sources. A common cause of surface impurities is the surface irregularities in the crystalline structure. The

phase changes induced by temperature variation during the colloidal synthesis could introduce unannealed surface atoms caused by various sources including violent heating or uneven cooling. Additionally, irregular stacking patterns could arise from these processes as well, which may exhibit "dangling" bonds that contribute to undesirable optical-electrical features. As discussed in later sections in this thesis, these dangling bonds could be utilized to combine with passivating ligand molecules, including fatty acids and amines particularly, for surface functionalization purposes such as modifying their hydrophobicity properties. However, they are also susceptible to unintentional bonding with surface ligands such as oxygen[13] or hydroxyls[14]. Proper treatment of the surface is important in that it could potentially remove excess charges of the particle and thus reduce chances of unintentional bonding, introduce trap states, or act as an electron donor[15], in addition to provide chemical stability of the particle.

An additional challenge of dopant incorporation is the self-purification of nanoparticles. Interestingly, it was mentioned in literature[16] long ago that smaller crystalline structures tend to have fewer defects, as they're more likely to remove these defects from the system. Dalpian *et al.*[17] proved theoretically that dopants suffer from reduced solubility in the nano-sized host material compared with that in the bulk material as the formation energy of impurities increases while the particle size decreases (Figure 1.3). Dopants that end up inside the host particle during synthesis undergo a thermodynamic process where the dopant atoms are expelled out of the system through gradual diffusion.

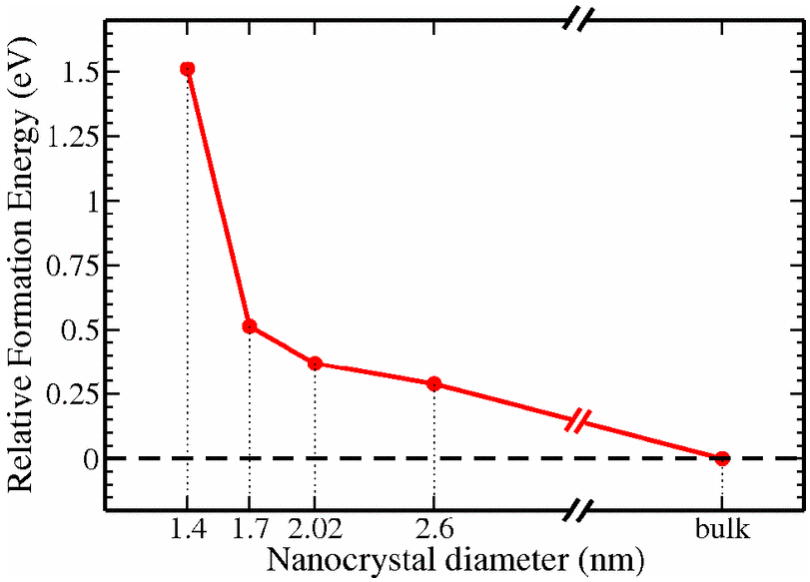

Figure 1.3 Formation energies of Mn dopant in CdSe nanocrystal with respect to particle size. (Reprinted with permission from ref. 17. Copyright © 2006 American Physical Society.)

Doping Strategies

Currently two major strategies of doping include "nucleation doping" and "growth doping", which are summarized in Table 1[18]. In nucleation doping, the dopants are incorporated into the precursor molecule and serve as nucleation centers, thus resulting in all nanoparticles being doped. Since all precursor molecules contain the dopant atoms, the doping is uniform for all particles. In growth doping, dopants are introduced separately into the reaction mixture alongside precursor molecules, such as in forms of salts of the dopant element. The dopants then distribute during growth following Poissonian statistics into individual particles. Therefore, this method of doping is nonuniform due to its highly statistical nature. In both methods, the dopants are subject to self-purification of the host particle and could be rather unstable. And due to increased potential of the dopant-host interface, growth of certain crystal facets could become unfavorable.

Table 1 Summary of Nucleation Doping and Growth Doping[18]. (Reprinted with permission from ref. 18. Copyright © 2013 Royal Society of Chemistry.)

Strategy	Diagram	Uniformity of dopants	Stability of dopants	Effects on nucleation and growth
Nucleation Doping	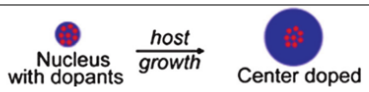	Uniform; all nanoparticles are doped	Unstable	Dopants serves as nucleation centers; dopant could impede growth of certain crystal facets
Growth Doping	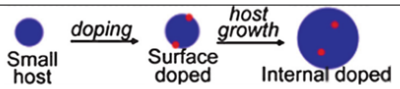	Nonuniform doping; dopant distribution follows Poisson distribution	Unstable	Dopant could impede growth of certain crystal facets

Capping Agents

As mentioned in the previous section, ligands have proven to be an effective method of controlling the nanocrystal's surface functionalization and other characters such as reducing dangling bonds, unintended bonding with oxygen and hydroxyls, acting as electron donor, providing trap states, and so on. Therefore, understanding of the capping agents and their interaction with the quantum dot surface is another important aspect of such material.

Surfactants could be easily attached to the surface of CdSe quantum dots during synthesis. Ligand molecules surround the CdSe nanoparticle as a stabilizing layer that prevents coalescing driven by the lowering of surface tension. In general, surfactants of different properties could be attached to achieve certain properties such as hydrophobicity or hydrophilicity. Additionally, as Embden and Mulvaney[19] have pointed out, the capping agent plays a key role in the growth kinetics of CdSe nanoparticles as well. It is understood that the capping agent has an effect on the critical nucleus radius, and eventually the size and size distribution of the ensemble. Different surfactants also have different affinities to the particle surface compared to the monomers, thus changing the surface free energy.

Weiss *et al.*[20] have also mentioned in their study that the surfactants alter the rate of surface reactions, which include adsorption/absorption of monomers. The surfactants act as a passivating layer on the particle. A dense layer of surfactant would lower the chance of monomers or other reactants entering the surface of the particle, thus lowing the surface reaction rate. The affinity of the specific surfactant towards the reacting molecule in solution also greatly affects the reaction rate.

Why Study CdSe Quantum Dots

CdSe quantum dots have been studied extensively in the past few decades as a model system to investigate the various effects related to syntheses and properties of semiconducting nanoparticles, and notably because their band gap can be tuned in the visible light region between 400−800 nm by controlling the size of the particles. A query in Web of Science database generated over 10,000 results related to CdSe quantum dots. They has already seen applications in areas such as solar cells[1], batteries, bio-imaging[2], catalysis[3] and data storage[4], although with the drawback of health and environmental issues. Selenides are in general toxic compounds and cadmium is a heavy metal, which causes concerns during their production and usage. CdSe has also been identified to induce cancer in humans. Nevertheless, this thesis continues to use CdSe quantum dots as a platform to study and demonstrate the experimental and theoretical discoveries of semiconducting quantum dots in general, which could be readily applied to other similar but safer and more environmentally friendly materials as well.

3. Current Understandings, Limitations, and Motivation for This Thesis

Progress in the study of the synthesis and experimental and theoretical understanding of semiconductor nanoparticles is a crucial part of the nanoscience and nanotechnology. The quantum confinement effect gave rise to various size- and shape-dependent properties at the nanoscale where radius of the particles is smaller than the Bohr exciton radius of the material. In general, binary semiconductors are semiconductors that consist of two different groups of elements. Such semiconductor material has superior properties over conventional semiconductor material such as silicon, which generated intense research interests in recent years for their potential application in the micro-electronics industry. Colloidal semiconducting quantum dots have sizes in the nanometer regime and are grown in solution. They're typically stabilized by a layer of organic ligands which prevents aggregation of the particles. By tuning the size, shape, composition, crystal structure and surfactants of the particles various useful properties can be obtained, which makes it possible to utilize them in making more complicated structures and devices as building blocks, for example, as inorganic fluorophores in biomedical assays, light emitting diodes, lasers and solar cells.

Colloidal Synthesis of CdX (X = Se, Te, S) Quantum Dots

Many properties of colloidal nanocrystals such as size-tunable band gaps and luminescence energies which are a result of their electronic states, can be easily tuned by controlling their composition, size and shape. The ability to achieve uniform size, shape and control of their composition, crystal structure and surface properties is crucial in understanding and manipulation of desired properties of these nanoparticles. Colloidal nanocrystals have an inorganic core that is stabilized by a layer of surface surfactants. In general, semiconducting nanoparticles are synthesized by the reaction between metal ions or their complexes and precursors containing appropriate ions in a stabilizing solvent such as hexadecylamine (HDA), followed by nucleation and growth of the particles, particularly the "hot-injection" method[21] and "heating-up" method[22].

Hot Injection Synthesis of QDs

Hot injection method has been widely used in the past 20 years in synthesis of colloidal nanocrystals.[23] Bawendi and co-workers first introduced the hot-injection method in their synthesis of cadmium chalcogenide nanocrystals[24]. The method is based on the homogeneous nucleation and growth through rapid injection of precursor into the reaction mixture at elevated temperature.[5] The rapid injection causes a short period of high precursor concentration, which induces a "burst" nucleation stage. This method achieves small size distribution by minimizing the growth during nucleation, since the size distribution is mainly determined during the nucleation stage.

Murray *et al*.[24] produced CdSe, CdS, and CdTe nanoparticles by thermolysis of the complex $[MeCdSe_2CNEt_2]_2$(E=S,Se) in a high-boiling coordinating solvent with the hot injection method. In another synthesis by the same author, the TOPSe or TOPTe stock solution is prepared by addition of Se or Te to TOP.[25] Two separate solutions, one containing dimethylcadmium in TOP, and one consisting of 1 M TOPSe solution were mixed and injected into TOPO at 250 °C. TOPO-capped nanocrystallites of CdSe were also produced by replacing the phosphine chalcogenide precursors with $(TMS)_2S$, $(TMS)_2Se$, and $(BDMS)_2S$ and carrying out the reaction at 290−320 °C. The size of the particles is principally controlled by the temperature of the

reaction, with larger particles being obtained at higher temperatures. The sizes of the particles can also be controlled by the temperature of heating during the synthesis. The absorption spectrum (figure below) shows that the size distribution is actually quite narrow. The size distribution obtained from TEM images showed a standard deviation of around 5%. Furthermore a size-selective precipitation of the final material is employed.

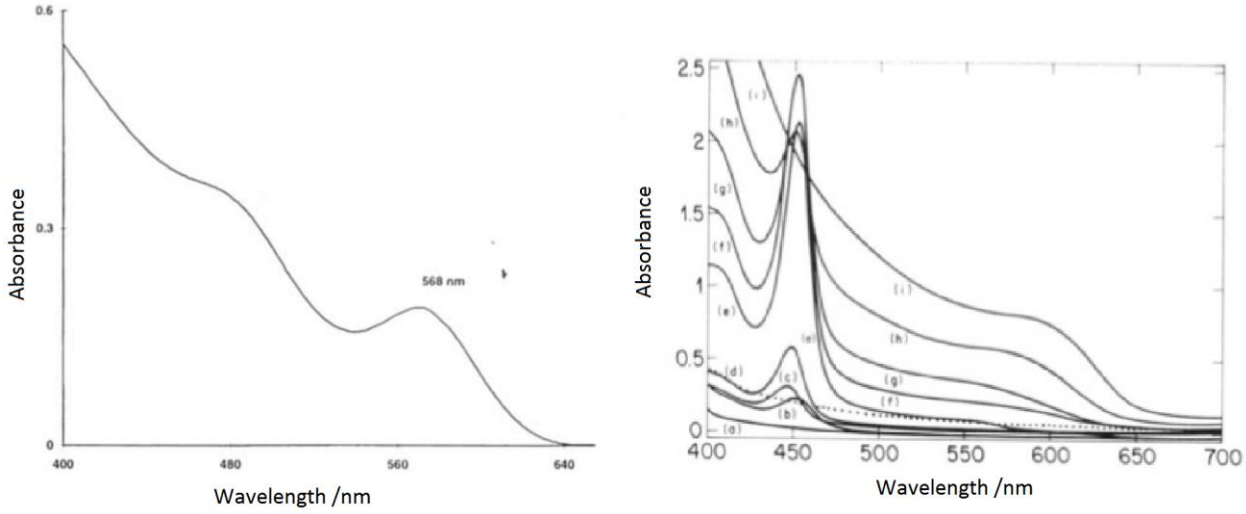

Figure 1.4[25] Left: Optical absorption spectrum of CdSe nanocrystallites dispersed in toluene; Right: Evolution of UV-visible absorption spectrum during thermolysis of the precursor. (Reprinted with permission from ref. 25. Copyright © 1989 American Chemical Society.)

Single-source precursor synthesis of Cd-based nanoparticles

Although hot injection method provides an approach to increase the nucleation rate and therefore narrow down the size distribution of the particles, it is restrictive in that the precursor molecules in solid form could not be used, thus severely limiting the range of reactions and choice of precursors. Additionally, since the precursor is injected into the reaction mixture at elevated temperature, they could not be pre-mixed to achieve higher uniformity. Local variation of precursor concentration during the mixing stage becomes a major drawback that could result in broadened size distribution of initial nuclei. However, by using a single precursor these issues could be resolved. Cumberland *et al*.[26] later developed a convenient single-source precursor method for the preparation of CdSe Quantum Dots (QDs) by utilizing the inorganic cluster

$(Li)_4[Cd_{10}Se_4(SPh)_{16}]$, in which the complex was heated in hexadecylamine (HDA), an amine that acts as both solvent and a stabilizing agent that caps the nanoparticles' surface. The resulting QDs have sizes ranging between 2.5-9.0 nm depending on experimental parameters, and a size distribution of ~12%, and ~5% after size-selective precipitation. Microwave synthesis of various types of nanoparticles have also been reported by Gerbec *et al.*[27], which removes the need for hot injection and allows for faster heating rate. In a typical MW synthesis a 2.45 GHz, 300−400 W/cm^2 MW will be used. The precursor will be heated up to the boiling point of the solvent, same as in induction heating, but in 20 min.

Numerous complexes have been used as precursors for the syntheses of Cd-based nanoparticles. Dithiocarbamato complexes $[M(S_2CNR_2)_2]$ (M = Zn or Cd, R = Alkyl) were used to synthesize CdS and CdSe nanoparticles by O'Brien and co-workers. $[Cd(E_2CNEt_2)]$ (E = S, Se)) is a 3-electron donor ligand which is capable of stabilizing the metal centers in different oxidation states[28]. The complexes have been widely used in the rubber industry[29], analysis, and the petrochemical industry,[30] due to their advantage of being air-stable. In a typical synthesis, $[Cd(E_2CNEt_2)]$ (E = S, Se) were dissolved and refluxed in 4-ethylpyridine, which is a high-boiling (168 °C) coordinating solvent, and dilute solutions of bis(dithio- or diselenocarbamato)cadmium . The solution were able to remain optically clear for days. Murray *et al.*[31] used a similar TOPO method to produce TOPO-capped CdSe and CdS nanoparticles by using mixed alkyl compounds $[MeCdE_2CNEt_2]_2$ (E = S, Se)[32] as complex. These particles were also used as starting materials to prepare composites using other organic ligands such as 2,2-bipyrimidine. This method avoids the use of dimethylcadmium at high temperatures, which is an advantage of the single-source precursor approach. This method is also superior to other methods in that it is possible to produce a variety of different kinds of nanoparticles by changing the design of precursors. In various applications of these nanoparticles, morphological properties, which depend on the structure of the precursor, are essential. Elemental Se and hexagonal CdSe NPs are the major product of $[Cd(Se_2CNEt_2)_2]$ as precursor, while $[Cd(S_2CNEt_2)_2]$ produced CdS nanoparticles.[33] $[NpCd(E_2CNEt_2)]_2$ (E = S, Se) and other mixed alkyl compounds of cadmium were also reported to be able to produce CdSe and CdS nanoparticles. CdS nanoparticles obtained from using $[Cd(S_2CNEt_2)_2]$ as precursor show a red shift as compared to those particles obtained from $[RCd(E_2CNEt_2)]_2$, indicating that larger particles were produced under similar reaction conditions.[32] It is also reported that $[EtCd(E_2CNEt_2)]_2$[34] and $[EtZn(E_2CNEt_2)]_2$ [35] were

used to synthesize TOPO-capped ZnSe and ZnS nanoparticles by such similar single-source precursor route.

Although these mixed alkyl derivatives as single-source precursors were able to produce nanoparticles with relatively good size distribution (with σ≈5%-15%) and quality, the particles have the disadvantage of being air-sensitive and therefore cannot be stored for a long period of time. On the other hand [$Cd(S_2CNEt_2)_2$] has the advantage of being stable for years, but the yield was lower than the former method and quality of nanoparticles was not as good. Later Revaprasadu and co-workers reported[36] that [$M(ECNMe^nHex)_2$] (M = Cd, Zn; E = S, Se) are better alkyl derivatives for growth of Cd-based nanoparticles. They used a so-called "one-pot" synthesis in TOPO with [$M(E_2CNMe^nHex)_2$] as complex. The produced nanoparticles have narrow size distribution and good quality. In a similar approach[37], [$Bi(S_2CNMe^nOctadecyl)_3$] was synthesized and used for the preparation of self-capped Bi_2S_3 nanoparticles. [$Cd(S_2CNMe^nOctadecyl)_3$] was also used to produce self-capped CdS quantum dots with the same method. In this study IR and NMR spectroscopies were used to characterize the capping agent and it showed that the CdS nanoparticles prepared at 150−250 °C were cubic, and those prepared at 300 °C were hexagonal.

O'Brien and co-workers first reported[38] that monodispersed nanoparticles can be prepared in TOPO using cadmium salts. Murray and co-workers[24] and Peng *et al.*[39] then modified this approached and further developed it to synthesize CdTe, CdSe, and CdS quantum dots with CdO, TOPO, and hexylphosphonic acid (HPA) or tetradecylphosphonic acid (TDPA) under 300 °C. By adding tellurium, selenium, and sulfur stock solutions the corresponding nanoparticles can be produced.

[$M_{10}E_4(EPh)_{16}$]$^{4+}$ (M = Cd; E = S, Se) and [$M_8E(EPh)_{16}$]$^{2-}$ have also been used to produce near-monodispersed nanoparticles[40]. These complexes are air-stable inorganic molecular clusters[26]. $Cd[(SeP^iPr_2)_2N]_2$ was also used to synthesize QDs in a so called one-step size-controlled[41] approach. The sizes of the QDs produced by this method can be controlled fairly precisely by varying the reaction time. The QDs have emission over the visible light range varying up to 650 nm depending on the particle size.

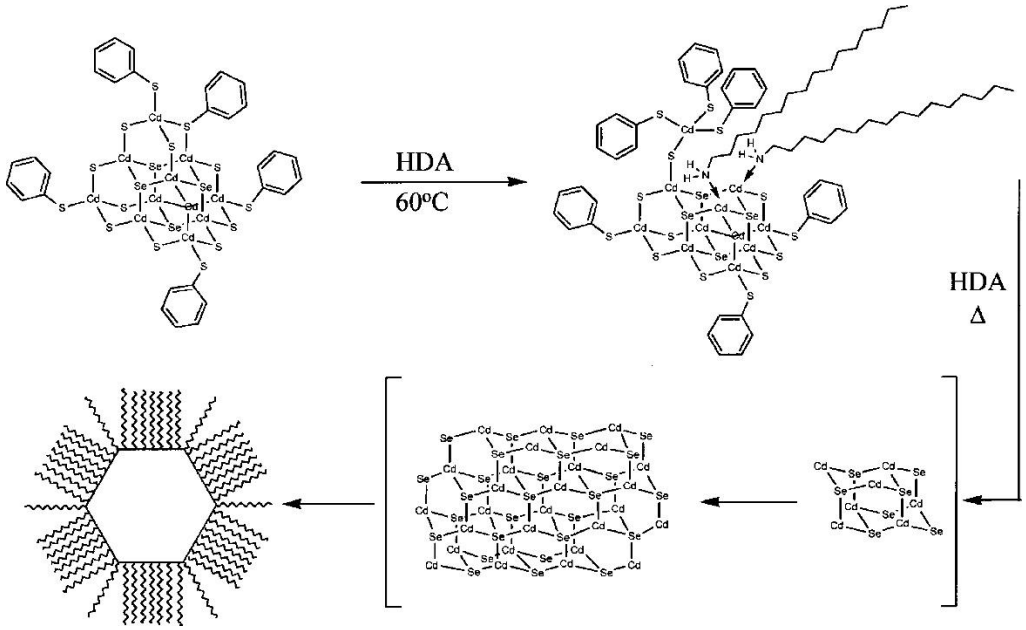

Figure 1.5[26] Proposed reaction mechanism for formation of CdSe nanocrystals from cluster precursors. (Reprinted with permission from ref. 26. Copyright © 2002 American Chemical Society.)

Thiourea and *N*-alkylthioureas (with alkyl groups methyl or ethyl) cadmium complexes have also been used[42] as precursors to prepare TOPO-capped CdS nanoparticles (Figure 1.6). These complexes have the advantage of being air-stable, low-cost, and easy to prepare.

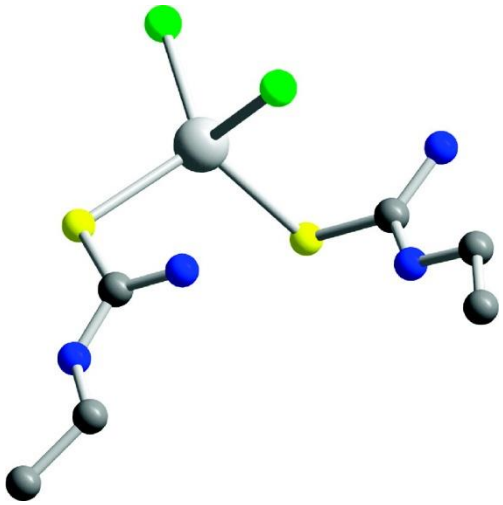

Figure 1.6 Molecular structure of $CdCl_2(CS(NH_2)NHCH_2CH_3)_2$.

O'Brien and co-workers reported[43] that cadmium diisopropyldiselenophosphinate $[Cd(^iPr_2PSe_2)_2]$ can be used as a single-source precursor as an easy and convenient technique to mass produce high-quality CdSe nanoparticles. In a microfluidic reactor (fused silica microcapillary tube) the precursor is dissolved in TOP and oleylamine at 200 °C. The CdSe

nanoparticles produced were then mixed with [Cd(S_2CNMe^{n}Hex)$_2$] and returned to the reaction vessel for the growth of the CdSe/CdS core−shell structures. The quantum yield increased from 12% for CdSe to 33% for CdSe/CdS and are highly luminescent.

Single-source precursor synthesis of nanoparticles based on elements other than Cadmium

Single-source precursor methods have been used for the preparation of nanoparticles based on various elements other than Cadmium such as AlN, GaN, InN, InP, GaP, In_2Se_3, GaSe, In_2S_3, PbS, etc.

Polymeric gallium imide, [Ga$(NH)_{3/2}]_n$, and gallium azides, [$Et_2GaN_3]_3$, $(N_3)_2$Ga[$(CH_2)_3NMe_2$], or $(Et_3N)Ga(N_3)_3$ have been used as precursors to synthesize GaN nanoparticles.[44] The sizes of the particles produced are controlled by the amount of precursors used. The particles are usually aggregates of 20−200 nm that consist of ~4 nm crystals. In this approach poly(imidogallane) precursor was used[44] to synthesize GaN nanoparticles. However it involves the use of pure ammonia, which is hazardous and difficult to manipulate. The complex has poor solubility, which makes it difficult to control the sizes. As a result only a small percentage of nanosized particles are obtained at higher reaction temperature. Patten *et al.* improved this method by pyrolysis of this compound.[45] This improved method increased the yield of GaN nanocrystals significantly and also does not involve the use of ammonia. This method is related to the ability of the coordinating ligands to cap the particle surfaces as soon as GaN nuclei are formed. The reaction does not produce any GaN without the presence of HDA, which suggest transamination by HDA[45].

Wurtzite (hexagonal) QDs of AlN, GaN, and InN have been synthesized[46] by using [M$(H_2NCONH_2)_6]Cl_3$ (M = Al, Ga) and In$(H_2NCONH_2)_3Cl_3$ as precursors and refluxing the precursors in *n*-trioctylamine. The resulting GaN QDs have sizes between 2−3 nm in diameter and showed two emission bands at 380 and 340 nm. In the synthesis of In nanoparticles[47], a small amount of indium oxide is also produced. The indium analogue of $(N_3)_2$Ga[$(CH_2)_3NMe_2$] undergoes thermolysis in TOPO and the resulting InN nanoparticles are cubic, with sizes ranging between 2−10 (Figure 1.7). The particles are fractionated by size-selective precipitation and particles with an average diameter of 4.5 nm have emission at 690 nm (1.82 eV), which is consistent with the band gap of the bulk InN near 0.7 eV.

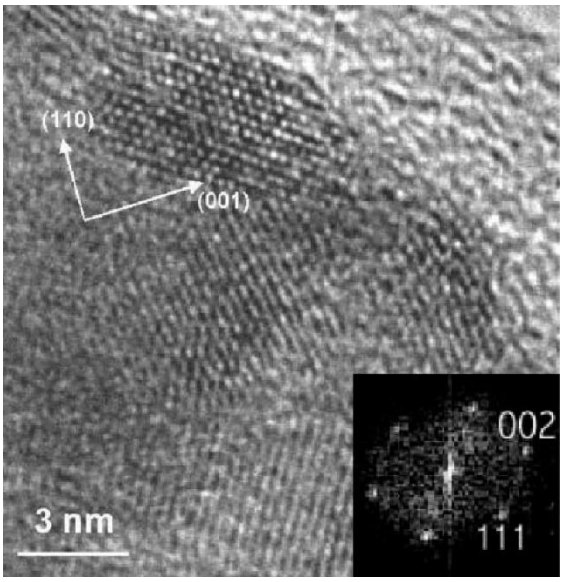

Figure 1.7[48] HR-TEM image of InN nanoparticles. The principal zone axes of the cubic unit cell are indicated for the top particle. (Inset) Fourier transform electron diffraction pattern of the particle in the top of the image. (Reprinted with permission from ref. 48. Copyright © 2006 Royal Society of Chemistry.)

In a similar method, Gillan *et al.*[49] produced wurtzite InN QDs in superheated toluene which is then refluxed in hexadecane at 280 °C. Characterization of the resulting QDs shows that lower temperature reactions produced less crystalline nanoparticles with a zinc blende (cubic) structure whereas mixed metal nitrides, $Ga_{1-x}In_xN$, where x is 0.5 and 0.75, were produced in mixed indium and gallium azide precursors in toluene. Both InN and Ga−In−N QDs showed emission in the red and green visible light region. Furthermore, Mishra *et al.*[50] used ammonium hexafluoroindategallate $[(NH_4)_3In_{1-x}Ga_xF_6]$ as precursor and produced a mixture of cubic and hexagonal (InGa)N particles. Characterization of the synthesized material shows a ratio of 9:1 for the cubic to hexagonal structures and emission in the visible region at around 735 nm (1.69 eV) at room temperature.

Diorganophosphides $[M(P^tBu_2)_3]$ (M = Ga, In)[51] were used to synthesize InP and GaP nanoparticles in dry alkylpyridine. A complicated mix of reductive and β-hydrogen elimination is involved in the mechanism of the thermolysis of the precursor, which also produced metal phosphide and metallic impurities. The reaction produced capped QDs which showed distinct optical quantum size effects. Wells *et al.*[52] used $[X_2GaP(SiMe_3)_2]_2$ (X = Br, I) or $(Cl_3Ga_2P)_n$, to synthesize crystalline monodispersed GaP. The precursor decomposes at relatively low

temperatures under vacuum. Guzei *et al.*[53] used $[H_2GaE(SiMe_3)_2]_3$ (E = P, As) to produce GaP and GaPs NPs. The complex decomposes at 450 °C in xylene and the resulting QDs have diameters around 5 nm. Helliwell *et al.*[54] and Hamilton *et al.*[55] reported the synthesis of HDA-capped InAs and GaAs nanoparticles from dimeric compounds $[^tBu_2AsInEt_2]_2$ and $[^tBu_2AsGaMe_2]_2$ respectively. Both InAs and GaAs NPs produced in this synthesis showed a blue shift in their absorption spectra compared to their bulk materials.

Dimitirjevic and Kamat[56] reported the synthesis of In_2Se_3 by using either poly(vinyl alcohol) (PVA) or sodium metaphosphate (SMP). The produced nanoparticles have diameters of around 2−3 (with SMP) and 30 nm (with PVA) and showed absorption maximum at 375 and 250 nm (with SMP) and 550 nm (with PVA). By a similar approach they also produced[57] In_2S_3 QDs in acetonitrile with diameters ranging between 100 and 200 nm. Barron *et al*.[58] used cubane precursors $[(^tBu)GaSe]_4$ and $[(EtMe_2C)InSe]_4$ to produce GaSe and InSe nanoparticles. Characterization by TEM showed that the resulting GaSe NPs have a mean diameter of around 42 nm with standard deviation of 13 nm and InSe particles have a mean diameter of around 88 nm with standard deviation of 30 nm. O'Brien *et al.*[59] used $[In(E_2CNEt_2)_3]$ (E = S, Se) to produce InS and InSe nanoparticles capped with TOPO and InSe nanoparticles capped with 4-ethylpyridine (Figure 1.8).

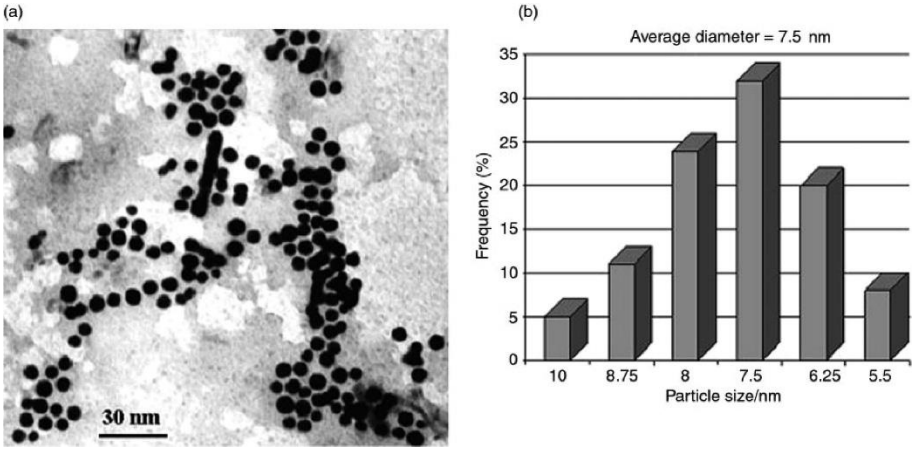

Figure 1.8[59] 4-Ethylpyridine-capped InSe nanoparticles from $[In(Se_2CNEt_2)_3]$: (a) TEM micrograph and (b) size distribution histogram. (Reprinted with permission from ref. 58. Copyright © 1999 Royal Society of Chemistry.)

Dutta *et al*. used methylindium thiolate complexes to produce In_2S_3 nanoparticles.[60] However the produced indium sulfide nanoparticles had poor quality. Later

they used indium xanthates as precursors and the quality of the QDs improved significantly. They also synthesized Ga_2S_3 and In_2S_3 NPs with polymeric indium and gallium precursors $[MeM(SCH_2CH_2S)]_n$ (M = In, Ga). These precursors were prepared by the reaction of trimethyl gallium/indium ether adduct ($Me_3Ga/InOEt_2$) with 1,2-ethanedithiol ($HSCH_2CH_2SH$) with 1:1 stoichiometric ratio. The reaction takes place in a tube furnace and at the temperature between 300 and 500 °C.

O'Brien *et al.*[61] first reported the synthesis of PbS NPs from diethyldithiocarbamate. The resulting material showed to have well-defined cubic structure. Later Cheon *et al*.[62] showed that shape control was possible with changes in the reaction conditions. Vittal *et al*. synthesized PbS nanoparticles by employing a Lewis-base-catalyzed approach[63] to decompose metal alkyl xanthates by using alkyl amines as a solvent. When long-chain alkylamines were used the resulting PbS nanoparticles had a spherical shape and diameters between 5−10 nm. Such above-mentioned precursors have the advantage of being air-stable for months and easy to synthesize, and having high yields. Cheon and co-workers also discussed[64] the ripening process observed with the PbS nanoparticles from a single-source precursor. They showed that by varying the precursor solvent ratio and reaction temperature, it is possible to obtain materials with shapes like rods or cubes.

Rosenthal *et al.*[65] used tin dithiocarbamate $[Sn(S_2CNEt_2)_2]$ with oleylamine as solvent to produce SnS nanoparticles. Their method compared with previously reported ones does not involve the use of phosphines and some other organometallic compounds which are volatile and hazardous. The resulting SnS NPs has well-defined crystalline structure and showed strong optical absorption in the visible and near IR regions.

Limitations of Current CdSe Quantum Dots Synthetic Methods and Motivation of this Work

Although lots of work is presented in the literature, these methodologies leave much room for improvement on the particles' size uniformity. In the hot injection method, excess amount of precursor is rapidly injected into heated solvent. The monomer concentration is rapidly increased and the excess free energy from super-saturation is released through rapid nucleation of nanoparticles and the monomer concentration decreases quickly. The nucleation

process typically completes in a few seconds timescale. Although this method is able to produce nanoparticles of fairly narrow size distribution, the composition of the particles is hard to control because of more than one precursor used. By using the single-precursor heating-up method, composition of the particles can be tuned by controlling the composition and nature of the precursor complex, while still maintaining the advantage of producing narrow size distribution. In this method the single-precursor and solvent are mixed at a lower temperature and then heated up to a higher temperature for the nucleation to begin. This method also has the advantage of simplicity and ease of control due to prolonged reaction time[6, 7]. Due to the short reaction time this method has poor reproducibility. The composition and size distribution of the nanoparticles are also difficult to control by this method.

Size-selective precipitation in particular is an inefficient and tedious process, which is unsuitable for large-scale industrial production. Another challenge remaining is the ability to produce sub-2nm QDs, a type of QD referred to as magic size QDs because of its particular stability.[19] In a typical QD growth, after the initial nucleation stage the particles are allowed to grow in order to narrow the size distribution, a process dominated by Ostwald ripening and monomer diffusion. Larger particles grow at the expense of smaller particles' re-dissolving. Due to their particular size (<2nm), these magic size QDs do not go through Ostwald ripening and are stable.[66] Investigation of the magic size nanoparticles could give interesting insights into their photo-electronic properties at the molecule-cluster transition regime.[67] They also have potential application in white light LEDs[68], biological detection[69], and seeding growth of larger particles. The Cumberland[26] method could not achieve such small size and uniformity at the same time. As the nucleation initiates, the precursor complex decomposes and nuclei start forming. However, the nucleation stage and growth stage could not be separated because the precursors do not decompose fast enough. In fact, the nuclei already started growing as the complex is still decomposing. After most precursor molecules have completed decomposition, some of the earliest nuclei have already grown significantly larger than the newer ones, creating a broad initial size distribution. Moreover, in order to narrow such broad size distribution, prolonged growth is needed and therefore small particle size can not be achieved.

The induction heating method described in Chapter 5 could resolve these issues. Our data have shown that it provides a heating rate of at least 110 °C per second, 6,600 times faster than using a typical heating mantle (1 °C per minute). As indicated by calculation, induction heating

would provide far greater power and heating rate compared to MW method as well. It is expected that induction heating will produce smaller particle sizes and initial nuclei size distribution compared to both the heating mantle and the microwave synthesis.

Colloidal CdSe Quantum Dots Growth Kinetics

Besides the experimental aspects, this thesis also investigated the growth kinetics of CdSe quantum dots in colloidal solution from the theoretical perspective. Classical nucleation theories consider the particles as bulk material. From the general perspective, there should be two terms that determine the growth rate: one responsible for the formation of new bonds, and the other the energy required to form new interfaces between different phases. These two terms compete with each other in the equation of free energy of the system, and therefore a maximum could be found. And since these terms are expressed as functions of particle radius, a so-called critical radius could be determined, where the particle size is thermodynamically favored. In simple terms, the free energy could be expressed as[70]:

$$\Delta G = -\frac{4}{3}\pi r^3|\Delta G_V| + 4\pi r^2\gamma,$$

where ΔG_V is the unit volume free energy difference between two phases, and γ is the unit area surface free energy, with r being the particle radius. It is clear from the expression that it assumes the particle to be spherical, which is a reasonable approximation. The center issue therefore is finding out the state of related parameters where $d\Delta G/dr = 0$. In order to achieve this, several assumptions and approximations need to be made regarding the chemical potential of absorbing/dissolving a monomer, flux of monomers towards/away from the nuclei, and initial monomer saturation. The theory utilized in Talapin *et al.*'s simulation[71] could be adopted, which gives

$$\frac{dr}{dt} \propto S,$$

with S being the dimensionless initial supersaturation ratio. Then, another assumption could be made regarding the rate of nucleation in solution described by Nielsen as follows:

$$J_N = B_N \exp(-\frac{\Delta G^N}{RT})$$

$$\Delta G^N = \frac{16\pi\gamma^3 V_M^2}{3(RT ln S)^2}$$

Here B_N is the preexponential factor relating to factors such as desolvation of species, ΔG^N is the activation energy for nucleation, γ is the specific surface energy, and V_M is the molar volume. With these relations, we could see (Figure 1.9) within the regime of $1 < S < 1000$, the nucleation rate increases more rapidly compared to the growth. As the heating rate increases, the precursor molecules decompose more quickly, providing more monomers, which could either end up forming new nuclei, or grow onto other existing nuclei. But since the increase of nucleation rate is greater than that of growth, it is sensible to believe that by increasing the heating rate and therefore the initial saturation S, the solution will end up with more nuclei.

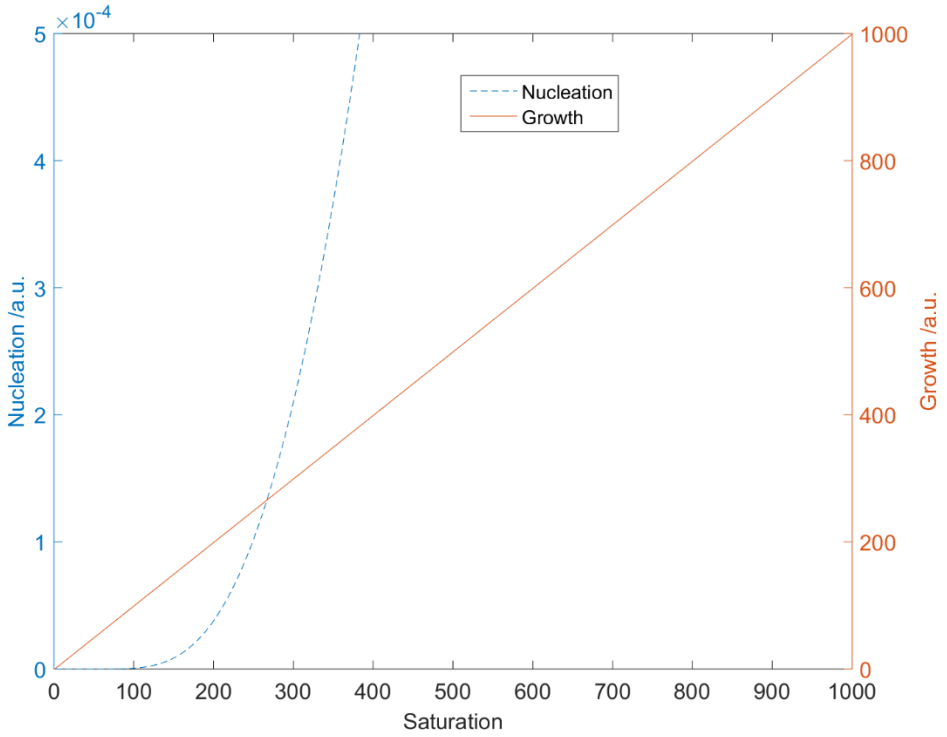

Figure 1.9 In the regime of 1<Saturation<1000, nucleation rate increases more rapidly than growth rate

Generally, theories including LaMer[72] burst nucleation and Ostwald ripening have been used to describe the growth of nanoparticles in solution. However, due to the nature of such process, it is difficult to monitor the growth experimentally. With such lack of empirical data, theories were crude until the advancement of several in-situ and ex-situ measurement techniques. UV-vis spectroscopy is a convenient technique to monitor the particle size in solution during and after growth, as the nanoparticles' sizing curve can be readily obtained through calculations[8] and

experiments.[73] Emission spectroscopy could provide important information on the electronic structure of these particles, and is crucial to understanding other affecting factors as well such as interaction with surfactants. More recent studies include use of small-angle X-ray scattering and liquid cell transmission electron microscopy.[74] These data have facilitated the development of much more refined models. But to date, there still lacks a successful model that describes the growth and especially the nucleation stage of CdSe QDs. Due to the difficulty of separating the nucleation and growth process, it is challenging to obtain experimental data pertaining to the two stages separately. As pointed out by Qu *el al.*[75], the crystallization of nanoclusters, especially the early nucleation stage has been a challenging area of study mainly due to lack of experimental data. Although numerous theoretical attempts at understanding such process have been done, it is not uncommon to have theoretical prediction differ by tens of orders of magnitude with experimental data.[70] The difficulty of gaining insights into the nucleation stage lies in the fact that nucleation and growth, including the appearance and disappearance of nuclei happen simultaneously in a dynamic fashion. Through separation of the nucleation and growth stage of the quantum dots, this thesis provides valuable data with controlled variables that address the different experimental conditions during growth and nucleation separately, which will facilitate greatly the development of a more accurate theory describing such processes.

Impact of Doping on Charge Carrier Density and Application in Solar Cells

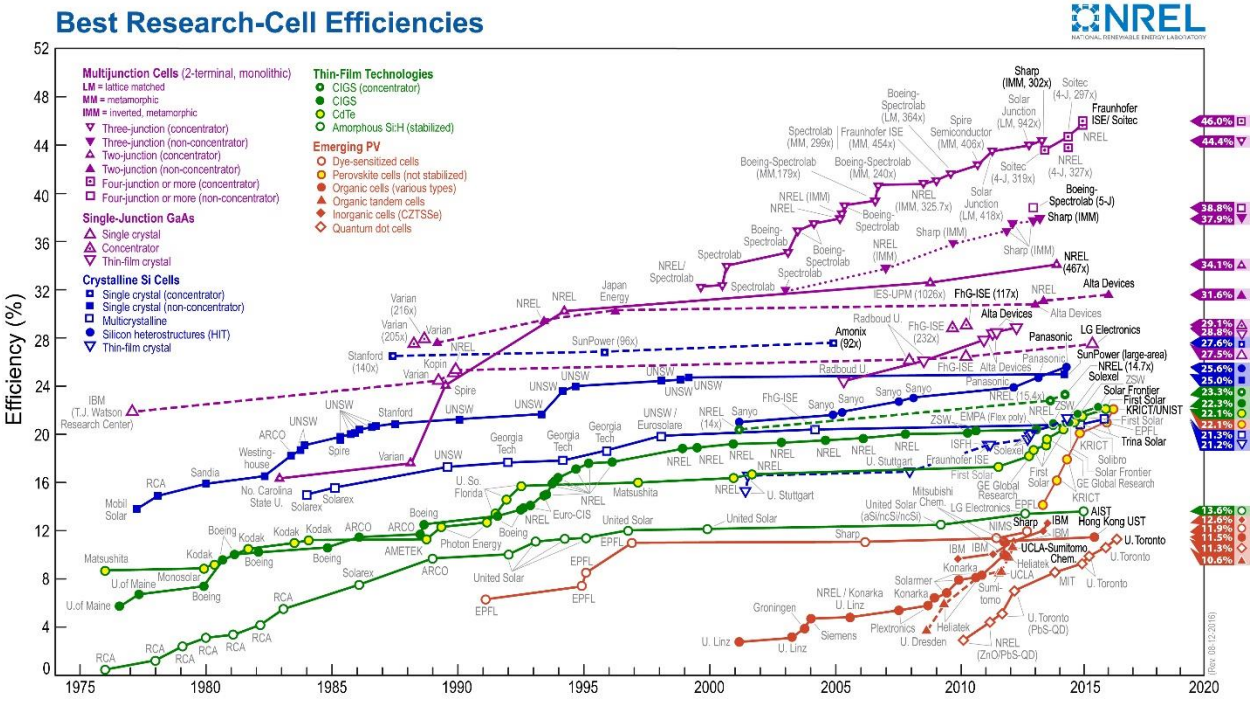

Figure 1.10 Progression of best research-cell power conversion efficiencies by NREL. (Reprinted with permission from National Renewable Energy Laboratory (NREL). Copyright © 2016 NREL)

The light harvesting potential of CdSe quantum dots is an attractive property that received much attention in recent years as part of a continuing global effort in developing photovoltaic technology to resolve the energy and environmental challenges the world is facing in the near future[76]. The currently most adopted solar cell solution involves devices based on single-crystal silicon material, which yields a conversion efficiency of about 28%. Although these devices have proven to be functional, they suffer from prohibiting high cost of manufacturing in the single-crystal preparation process which severely limits their scope of commercialization, and their PCE has seen only ~4% growth in the past 25 years. A second generation of solar cells based on polycrystalline semiconducting material has since emerged from research efforts, which could lead to significant lowering of manufacturing cost. However, there's still much room for improvement of their power conversion efficiency compared with that of the single-crystal silicon based devices. In recent years, focus has been turned to the so-called organic-inorganic heterojunction nanomaterial based solar cells, which could deliver

satisfactory efficiency at an economically viable cost. Nanomaterials with various structures including nanowires, nanotubes, nanorods, and quantum dots have been studied extensively for this purpose. In this thesis, the photoconductivity and charge carrier density characteristics of CdSe quantum dots have been explored for this consideration. The physiochemical properties of CdSe quantum dots, among other quantum dot material have been investigated since several decades ago[77]. Literature[78] has pointed out the following charge separation process in CdSe nanocrystals:

$$\mathrm{CdSe} + \mathrm{h}v \rightarrow \mathrm{CdSe}\left(\mathrm{e_p} + \mathrm{h_p}\right) \rightarrow \mathrm{e_s} + \mathrm{h_s}$$

$$\mathrm{CdSe}(\mathrm{e_s} + \mathrm{h_s}) \rightarrow \mathrm{CdSe} + \mathrm{h}v'$$

where s and p indicates the states of the electrons (e) and holes (h). Various theories and experiments have shown that defects affect this process in significant ways, as discussed in detail in Chapter 4. It was previously mentioned in this chapter that surface ligands on CdSe quantum dots serve as a stabilizing agent that prevents coalescence of the particles. However these capping agents could pose a challenge in its optoelectrical device application since they decrease the conductivity of such material by inhibiting electron transfer in the material[79]. A power conversion efficiency chart was compiled by National Renewable Energy Laboratory as shown in Figure 1.10, demonstrating progression of highest confirmed conversion efficiencies for research cells, among which QD cells have seen significant development in the past five years (red hollow diamond, lower right). Zhou *et al.*[48] reported improved 2% power conversion efficiency of (P3HT):CdSe QD solar cells after a simple hexanoic acid washing to reduce the hexadecylamine shell around the particle. 4.94% PCE were reported[80] for cells based on TiO_2/ZnSe/CdS/CdSe cascade structured electrodes. Firdaus *et al.*[81] improved PCE of PbS QDs up to 0.91%. Guyot-Sionnest *et al.*[82] have demonstrated that by doping with potassium, the conductivity of n-type CdSe thin film could be increased by up to 12 times. Based on this evidence, it is intuitive to postulate that doping would have significant impact on the charge carrier density and conductivity of CdSe quantum dots as well.

Another crucial aspect of the effect of doping in the application of solar cells is its behavior under elevated temperatures. Photovoltaic devices for energy harvesting purposes are expected to operate under higher than normal room temperature, as the nature of such operation requires prolonged exposure to direct sunlight. Given the relative energy conversion rate, such device would not be efficient if it requires active cooling. Therefore the performance of the solar

cell under higher temperature is of critical importance for such application, an aspect rarely explored in current studies.

For the above arguments, this thesis will demonstrate experimentally a simple method to dope and control the photoconductivity and charge carriers of CdSe QDs, showing increased photoconductivity leading to a more efficient hybrid solar cell. The chemical dopants (Ga, In and Sn) of CdSe QDs not only result in a controllable photoconductivity, but also a stronger electronic interaction at elevated temperatures. The high conductivity and stronger electronic coupling of doped CdSe QDs can largely enhance charge separation and transport efficiency, which are essential for hybrid inorganic-organic solar cells. The results shown here represent a potentially powerful tactic for increasing the efficiency of hybrid solar cells via enhancing the photoconductivity and controlling electronic interaction between the organic and inorganic materials.

4. Thesis Outline

The goal of this thesis is to understand the role of defects and the control of defects through doping in quantum confined systems, particularly CdSe quantum dots. Various experimental techniques are utilized to achieve this goal including single-source precursor synthesis and doping of quantum dots, magnetic heating for achieving extreme high heating rate and rapid quenching, spectral measurements and monitoring of QD growth, infusion withdrawal dip coating technique for preparation of the TMOS and PTMOS gradient film, and finally reflection on some of the limitations of these techniques and areas for potential improvements. They are described in the Experimental Techniques Chapter 2.

The work described in Chapter 3 aimed at controlling various chemical, electrochemical and spectroscopic properties of CdSe quantum dots through doping. To achieve this, CdSe QDs doped with gallium was synthesized. TEM, XRD and elemental analyses was done to obtain the size distribution of the particles and confirm the presence of dopant atoms as well as determined its crystal structure. Cyclic voltammetry was used to investigate the band-edge electronic states of the doped QDs and computational modeling was performed to understand the dopant atom's role in the host's crystal lattice.

In Chapter 4 I describe work whose goal is to explore the possibility and advantages of doped CdSe quantum dot for hybrid solar cells. Indium and gallium doped CdSe QDs were prepared and CdSe/P3HT hybrid bi-layer solar cells were constructed. Their photovoltaic current density-voltage characteristics and quantum efficiency was measured. The conductivity of solar cells based on doped QDs was compared with that of the undoped to measure its performance. The effect of temperature on conductivity of QDs was also explored.

Chapter 5 focuses on achieving greater control of size distribution and preparation of ultra-small quantum dots through induction heating. The chapter will demonstrate the advantage of induction heating through a series of syntheses with induction heating and microwave heating. The effect of solvents, ligands, and quenching will also be explored through according comparative syntheses. The chapter will also discuss the effects of extreme high heating rate on nucleation and growth of such nanocrystals.

Chapter 6 describes study of the blinking behaviors of CdSe nanorods under polar environments. Infusion withdrawal dip coating technique was used to prepare a polarity gradient film where the CdSe NRs are placed. Various analyses of data including count of number of blinking spots, spectral shift over time, on-off time frequency, spots intensity distribution and mean intensity time sequence were performed to investigate variation of their blinking statistics with respect to different polar environments and NR orientation.

Chapter 2 - Experimental Techniques

1. Single-source Precursor Synthesis and Doping of Quantum Dots

CdSe quantum dots were prepared by the single-source precursor method reported[26] by Cumberland *et al.* (Figure 2.1). The inorganic cluster precursor $(Li)_4[Cd_{10}Se_4(SPh)_{16}]$ can be synthesized as reported in literature[83]. In 1983, Dance *et al*.[83] described the synthesis, properties, and molecular and crystal structures of $(Me_4N)_4[E_4M_{10}(SPh)_{16}]$ (E=S, Se; M=Zn, Cd), a molecular fragment of the cubic metal chalcogenide lattice. $(Me_4N)_2[Cd_4(SPh)_{10}]$ was first prepared by adding $Cd(NO_3)_2 \cdot 4H_2O$ into thiophenol and triethylamine, followed by addition of tetramethylammonium chloride. Selenium metal was then added to the product to produce $(Me_4N)_4[E_4M_{10}(SPh)_{16}]$. Then, CdSe quantum dots were synthesized in hexadecylamine, dodecylamine, and other possible amines. The different solvents acting as capping agent would alter the rate of the dissociation of precursor molecules, as these surfactants can "capture" partially decomposed precursor molecules at different rates. During the growth stage, different solvents would also result in different growth rate, as surfactants greatly affect the surface reaction.

For doping, the appropriate metal chloride was added into reaction mixture before synthesis. To insure precise molar ratio of metal chloride added since the amount could be as low as a few milligrams, a larger amount of metal chloride might be first dissolved in solvents, and then have the proper amount added to the reaction mixture before the solvent vaporizes.

Figure 2.2 shows the TEM image of a sample obtained with this method. The quantum dots are spherical in shape and relatively uniformly sized.

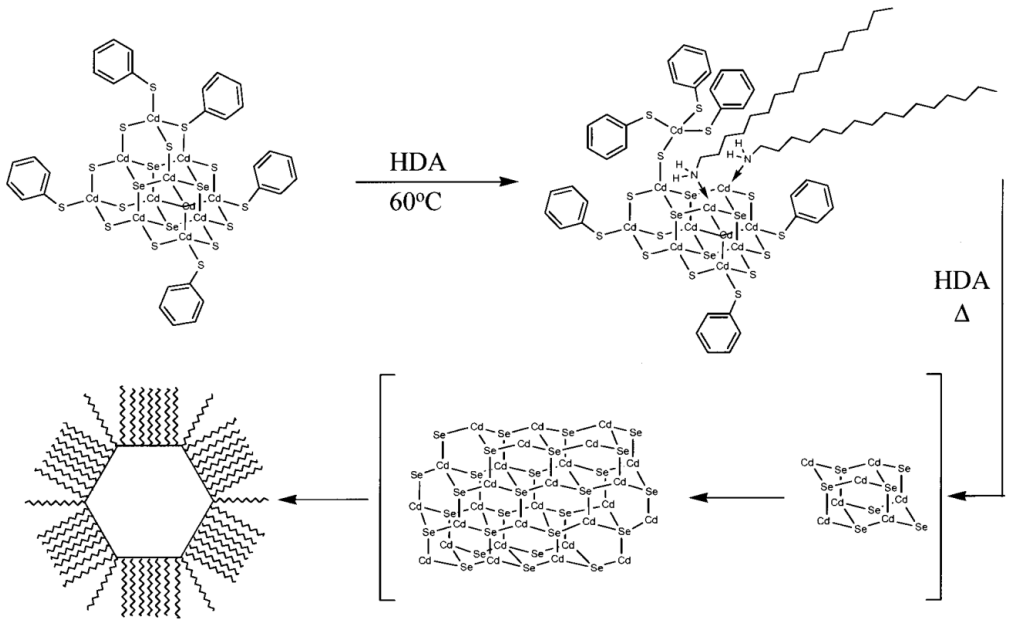

Figure 2.1 Reaction mechanism for formation of CdSe nanocrystals from cluster precursors. (Reprinted with permission from ref. 26. Copyright © 2002 American Chemical Society.)

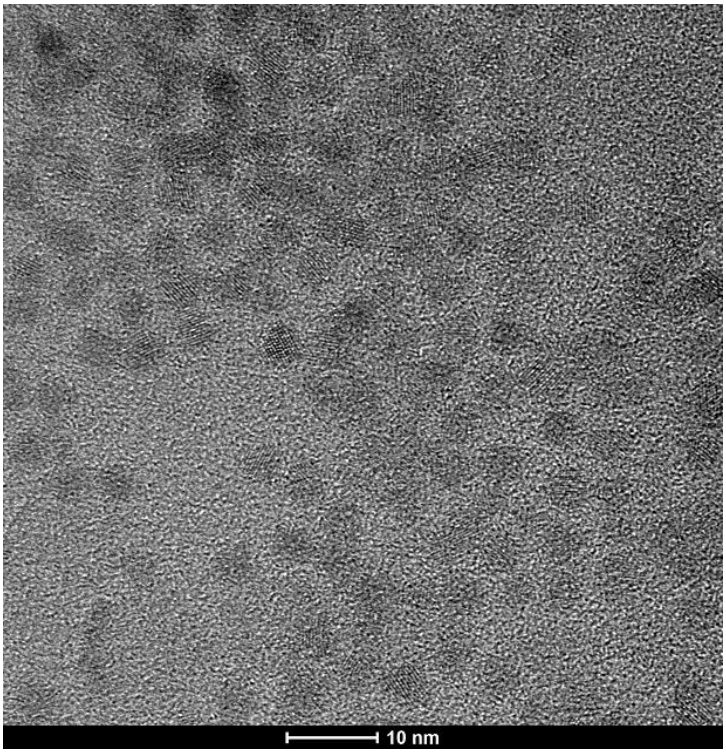

Figure 2.2 CdSe quantum dots synthesized with single precursor[84]. (Reprinted with permission from ref. 84. Copyright © 2015 American Chemical Society.)

2. Magnetic Heating

Mechanism of Heating and Experimental Setup

Induction heating utilizes electromagnetic induction to generate heat by the internal resistance of a conducting metal. High frequency AC is run through an electromagnet, which generates Eddy current in the workpiece. The method has application in processing various types of metals for the ability to raise the temperature of the metal to their melting point in a short period of time. In the experimental setup, the precursors were placed in a glass container (Figure 5.1 top right) filled with steel beads to allow for semi-uniform heating. Glass beads can be mixed with the steel beads to control the heating rate, and heating uniformity can be controlled by the steel bead sizes. An optical temperature probe was placed inside the solution. The container was filled with argon to purge out any oxygen for 1 min prior to heating. Figure 5.1 left shows the rise of temperature of the solvent over time. In 12.8 seconds, temperature of the solvent rose from 28 °C to 186 °C, at a rate of 12 °C/s. However, dodecylamine has a boiling point at 247 °C and during actual heating the solvent was observed to start boiling in under 2 seconds. Due to limitation of the temperature probe's response time, actual heating rate could instead be as high as 110 °C/s. In a conventional synthesis, a heating mantle and temperature controller were used to first melt the solvent at 70 °C, followed by raising the temperature to 275 °C in 3 hours and 25 min, or 1 °C /min.

Unique Characters of Magnetic Heating

This method has the advantage of injecting a massive amount of heat into the reaction solution within a short period of time. With this method, as the heating starts, the precursor rapidly decomposes, creating a large number of small, uniformly sized nuclei, before growth could even start. Compared to conventional synthesis in a heating mantle, or the relatively faster microwave method, when Ostwald ripening comes into effect, a larger portion of precursors will be depleted, producing the final small, uniformly sized nanoparticles. The faster depletion of the complex also leads to possibility of separating the nucleation and growth stage completely, by tweaking the amount of complex used and the current applied in heating. By decreasing the

complex used in the synthesis, we could reach a point where all of the precursor molecules have decomposed after the few seconds of heating.

Because of all these unique characters of magnetic heating, we are able to achieve preparation of sub-2nm magic sized CdSe crystals with improved size uniformity and white light emission, and to investigate the kinetics impact of extremely high heating rate.

Adaptation for Industrial Implementation

Additionally, this setup could be easily modified to drastically increase the amount of product produced in a reproducible manner compared to conventional method, considering that the ability of cheap, bench-top mass production is one of the key attractions of nanoparticles in industrial application. Such setup consists of a continuous production system utilizing a flow-thru tube design (Figure 2.3).

The system includes a setup where the complex solution is continuously supplied by being pumped into a narrow tube that goes through the induction coil. The part of tube inside the coil is filled with steel beads and trapped in between two filters. As the solution passes through the heating chamber, reaction occurs and nanoparticles are formed. The solution continues to flow through a passage where external cooling is applied. The cooled product will stay in liquid form at 40 °C and can be collected. This system would be fully concealed from atmosphere, therefore eliminating oxygen and water, substances that the complex and quantum dots are sensitive to under high temperature. The cooled product can be conveniently collected under atmospheric conditions in liquid form since at 40 °C no significant reaction would occur even with the presence of oxygen and water. The collected product will further solidify as temperature drops below 30 °C and can be stored for a long period of time. With our current setup, 2 grams of solution could finish reaction in 2 seconds. With a more delicate cooling setup to match the reaction speed, the system could theoretically process 3.6 kilograms of raw material per hour.

Figure 2.3 Schematic Diagram of Continuous Synthesis Setup

3. Rapid Quenching

In this thesis, a rapid quenching method was utilized to study the effects of fast cooling on the growth kinetics of these nanoparticles. For the quenching experiments, CdSe complex dissolved in the amine solvents are placed in a glass vial with an injection cap. An optical temperature probe is inserted inside the vial, and two needles are injected through the cap to allow for entry of argon and exhaust gas exit. The vial is similarly placed inside the coil, held with a clamp on a ring stand. Liquid nitrogen is placed under the vial to allow for quick transfer of the sample. After heating has finished, the clamp is quickly let loose and the vial is dropped inside liquid nitrogen immediately. As described in details in later chapters, the data show that temperature of the solution could be dropped to 40 °C within 60 seconds in nitrogen. It is notable that due to the nature of such cooling method, solution around the outside of the vial cools far more quickly than solution in the center. Data is taken of the temperature at the center of the solution to ensure the entirety of the sample has been cooled.

4. Growth Monitoring and Sample Characterization Techniques

In-situ fluorescence spectroscopy and absorption spectroscopy can be employed to monitor the growth of the particles in solution. The presence of complex remaining in the solution after synthesis has completed could be detected with NMR. We could also employ in-situ PL monitoring of the solution to detect newly formed small nuclei and the growth of such nuclei as they will appear at the shorter wavelength end of the spectrum. FWHM of the fluorescence can be obtained to account for the size distribution of the particles. TEM images can be taken of the final product to confirm the presence of the particles and their size distribution.

5. Infusion Withdrawal Dip Coating (IWDC)

Infusion withdrawal dip coating (IWDC)[85] is a method utilized in Chapter 6 to prepare tetramethoxy silane (TMOS)/phenyl trimethoxy silane (PTMOS) gradient film. The process involves preparation of first the tetramethoxy silane sol for the base layer, and then followed by

preparation of the TMOS base layer on a coverslip and tetramethoxy silane and phenyl trimethoxy silane sols for gradient deposition, and finally the gradient film with dip-coating.

Preparation of tetramethoxy silane sol for the base layer

Several small vials were plasma-cleaned and left in the glove box along with several 200 μL and 1mL pipettes. A small magnetic stir bar was also rinsed with water and dried with nitrogen. A solution of 0.1M hydrochloric acid and 200 proof ethanol was prepared. 200μL of TMOS (0.207g) was taken out of the glove box and added to 2491 μL 200 proof ethanol. The mixture was then stirred with the magnetic stir bar for 1 minute followed by addition of 135 μL 0.1M HCl and then stirred again for 1 hour. The TMOS sol was then taken out and put in a glass desiccator for aging for 23 hours before spin coating on the coverslip.

Preparation of the TMOS base layer on coverslip

A piece of wrapping foil and the metal substrate of the spin coater were cleaned with ethanol and dried. Then it was made sure the vacuum was working properly by placing a coverslip on it. 10-12 very clean microscopic glass coverslips were taken from the petri dishes with the dust cleaned off by nitrogen gas and then plasma-cleaned (in batches of 4) for at least 5 minutes. Then one piece of the plasma cleaned coverslip was placed on the spin coater and centered with tweezers. Vacuum was then applied to keep the coverslip in place. The 23-hour-aged sol was then taken out for spin coating. 150 μL of the aged TMOS sol was pipetted onto the center of the coverslip and then spin coated for 30 seconds at 5000 rpm. The coated coverslip was then transferred to a petri dish. The same process was repeated for all plasma cleaned coverslips with the goal to achieve as smooth and uniform TMOS base layer as possible. Then, all the petri dishes with TMOS base layer were placed in the glass desiccator to dry. Such prepared TMOS base layers can be used after 12 hours to up to a week old.

Preparation of tetramethoxy silane (TMOS) and phenyl trimethoxy silane sols for gradient deposition

TMOS: 1200 μL (1.23g) of TMOS was taken from glove box into a large vial and added to 28 mL 200 proof ethanol. A clean and dry stir bar was put into the TMOS and stirred for 1 minute, followed by addition of 830 μL 0.1M HCl and then stirred again for 5 minutes. 600 μL 1M

NH_4OH was then added to the mixture and stirred for 35 minutes. An appropriate amount of CdSe solution was added based on specific experimental needs. The TMOS sol was then left in the desiccator for aging for 4-5 hours.

PTMOS: 500 μL (0.531g) PTMOS was taken from the glove box and put into a large vial and added with 9500 μL 200 Proof ethanol. A clean and dry stir bar was put into the solution and stirred for 1 minute followed by addition of 290 μL 0.1M HCl. The mixture was then stirred for 10 minutes then added with 200 μL 1M NH_4OH and stirred again for 30 minutes. An appropriate amount of CdSe solution was added based on specific experimental needs. The PTMOS sol was then left in the desiccator for aging for 4-5 hours.

Preparation of gradient film with Infusion Withdrawal Dip Coating (IWDC)

The syringe pumps were set up from the 3rd hour of aging time of the TMOS and PTMOS sol. The infusion and withdrawal rate were first determined for the syringes and set accordingly. The motor that moves the coverslip up and down during the dip coating was checked to be in working order to prevent occasional jamming, which could take a bit effort to fix up. The cell, syringe and tubings were then placed in the dip coating room with the syringes fixed along with the tubings in the syringe pumps and connected to the opening (hoses) of the cell. A smooth base layer was picked to be plasma cleaned for one and a half minutes with the rest discarded. The infusion syringe was then loaded with the TMOS that has been aged for 4-5 hrs. The plasma-cleaned base layer was then clipped in the dip coater such that the base layer faces the operator. The stir bar was then transferred from the vial containing the PTMOS into the cell with 9.5 mL of PTMOS sol that was also aged for 4-5 hours pipetted into the cell. The cell was then put right below the clipped base layer in such a way that when the base layer was lowered it will move right across the middle of the meniscus. To achieve this, the cell can be moved very slightly so as to avoid the slashing of meniscus since it was where the deposition was performed and extra care needs to be taken in its handling. The base layer was then lowered into the cell that is partially filled with PTMOS sol controlled with computer at 200 rpm. The motor was stopped when the bottom edge of the base layer (coverslip) was just above the outlet opening to fix the coverslip at its place. At the same time, the sol in the cell (i.e. PTMOS sol) was stirred slowly. Once the meniscus was stable, the opening of the dip coater was closed and both the pumps were turned on such that the infusion and withdrawal could start simultaneously (Figure 2.4).

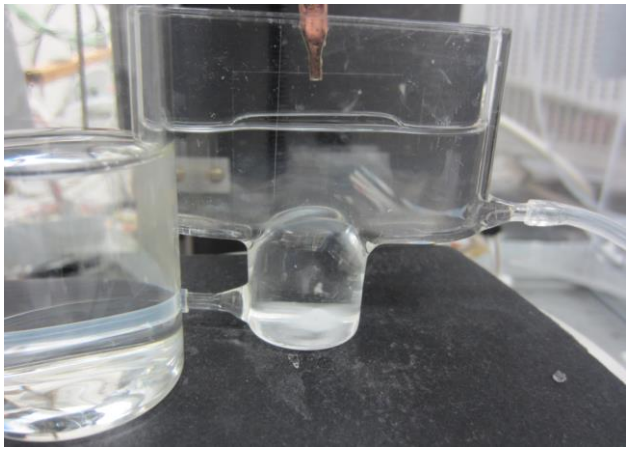

Figure 2.4 Experimental setup of Infusion Withdrawal Dip Coating

6. Limitations, Future Work and Improvements

In the magnetic heating synthesis setup, the sizes of the steel beads used in induction heating would affect the uniformity of heating. Theoretically, the difference of amount of heat received by solution from different distances to the beads can be decreased by using smaller beads. However, smaller sizes will also leave smaller spaces between the beads, reducing the amount of solution that could be used in one synthesis. Therefore, it is both theoretically and practically impossible to achieve absolute uniform heating by infinitely decreasing the sizes of the beads. With the parameters employed as discussed above, a reasonable approximation could be achieved to study the effects of induction heating.

The experimental techniques discussed in this chapter will also enable possible future efforts at making proper predictions of the effect of our experimental conditions using theories reported in literature for such systems. It is possible to fit the experimental data with numerical simulations accounting for varying parameters, and performing a series of simulations based on theoretical models discussed in Chapter 1. It is easy to implement simple simulations of the growth accounting for different conditions. A Monte Carlo simulation similar to that described by Talapin *et al.*[71] can be performed to reflect the high heating rate of induction heating, whose result could be compared with that from experimental data.

Chapter 3 - Synthesis and Characterization of Gallium Doped CdSe Quantum Dots

1. Introduction

Doping quantum confined semiconductor nanocrystals (quantum dots or QD's) will allow for a new generation of electronic devices built on a bottom-up construction model that are smaller and more powerful than devices currently fabricated by photon-lithography.[86] The ability to synthesize high quality quantum dots[24, 87] via bench-top chemistry makes doping quantum dots to enhance electrical properties of the utmost importance. Despite several drawbacks such as the low availability of elements in earth's crust and highly negative environmental impact,[88] CdSe quantum dots produced through colloidal synthesis are the ideal system for doping studies simply due to extensive investigation over the past 20 years.[89] Because of the small number of atoms composing the QD, successful doping was initially thought to be unlikely because even a single dopant atom would lead to dopant/cm^3 values more consistent with alloy materials.[90] Several obstacles, such as self-purification[17] and low dopant solubility, would have to be overcome. Reports of successful incorporation of aluminum,[91] chromium,[92] cobalt,[93] copper,[94], indium,[91, 95] iron,[96] manganese,[97] silver[98] and tin[95a] introduced magnetic properties to CdSe and ZnSe[10] QD's. Creation of n-type CdSe via "charge injection" of an electron into the conduction band using reducing agents has been used to study electron relaxation in the absence of an accompanying hole.[82] However, up until several years ago there were no reports of attempting n-type doping of CdSe QD's. Indium has been used in doping CdSe thin films[99] and CdSe nanowires,[100] which creates electron donor states below the conduction band characteristic to n-type semiconductors. Indium doped CdSe QD's were also reported by Knox *et al.*[101] However, little evidence of the dopant atoms' impact on the properties of the QD's was presented.

Previous reports of successful doping of CdSe QD's with indium[95b] showed that the presence of indium had dramatic effects on the growth of CdSe:In. Briefly, CdSe dots grown in the presence of $InCl_3$ showed increased growth rates in the "heterogeneous growth regime" along with rapid size focusing. Indium was found to activate the growth of QDs, resulting in larger particles than QD's grown in the absence of dopant and significant quenching of band-edge

photoluminescence in spite of a ZnS passivating shell and corroborating results reported with "charge-injected" particles[8] as well as with indium doping in thin films.[9] Further work on indium and tin doped CdSe showed that donor electrons are not ionized into the conduction band until temperatures well above room temperature.[95a] In an ideal n-type semiconductor, electrons from the donor level are ionized into the conduction band at room temperature due to the extra electron being weakly bound to the dopant atom. Gallium had been reported as an n-type dopant in thin films of CdSe.[102] Due to the higher ionization temperature shown by tin and indium, gallium was chosen for investigation in the hopes that the 4p orbital would align with the QD's $1S_e$ conduction band level at room temperature to provide increased donor electron occupation.

Here the synthesis of gallium-doped CdSe QDs are reported. Structural characterization of the CdSe QDs show no significant changes in the CdSe wurtzite structure upon introduction of gallium atoms. Experimental data on the growth of the CdSe QDs from $Li_4[Cd_{10}Se_4(SPh)_{16}]$ suggest that the gallium may exchange into the complex at the early stage of the nucleation. The resulting doped CdSe QDs exhibit more reducing character confirmed by oxidative etching and cyclic voltammetry experiments. Spectroscopic characterization reveals that the gallium-doped QDs show a stronger temperature dependent photoluminescence quenching and shortened excitonic lifetime as a result of the increased dopant ionization above room temperature.

2. Experimental Section

Chemicals: All chemicals are used as purchased with the exception of hexadecylamine, which is vacuum distilled at 2 torr. $InCl_3$, $SnCl_2$, $GaCl_3$, diethylzinc, hexamethyldisilithiane and tri-n-octyl phosphine (TOP) are all stored in an inert atmosphere/low water vapor concentration glovebox. Zn/S stock solution is prepared according Hines *et al.*[103] by mixing 7 mL of diethylzinc with 1 mL hexamethyldisilithiane and 32 mL of distilled TOP. Tri-n-octylphosphine oxide (TOPO), 2-amino-propanol (APOL), N,N-dimethyl sulfoxide (DMSO) and a supporting electrolyte (Tetrabutylammonium perchlorate (TBAP)) are used as purchased and stored under ambient conditions.

Synthesis: Doped and undoped CdSe core particles are synthesized using the $Li_4[Cd_{10}Se_4(SPh)_{16}]$ single source precursor (SSP) prepared as reported by Cumberland[26] in hexadecylamine with metal chloride as the doping agent. In this work, the gallium doped CdSe quantum dots are synthesized either with ZnS shell for the photoluminescence experiments or without ZnS shell for the electronic characterization.

Ga:CdSe quantum dot synthesis: 25 g of distilled hexadecylamine and 0.3 g of SSP are loaded into a three-neck flask and passed into a glovebox where the appropriate amount of metal chloride is added. All dopant load percentages are based on the total selenium content of the reaction. The reaction flask is purged on an Ar gas line for 3 minutes and heated to 70°C at 1.5 °C/min temperature ramp. The mixture is then heated to 275 °C at 1 °C/min and kept for 1 hour to allow growth of the particles, and cooled to 180 °C and kept for 18 hours to narrow the size distribution of the particles.

Ga:CdSe/ZnS Quantum dot synthesis: 50 g of distilled hexadecylamine and 0.6 g of the (SSP) are loaded into a three-neck flask and passed into a glovebox where the appropriate amount of metal chloride is added. All dopant load percentages are based on the total cadmium content of the reaction. The reaction flask is purged on an Ar gas line for 20 minutes before being very slowly heated to 120 °C with careful attention made to minimize temperature overshoot, as the stability of the magic sized nanocluster is extremely sensitive to temperature. The solution is stirred at 120 °C for 18 hours while in-situ fluorescence spectra are collected.[95b] After 18 hours the temperature is increased to 240 °C and the particles grow to their final size over 3 hours. ZnS shell growth is accomplished by using an automated syringe pump to dispense a solution of 2 mL of the Zn/S stock solution diluted with 8 mL of TOP over one half hour followed by one hour of growth at 250 °C. After one hour of shell growth, cooling studies are performed. Following the cooling studies described below, another layer of shell material is grown by repeating the slow Zn/S injection at 250 °C. This sequential shell growth is repeated for a total of four injections.

Monitoring ZnS Formation via Temperature Dependent Photoluminescence: Following the ZnS shell growth, the reaction mixture is allowed to cool from 250 °C to 60 °C with the flask covered with foil to ensure a slow, even cooling process. Photoluminescence spectra are recorded every second. This cooling process is repeated five times without exposure to oxygen. A surface reflection probe equipped with a 405 nm LED excitation source is used to collect the spectrum during all growth phases.[20]

Particle Preparation for Temperature Dependent Photoluminescence Studies: ~1 g of crude reaction solution is dissolved in 10 mL of toluene and gently heated until the crude solid is melted. This solution is centrifuged at 7000 rpm for ~5 minutes to allow all of the excess metal to precipitate out leaving a clean suspension of quantum dots. The toluene suspended quantum dots are refluxed in ~3 g TOPO for 4 hours followed by precipitation with methanol and re-suspension

in toluene and precipitated via methanol one final time. The solid is dried under vacuum for ½ hour after which 10 mL APOL is added to the centrifuge tube and sonicated until the quantum dots disperse in the APOL.

Temperature Dependent Photoluminescence Studies of Purified Quantum Dots: A dilute solution of quantum dots in APOL is made by filling a fluorescence cuvette with 3 mL of APOL and adding 1 mL of QD's in APOL described in "Particle Preparation for Low Temperature Photoluminescence Studies" above. The cuvette is fitted with a glass stem to allow accurate temperature measurement and sealed with a rubber o-ring to keep oxygen out. The experimental set up is a home-built 405 nm variable output laser diode equipped with UV-resistant fiber optic cables. Spectra are collected at a 90° angle from the excitation fiber. A small heating element is located at the base of the set-up and attached to a programmable power-supply. The cuvette is placed in the experimental set-up and heated to 80°C where the temperature is maintained at 80°C for twenty minutes to ensure uniform solution temperature. The apparatus is then cooled via water pump at a rate of 1 °C/minute down to 10 °C. During this time fluorescence spectra are collected every 10 seconds. For the time-resolved temperature dependent data, the 405 nm continuous excitation source is replaced by a pulsed laser source. The pulsed laser consists of a cavity dumped output of a mode-locked Ti:Sapphire laser (λ_{max} = 780 nm, repetition rate = 2 MHz, average power = ~80 mW), pumped by a diode laser (532 nm, 4.6 W). The 800 nm light is frequency doubled with the help of a nonlinear crystal (BBO) and gently focused on the sample. Detection is accomplished with a Hamamatsu MCP PMT and time-correlated single photon counting electronics (EG&G Ortec). Wavelength selection is accomplished using color filters.

Single Particle Fluorescence Study of the Zns/Gallium doped CdSe Quantum Dots with the Help of a Wide-field Microscope: Fluorescence images of the samples were also acquired by wide-field imaging.[104] The system employed is built upon an inverted epi-illumination microscope (Nikon Eclipse TiE). Excitation light in these experiments was either from a Nd:YVO_4 laser (Coherent, Verdi, 532 nm) or a diode laser (488 nm). The incident light was first focused into a spinning optical diffuser and subsequently collected and passed through a polarization scrambler before being directed into the epi-illumination port of the microscope. The light was reflected from a dichroic beam splitter (Chroma Q555LP or Chroma, Q505LP), for 532 nm and 488 nm excitation, respectively) and focused into the back aperture of an objective (Nikon Apo TIRF 100X, 1.49 N.A.). Fluorescence from the sample placed on a heatable sample stage was collected

and separated from the incident laser light by passage back through the beam splitter and a 580 nm band pass filter having a 40 nm pass band. A back-illuminated EM-CCD camera (Andor iXon DU-897) was used as the detector.

High Resolution Transmission Electron Microscopy (HR-TEM): HR-TEM imaging is done on a FEI Tecnai F20 XT Field Emission electron microscope. Samples are prepared by dispersion in chloroform and dropped onto a lacey carbon nickel grid. Nickel grids are necessary to eliminate Cu-K and Cu-L lines from obscuring Ga-K and Ga-L lines. The resolution of the instrument is 0.25 nm in TEM mode and 0.18 nm in Scanning Transmission Electron Microscopy with High Angular Annular Diffraction (STEM-HAADF) mode for elemental analysis.

Etching study of doped CdSe QDs: After washing the CdSe QDs with methanol three times, the particles are dissolved in APOL (3-amino-1-propanol, Sigma Aldrich) and then precipitated with acetone to remove the TOPO ligands from the surface. This precipitate is then re-dispersed in APOL. The concentration of the doped and undoped quantum dots is prepared so that the first electronic absorption peaks are at 0.4 optical density. These CdSe solutions are then placed into a cuvette holder, which is set up for temperature control and *in situ* photoluminescence (PL) recording. The PL setup consists of a 405 nm laser diode exciting the nanoparticles in the cuvette, and a fiber optic spectrometer recording the PL at 90^0 to the excitation source to minimize scattered light. A constant stream of air is passed into the holder, monitored by an air flow meter. For this experiment a flow rate of 290±10 sccm (standard cubic centimeters) is maintained. Before passing into the holder, the air is passed through a bubbler heated to 30 ^{0}C to minimize the effects of humidity fluctuations. The samples are heated for 16 hours at 80 ^{0}C. UV-Vis absorbance was taken before and after the 16 hours of annealing. Because shifts in the peak maximum wavelength are not a good indicator of actual rates of etching, we determined the cadmium flux across unit surface area. By calculating flux we obtain size independent data that allows us to make an accurate comparison. To do this, we first obtain the total amount of cadmium atoms in a particle at a given time. First, the diameter of the particle is calculated by using the empirical fitting function[15] of the CdSe sizing curve, which is given by the equation below.

$$\text{CdSe: } D = (1.6122 \times 10^{-9})\lambda^4 - (2.6575 \times 10^{-6})\lambda^3 + (1.6242 \times 10^{-3})\lambda^2 - (0.4277)\lambda + (41.57)$$

where D (nm) is the size of a given nanocrystal sample and λ (nm) is the wavelength of the first excitation peak. Using the radius obtained in the above method we can the calculate the number

of cadmium atoms per particle (N_{Cd}/QD) using equation 3 in ref [103]: $N_{\mathrm{Cd/QD}} = \frac{4}{3}\pi a^3 \frac{2}{V_{\mathrm{unit}}}$, where a is the radius (nm) and V_{unit} is the volume of the unit cell containing two CdSe units. The bulk CdSe wurtzite unit cell is 112 Å^3.[16] The bulk volume as XRD studies have shown exhibited less than 0.5% lattice contraction for the QD unit cell compared with the bulk unit cell.[17] The number of particles in a given sample can be obtained by determining the concentration according to Beer's law and multiplying by Avogadro's number and the volume of our sample. Finally, the flux can be calculated by dividing the total number of cadmium atoms by the total surface area.

Computational Methods: Geometry optimizations were performed on the doped and undoped CdSe clusters using Density Functional Theory, as implemented in the ADF 2012.01 package.[105] The PBE exchange-correlation functional[106] and a triple-zeta polarized basis set with frozen core were used for all calculations. Scalar relativistic effects were included using the zeroth order regular approximation (ZORA).[107] Both gas phase and solvent calculations were performed. The solvent used is triethylamine and it is modeled as a continuum solvent with the COSMO model.[108] In COSMO, the solvent is modeled by a dielectric constant ε and a radius R. For triethylamine, ε=2.44 and Rad=3.81 Å. In order to investigate the effect of solvent size, radii of 2.5 and 4.0 Å are also investigated.

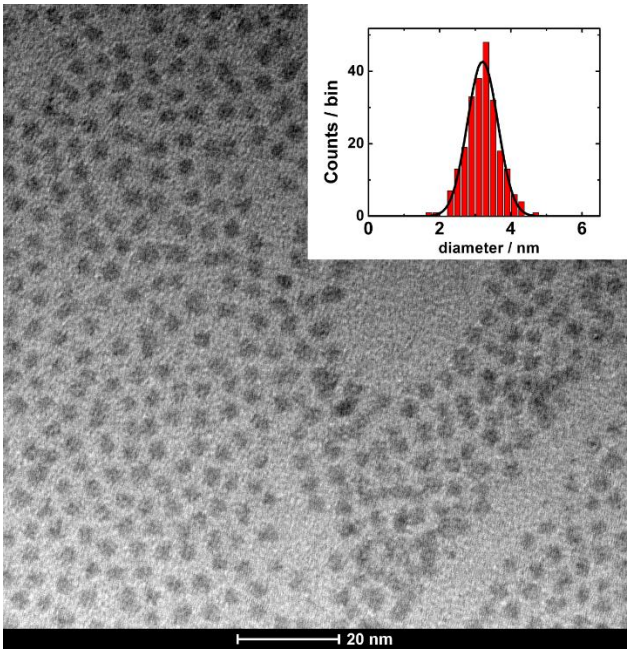

Figure 3.1[109] Low resolution TEM image of 4% gallium doped CdSe quantum dots. The inset indicates the size and size distribution of the dots. (Reprinted with permission from ref. 110. Copyright © 2015 American Chemical Society.)

3. Results and Discussions

In this work, gallium doped CdSe nanoparticles are obtained from a modified single precursor nanoparticle growth method.[26] TEM images of the 4% gallium doped particles (Figure 3.1) showed a relatively uniform shape and narrow normal size distribution, similar to that reported by Cumberland *et al*.[26] The HRTEM images (Figure 3.2) showed characteristic spacings of [100] plane from wurtzite structured CdSe crystals.

The presence of wurtzite structured CdSe was further confirmed by XRD analysis (Figure 3.3) where the characteristic (103) peak was identified, which is in accordance with statistical analysis of all spacings obtained from the diffractograms. The (012) spacings of the particles showed an increase when doped with gallium (Figure 3.3B), indicating possible lattice expansion as more dopants are introduced during the syntheses.

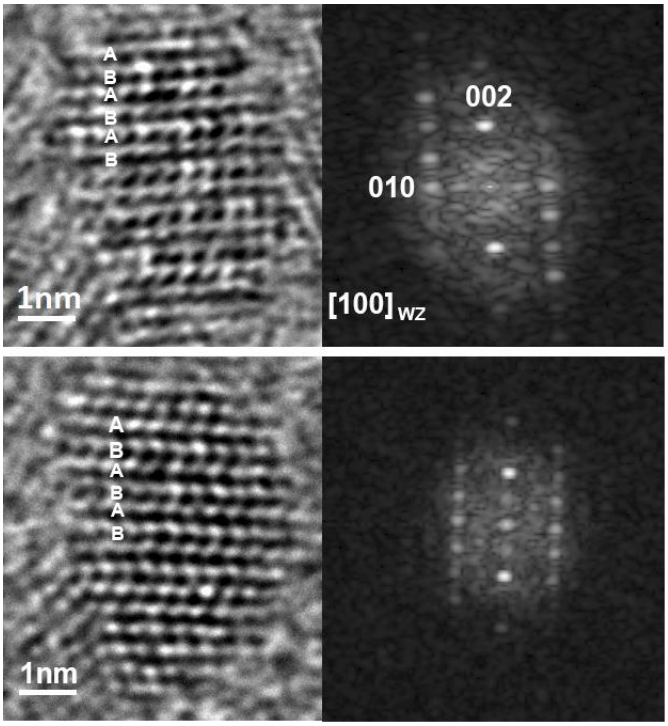

Figure 3.2 HRTEM image of 18% gallium doped CdSe dots indicating the wurtzite structure. (Reprinted with permission from ref. 110. Copyright © 2015 American Chemical Society.)

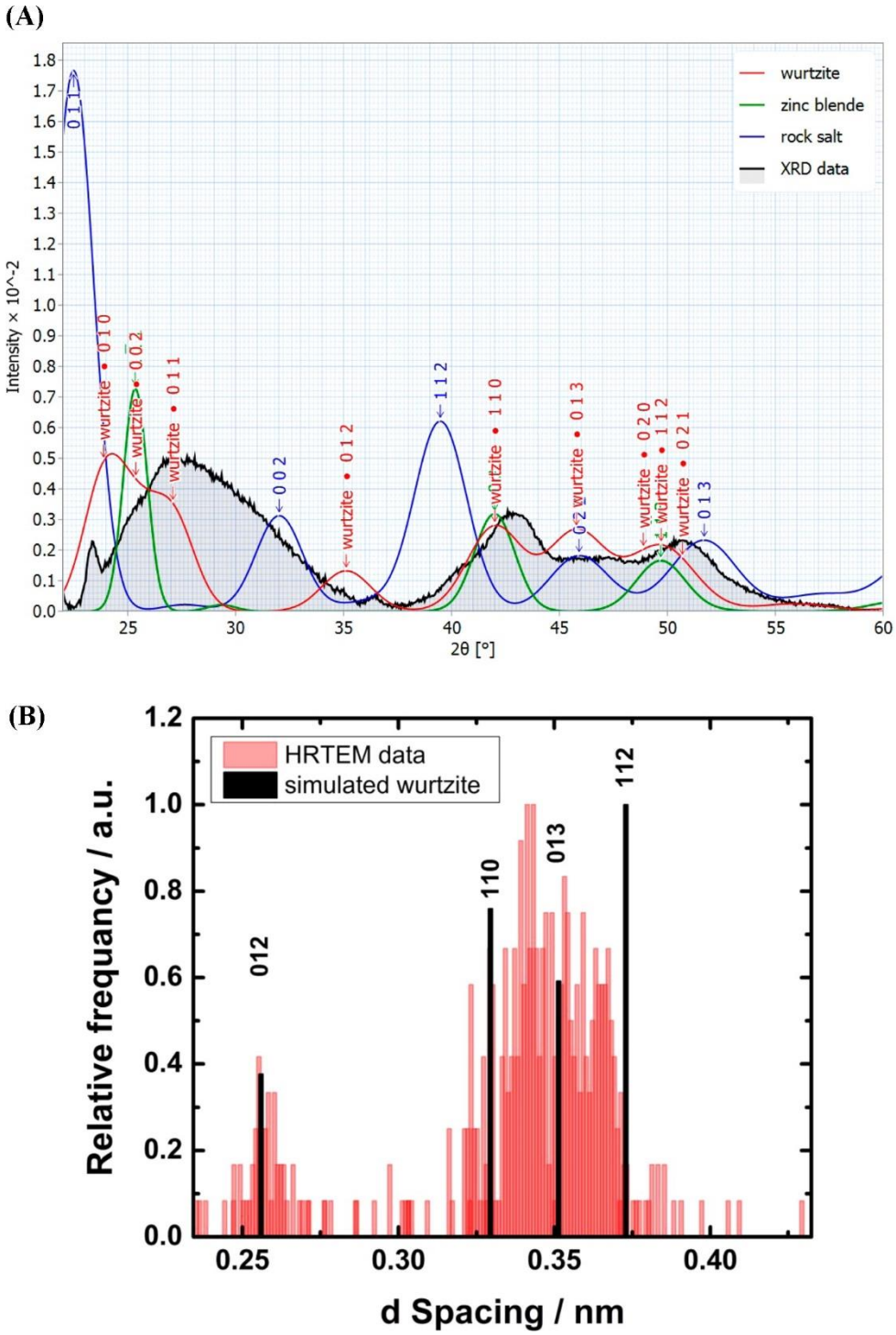

Figure 3.3 (A) Powder XRD of gallium-doped 5% CdSe quantum dots. The figure also contains the simulated CdSe XRD for wurtzite, zinc blende, and rock salt structures including size effect (4 nm) and lattice strain 1.5% lattice. (B) Histogram of lattice spacing determined from the HRTEM images of gallium-doped (2–18%) CdSe quantum dots. (Reprinted with permission from ref. 110. Copyright © 2015 American Chemical Society.)

Addition of an increasing amount of metal chloride to the quantum dot growth solution produced a nearly linear relation between the absorption maximum and the percentage of metal ion dopant (Figure 3.4). Particles doped with indium exhibited similar shifts in the absorption spectrum, but not with sodium (inset). It is plausible that during the early stages of crystallization, dopant ion exchange into the complex accelerates crystallization, producing larger particles, which gives rise to absorption of particles at longer wavelengths. As indicated in Figure 3.4, the atomic radii of the cadmium, gallium, indium and sodium are similar. The size of sodium atom (also shown in Figure 3.4) differs greatly from the cadmium atom, therefore no sodium exchange into the complex is expected resulting in little impact on the growth kinetics. How gallium and indium doping may produce the larger sized CdSe QDs is discussed below.

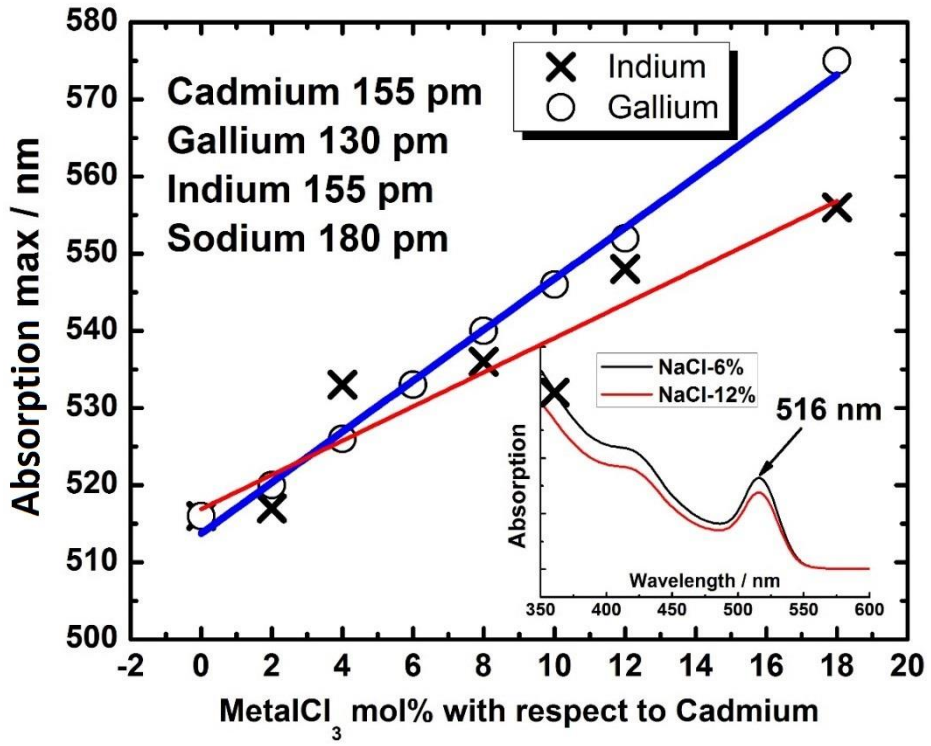

Figure 3.4 Impact of $InCl_3$ and $GaCl_3$ on the CdSe quantum dots synthesis. The final absorption peak maximum of the gallium- and indium-doped CdSe quantum dots produced from $Li_4[Cd_{10}Se_4(SPh)_{16}]$ complex. The inset shows that the addition of NaCl to the synthesis does not have any impact on the absorption wavelength of the CdSe QDs. The text inset shows the atomic radii of the metal ions relevant to this work in pms. (Reprinted with permission from ref. 110. Copyright © 2015 American Chemical Society.)

The original mechanism described by Cumberland *et al*.[26] has shown that a fragment of the $Li_4[Cd_{10}Se_4(SPh)_{16}]$ is held together during the quantum dot synthesis in HDA. These fragmented CdSe clusters aggregate to form larger CdSe quantum dots. This is in contrast to the CdSe hot injection synthesis in TOPO, which starts out with precursor molecules from basic constituents of CdSe. From the doping perspective, the TOPO synthesis contains organic phosponic acids that could inhibit the incorporation of transition metal dopants due to complexation.[110] In the presence of HDA, which is a weak organic base, this complexation is expected in a lesser amount. Previous work has shown that the HDA synthesis has been successfully utilized to produce various doped CdSe quantum dots.[97a] Previously, it has been found that tin and indium dopants accelerate the growth of quantum dots, resulting in larger particles. Here, the impact of the $GaCl_3$ is investigated on the final CdSe product following the synthesis. In these experiments, the amount of $Li_4[Cd_{10}Se_4(SPh)_{16}]$ is held constant while the relative amount of $GaCl_3$ is varied. The finite amount of complex used in the experiments also implies that the number of dots vs. their final size has a fixed relationship determined by the conservation of mass if all the precursor molecules are reacted. Figure 3.4 shows that the final size (bandgap in wavelength) exhibits a pseudo-linear relationship in the concentration regimes investigated. An increasing amount of $GaCl_3$ produces CdSe quantum dots where the bandgap is shifted to longer wavelengths. This red-shift is primarily associated with the size change and no significant band bending is observed. Figure 3.5 shows the bandgap variation of gallium doped (0-18%) CdSe quantum dots vs. the size determined from TEM analysis. The experimental sizing curve for wurtzite CdSe quantum dots is also shown.

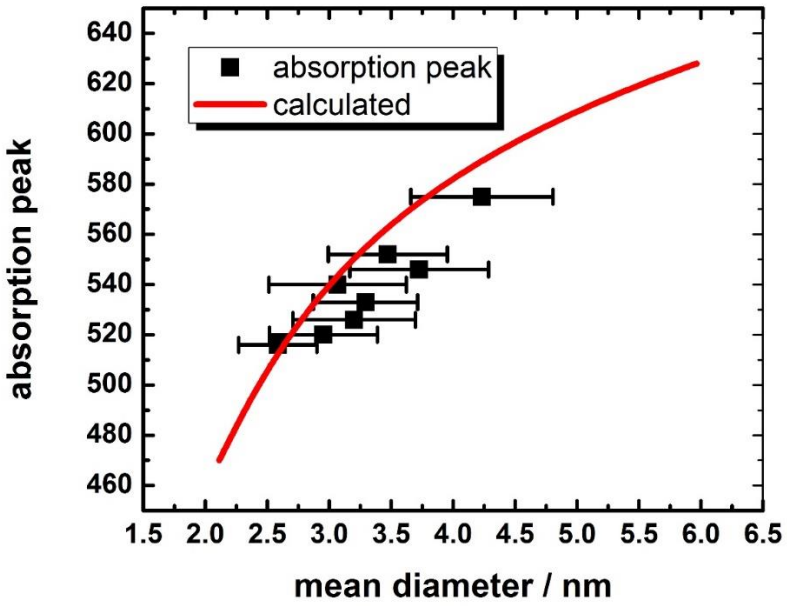

Figure 3.5 The absorption peak maximum position of gallium doped CdSe quantum dots (0-18% gallium content) with respect to the measured size of the dots. The error bar indicates the measurement error determined from TEM analysis. The red curve taken from literature is the calculated bandgap vs. size of wurtzite CdSe quantum dots. (Reprinted with permission from ref. 110. Copyright © 2015 American Chemical Society.)

Since the nucleation and growth are competing processes in this synthesis due to the finite amount of precursor available in the synthesis, the result of the $GaCl_3$ producing larger CdSe dots can be interpreted either as the effect of dopant on the nucleation reducing the barrier height for forming the initial nuclei or the impact of dopant on the growth of the particles. Previously, it has been observed that tin and indium chlorides enhanced the growth rate of the quantum dots under very similar synthetic conditions. Here, we think both nucleation and growth have been accelerated due to the impact of the presence of gallium chloride. We propose that the origin of the increased growth rate of the dots is via exchange of the metal ion to the $[Cd_{10}Se_4(SPh)_{16}]^{4-}$ complex by replacing the Cd^{2+} with a single or multiple Ga^{3+} ions. The resulting $Li_{4-x}Ga_xCd_{10-x}Se_4(SPh)_{16}]^{4-x}$ complex will lead to the decreased overall charge of the cadmium and selenium containing complex anion, leading to the increased relative reaction rate observed experimentally. Confirming this hypothesis, the addition of sodium chloride to the growth solution does not produce an observable change on the size of the CdSe quantum dots under these conditions (see Figure 3.4 inset). This is possibly because the size of sodium is significantly larger than gallium in comparison

to the cadmium in the $Li_4[Cd_{10}Se_4(SPh)_{16}]$ complex. In support of this hypothesis, the literature shows evidence of metal ion exchange into the analogues of $Li_4[Cd_{10}Se_4(SPh)_{16}]$ at relatively low temperatures.[111]

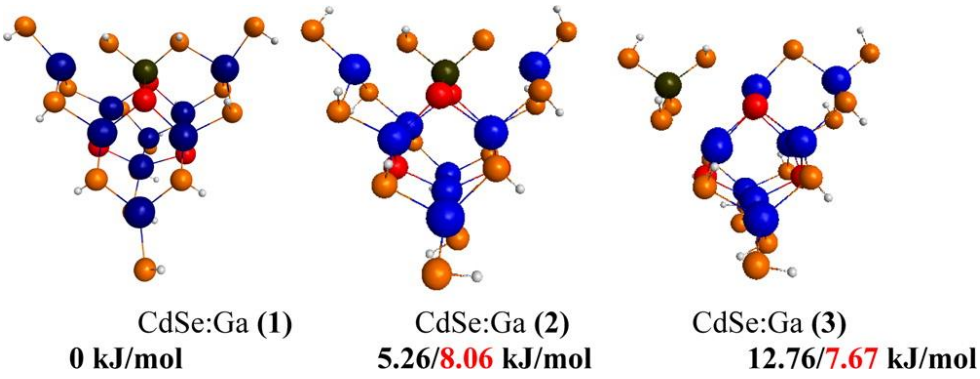

Figure 3.6 DFT optimized CdSe:Ga structures in the gas phase. The relative energies in black bold correspond to the optimized structures in the gas phase. The relative energies in red bold correspond to the optimized structures in triethylamine solvent. Structure 1 is the most energetically favorable. Color coding: blue = Cd, red = Se, orange = S, white = H, and dark green = Ga. (Reprinted with permission from ref. 110. Copyright © 2015 American Chemical Society.)

Our DFT calculations suggest that the gallium dopant could potentially be incorporated into the very core of the $Li_4[Cd_{10}Se_4(SPh)_{16}]$ complex, which would explain why the growth conditions can produce gallium doped CdSe quantum dots. The cadmium atom that is most likely to be replaced by the gallium is one of the core cadmium atoms in the complex, as also shown in Figure 3.6. In fact, the preferred doping position for Ga is one that coordinates to two Se atoms and two S atoms. On the other hand, coordination to four S atoms is highly unfavorable in the gas phase. It is interesting to see that complexes **(1)** and **(2)** are quite similar, with Ga coordinated to two Se atoms and two S atoms, yet complex **(2)** is higher in energy than **(1)**. One difference here is the *trans* arrangement of the hydrogen atoms coordinated to the two S atoms in **(2)** and the *cis* arrangement of these hydrogens in **(1)**. The Ga-Se bond lengths are both 2.42 Å for **(2)**. The Ga-Se bond lengths are 2.42 and 2.40 Å for **(1)**, which is quite similar. In addition, the Ga-S bond lengths for **(2)** are 2.41 Å whereas they are 2.40 and 2.39 Å for **(1)**. A slightly larger distortion occurs when one looks at the bond length between the sulfur atoms coordinated to the gallium and their adjacent cadmium atoms. In fact, for **(2)** these distances are 2.81 Å whereas for **(1)** they are 2.78 and 2.79 Å. We now compare the geometries of the undoped and doped complexes. Relevant bond distances are summarized in Table 2. For the undoped complex, the average Cd-Se distance is 2.70 Å (±0.01 Å). Upon gallium doping in **(2)**, the Ga-Se bond distance is 2.42 Å, which is

nearly 0.3 Å smaller than the corresponding Cd-Se bond length in the undoped complex. On the other hand, the average Cd-Se bond distance is 2.71 Å for **(2)**, similar to the undoped complex. For **(1)**, the Ga-Se distances and Cd-Se distances are similar to **(2)**. We label the position of the doping gallium atom in **(1)** D1 and the position of the Ga dopant in **(2)** D2. Due to symmetry, D1 and D2 have two nearly equivalent positions in the complex. The Cd-S distances at position D1 and its geometrical equivalent are 2.75 Å for the undoped complex with deviations smaller than 0.01 Å. For **(2)**, the Cd-S distances at position D1 and its geometrical equivalent are 2.70 Å on average, with deviations up to 0.02 Å. This value is 0.05 Å smaller than for the undoped complex. For **(1)**, the distance between the gallium at position D1 and the adjacent S atom is 2.40 Å on average. At the symmetrically equivalent position, the Cd-S distance is 2.72 Å on average, similar to the undoped complex and **(2)**. This yields an average metal-sulfur distance of 2.56 Å. Overall, gallium doping induces large distortions. At the D2 doping position and its symmetrical equivalent, the average Cd-S bond length for the undoped complex is 2.79 Å with deviation less than 0.01 Å. This value is 0.05 Å larger than the Cd-S length at the D1 position for this same complex. For **(2)**, the Ga-S distance at D2 is 2.41 Å whereas the Cd-Se distance at the symmetrically equivalent position is 2.75 Å. For **(1)**, the average Cd-S bond distance at D1 is 2.74 Å, which is 0.04 Å smaller than the undoped complex. For complex **(3)**, the average bond distances are very similar to the undoped complex but some bonds undergo very large distortions.

Table 2 Average bond lengths of the undoped CdSe complex and Ga-doped complexes in Å in the gas phase. M-S (M= Cd, Ga) bond at doping position D1 of (1) and D2 of (2) and their symmetrically equivalent position are averaged. (Reprinted with permission from ref. 110. Copyright © 2015 American Chemical Society.)

	CdSe Undoped complex	CdSe-Ga complex (1)	CdSe-Ga complex (2)	CdSe-Ga complex (3)
Cd-Se	2.70 (±0.01)	2.72 (±0.05)	2.71(±0.06)	2.69(±0.05)
Ga-Se	N/A	2.41 (±0.01)	2.42	N/A
M-S (D1)	2.75 (±0.01)	2.56 (±0.18)	2.70 (±0.02)	2.76 (±0.17)
M-S (D2)	2.79 (±0.01)	2.74 (±0.03)	2.58 (±0.17)	2.80 (±0.20)

The same complexes are optimized in triethylamine solvent. In this solvent, **(1)** is still the most stable complex. It is interesting to note that **(3)** becomes slightly lower in energy than **(2)** in triethylamine solvent, indicating that the solvent stabilizes this doping position. Also, **(2)** becomes much higher in energy than in the gas phase, indicating that the solvent destabilizes this doping position. Table 3 shows the relevant bond lengths of the undoped and three gallium-doped complexes. We can see that the bond distortions in **(3)** are smaller than in the gas phase. In order to investigate the influence of solvent molecule size, solvent molecule radii of 2.5 and 4.0 Å are investigated. The results are reported in Table 4. Regardless of the solvent radius, complex **(1)** remains by far the most energetically favorable. In case of a small solvent radius (Rad=2.5 Å), complexes **(2)** and **(3)** become similar in energy. For a solvent radius of 4.0 Å, **(2)** is 0.38 kJ/mol lower in energy than **(3)**. Note that for triethylamine which has a solvent radius of 3.81 Å, **(3)** is 0.39 kJ/mol lower in energy than **(2)**. Therefore, gallium doping is somewhat sensitive to the nature of the solvent.

Table 3 Average bond lengths of the undoped CdSe complex Ga-doped complexes in Å in triethylamine solvent. M-S (M= Cd, Ga) bond at doping position D1 of (1) and D2 of (2) and their symmetrically equivalent position are averaged. (Reprinted with permission from ref. 110. Copyright © 2015 American Chemical Society.)

	CdSe Undoped complex	CdSe-Ga complex **(1)**	CdSe-Ga complex **(2)**	CdSe-Ga complex **(3)**
Cd-Se	2.70 (±0.01)	2.71 (±0.05)	2.71 (±0.06)	2.69(±0.04)
Ga-Se	N/A	2.42 (±0.01)	2.42	N/A
M-S (D1)	2.74 (±0.02)	2.55 (±0.17)	2.70 (±0.03)	2.74 (±0.13)
M-S (D2)	2.77 (±0.01)	2.73 (±0.03)	2.57 (±0.17)	2.78 (±0.15)

Table 4 Relative energies of Ga-doped clusters in kJ/mol for different solvent radii with ε=2.44. (Reprinted with permission from ref. 110. Copyright © 2015 American Chemical Society.)

Complex	Solvent Rad=4.0	Solvent Rad=2.5

(1)	0	0
(2)	7.37	8.07
(3)	7.75	8.03

The gallium doped CdSe quantum dots are investigated with respect to the changes induced by the dopant. The replacement of the Cd^{2+} with a Ga^{3+} potentially produces an n-type material. In n-type material the Fermi level of the material is increased with respect to the intrinsic semiconductor. Previously, it has been found that due to quantum confinement these dopants may ionize at higher temperature compared to doping the same bulk semiconductor. Cyclic voltammetry is a valuable technique in characterizing the quantum dots because it can be used to find the band edge electronic states of the quantum dots including the defect states present.[112] Cyclic voltammetry is conveniently performed under mild experimental conditions and can be performed in solution.[113] One problem that must be taken into consideration is that the ligands on the quantum dots are extremely non-polar and will not dissolve in polar solvents; however, there are few non-polar solvents that are electrically conductive enough to effectively characterize the electrical properties of a sample. Therefore, the samples are dissolved in non-polar toluene and then mixed with polar N,N-dimethyl sulfoxide (DMSO) and a supporting electrolyte (Tetrabutylammonium perchlorate (TBAP)). Also, moisture, oxygen and CO_2 present in the air can interfere with potentiostat measurement; therefore, all reactions must take place in the inert atmosphere glovebox and all solvents used are anhydrous. According to the original paper, the bandgap will vary the electrochemical potential of both conduction band (CB) and valance band(VB); however, in the narrow size range we are investigating the CB and VB are roughly independent of size.

A key goal to achieve successful gallium doping is to increase the conductivity of QD films. This is demonstrated by measuring the current voltage characteristics of the QD films assembled from the purified doped and undoped QDs. Here, the gallium-doped and undoped CdSe QD film current voltage characteristics are presented along with the indium-doped CdSe QDs. The transport properties are sensitive to the type of ligand present on the surface of the CdSe QDs. The effect of ligand exchange, Ga- and In-dopants on the transport properties of doped CdSe films is demonstrated by the DC current density (J)–voltage (V) characteristics of

the electron-only devices. The CdSe-based electron-only device consists of Ag:self-assembled monolayer (SAM), CdSe, and Ag layers. The Ag:SAM layer blocks the hole injection to the CdSe. As shown in Figure 3.7, the treated electron-only device exhibits a strong enhancement of electron transport over the untreated device. In the treated device J decreases after EDT ligand exchange treatment, as shown in Figure 3.7. This result is again consistent with the fact that the ligand (EDT) exchange increases the electron transport in CdSe phase.

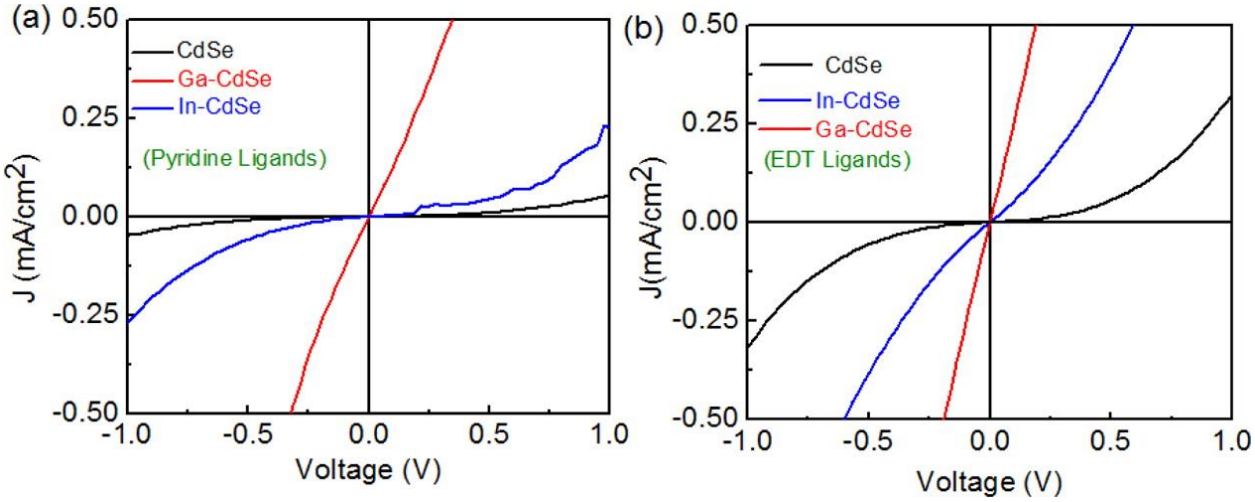

Figure 3.7 (a) J–V characteristics of an electron only doped CdSe (5% In–CdSe, 5% Ga–CdSe) device measured with incident light intensities from 100 mW/cm^2 AM 1.5 solar simulator using pyridine ligand exchange treatment. (b) J–V characteristics of an electron only CdSe device measured with incident light intensities from 100 mW/cm^2 AM 1.5 solar simulator after EDT ligand exchange treatment. (Reprinted with permission from ref. 110. Copyright © 2015 American Chemical Society.)

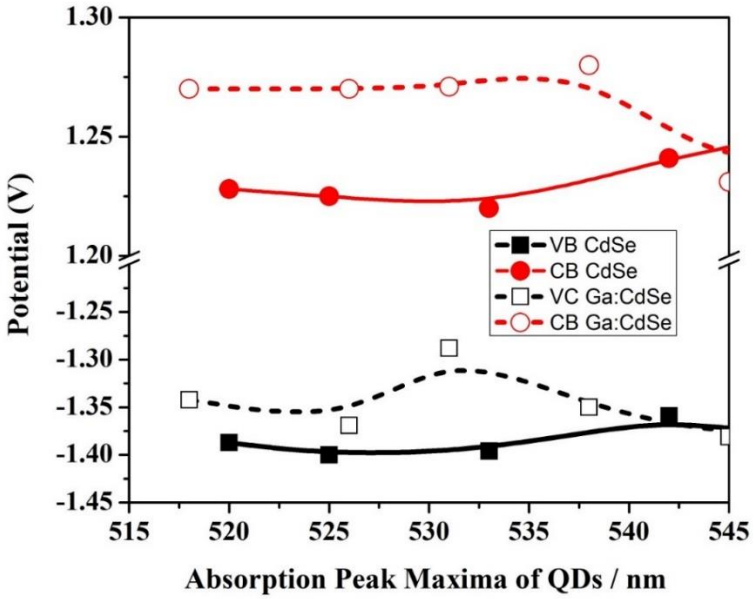

Figure 3.8 Cyclic voltametric measurements of the valance and conduction band of the CdSe quantum dot samples. (Reprinted with permission from ref. 110. Copyright © 2015 American Chemical Society.)

Here, undoped and doped CdSe QDs are grown with similar bandgaps to obtain accurate comparisons. From Figure 3.8 it appears that both the CB and VB of the gallium doped samples are consistently above the undoped CdSe quantum dots; however, the difference is small. It is thought that the introduction of n-type dopants will increase the Fermi level; therefore, this observation is consistent with the n-type nature of the CdSe dots upon gallium doping. The relatively small difference between the doped and undoped CdSe quantum dots is most likely due to the low ionization of the dopant at room temperature. We have attempted to obtain similar data at elevated temperature without success due to difficulty to stabilize temperatures above room temperature.

The increase of the Fermi level may be exhibited by the QD becoming a more effective reducing agent in redox reactions. This behavior is predicted by Guyot-Sionnest *et al*. in their early work.[114] In order to assess the difference between the reactivity of the undoped and doped dots in redox reactions, the dissolution kinetics of undoped CdSe compared to gallium doped CdSe is studied. The hypothesis is that after applying an oxidative etching method identical to the one developed by Li *et al*.,[115] the observed kinetics will be sensitive to the presence of dopant atoms introduced into the CdSe QDs. Specifically, it can be hypothesized that the introduction of 3+ ions

in place of Cd^{2+} will lead to more reducing quantum dots. In order to accurately compare the rates of removal of atoms from the different sized quantum dots, the flux of CdSe removal (# of CdSe units/surface area) across the unit surface area is calculated from the size changes. The results from etching experiments show a significant difference between doped and undoped systems. The flux of CdSe removal of tin-, indium-, and gallium-doped and undoped quantum dots is given in Figure 3.9. In addition to the gallium doped CdSe, indium and tin doped quantum dot are also prepared the data are also shown in Figure 3.9. Our results show gallium doped CdSe with the largest flux, followed by tin, and then indium, and with undoped having the lowest flux. When we compare this to calculations of activation energy levels an inverse trend is observed. The trend observed in the reactivity order of these differently doped CdSe Quantum dots is not surprising as gallium will much more readily donate electrons in comparison to tin or indium.

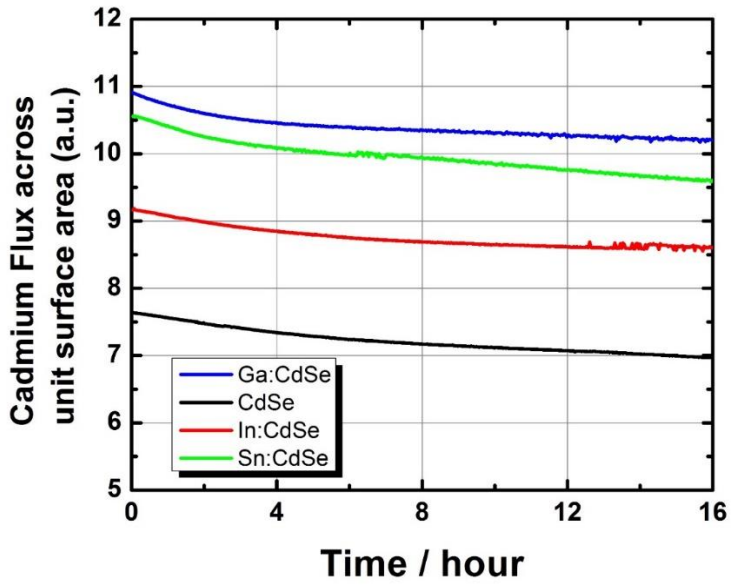

Figure 3.9 The relative rate of cadmium removal in various doped CdSe quantum dots. Each quantum dot is doped at 5%. (Reprinted with permission from ref. 110. Copyright © 2015 American Chemical Society.)

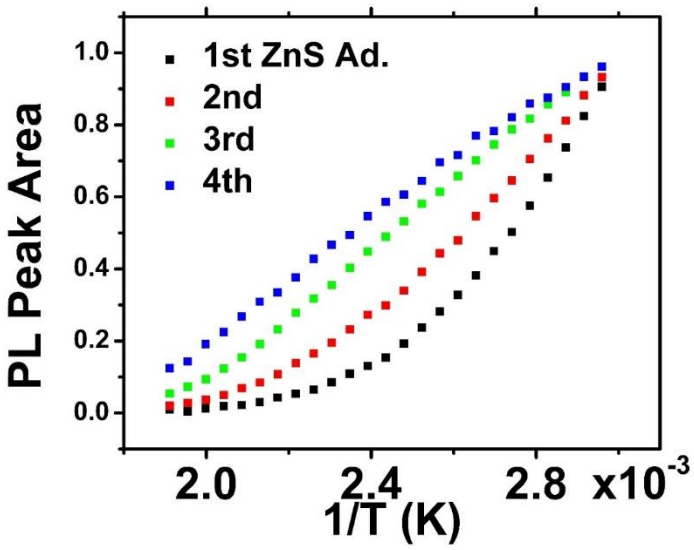

Figure 3.10 Photoluminescence vs 1/temperature of 2.5% gallium doped CdSe Quantum dots upon addition of more ZnS shell material. (Reprinted with permission from ref. 110. Copyright © 2015 American Chemical Society.)

In addition to the changes predicted by the chemical behavior of the doped quantum dots, doping has a significant impact on the photoluminescence properties of the quantum dots. In n-type semiconductors, the dopant atom will ionize followed by delocalization of the electron in the conduction band. In case of quantum confined systems, this delocalization is restricted to the discrete levels determined by the shape and size of the semiconductor. From the dopant ionization, the photoluminescence of the dots are quenched due to Auger type interaction of the delocalized electron with the excitation from photoexcitation. In doped quantum dots, the photoluminescence quenching is temperature dependent and it is related to the extent of ionization of the dopant (variation of the dopant levels with respect to the conduction band edge from non-uniform doping). In order to remove the temperature dependent quenching from surface defects, the gallium doped CdSe QDs is prepared with the addition of ZnS shell (type I core/shell structure). The completeness of the shell is monitored in situ during synthesis by temperature dependent photoluminescence quenching between 70 and 230 °C after injection of ZnS precursor material. Once the shell is complete, the temperature dependent photoluminescence becomes linear with the inverse temperature. This is the sample that is used for further characterization for both doped and undoped CdSe QDs. Figure 3.11 shows the Energy-dispersive X-ray spectroscopy (EDX) trace of ZnS

coated gallium doped CdSe QDs. The EDX trace confirms the presence of all the expected constituents of the material present in the material. The HRTEM image also shows the lattice fringes consistent with the presence of the ZnS shell.

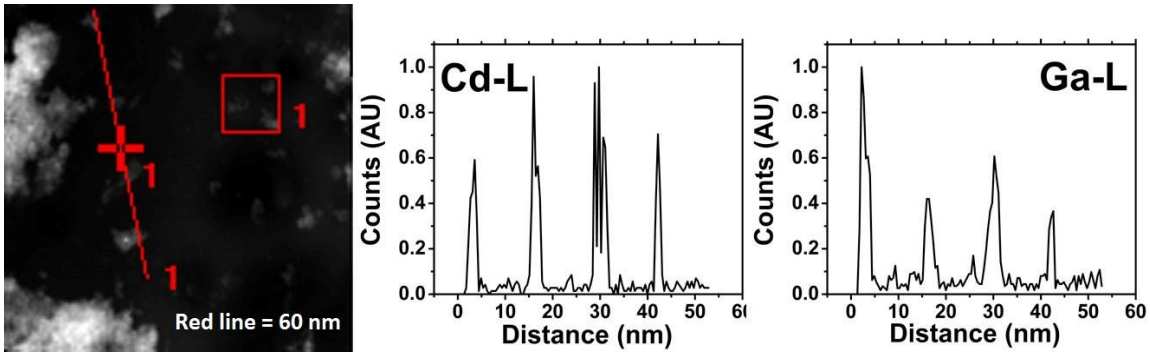

Figure 3.11 EDX line scan of 4 groups of gallium doped CdSe/ZnS core shell structures. The data clearly shows the presence of gallium and gallium together in the CdSe quantum dots. The EDX also confirms the Zn, S and Se atoms in these dots (not shown). (Reprinted with permission from ref. 110. Copyright © 2015 American Chemical Society.)

The temperature dependent photoluminescence of the ZnS coated gallium doped CdSe is investigated in the etching APOL solution, which is known to affect the surface of the dots resulting in strong variations in the photoluminescencewhen the ZnS shell is incomplete. However, we did not observe this variation during the time scale of the investigation; therefore, it is concluded that the variation of the photoluminescence is the result of the dopant ionization. The results are shown in Figure 3.12. The integrated photoluminescence of the QDs is plotted vs. inverse temperature and normalized to unity at 80 ºC. The error bar indicated the deviations over 5 subsequent measurements for both doped and undoped quantum dots. The results indicated the gallium doped dots have steeper temperature dependence in agreement with the expected dopant ionization. Since the difference is observable in the 20-80°C temperature range, we estimate that the dopant ionization is in the range of few tens of meV (room temperature would be ~25 meV). The temperature dependent time-resolved photoluminescence confirms this difference in that it shows a clear lifetime shortening of the bandedge emission (Figure 3.13). The solution based photoluminescence data provide information on how the ensemble average of the PL of the doped dots differs from the undoped QDs.

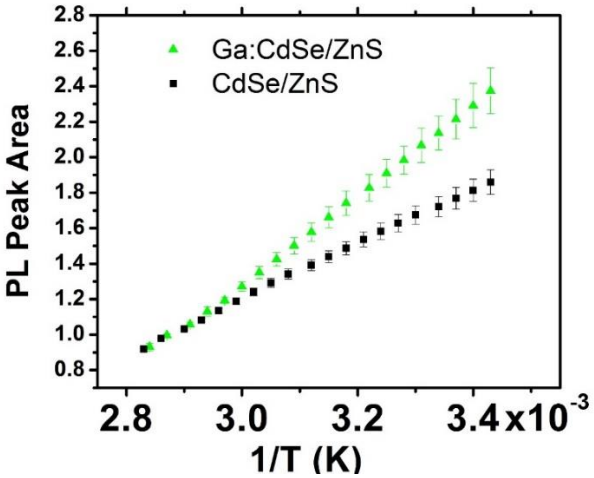

Figure 3.12 Temperature dependence of photoluminescence intensity of gallium doped and undoped CdSe/ZnS core shell quantum dots. (Reprinted with permission from ref. 110. Copyright © 2015 American Chemical Society.)

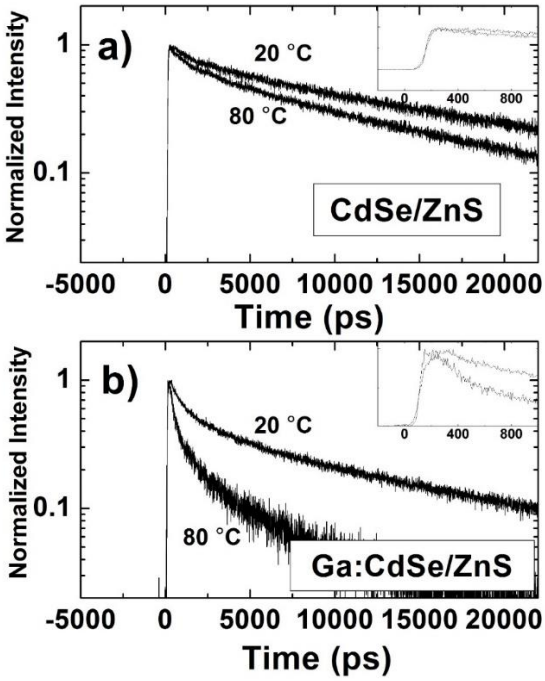

Figure 3.13 Photoluminesence lifetime of the bandedge emission of undoped and gallium doped CdSe/ZnS core shell quantum dots solution in APOL taken at room temperature and 80°C. (Reprinted with permission from ref. 110. Copyright © 2015 American Chemical Society.)

Bulk experimental measurements do not provide sufficient information about the variations of dopant from particle to particle. To investigate how dopant concentration may vary from particle-to-particle, single particle photoluminesence measurements of the gallium doped and undoped CdSe quantum are performed. All dots exhibit blinking behavior typical to CdSe QDs.[116] In these experiments, the QD blinking are investigated as a function of temperature to provide insight into how the ionized gallium dopant might affect the photoluminescence. The blinking statistics are fitted with a power law and the power law coefficient is investigated as a function of temperature. In Figure 3.14, the average height of the blinking is measured at the same excitation power levels, which shows the height of the blinking steps is smaller for the doped QDs. The smaller step size is indicative that the doped dots are less emissive due to the presence of the dopant levels, which provide recombination sites for the excitons generated in the material. In addition, the power law coefficient of the doped QDs appears much larger (shorter on-time) than the undoped CdSe QDs. This shorter on-time suggests that the dopant promotes the dynamical pathways that lead to the dark excitonic state of CdSe.[117] The power law coefficient of the doped QD also exhibit somewhat stronger temperature dependence as expected from the dopant ionization. Interestingly, the off-time power law is not influenced by the presence of the doped QDs.

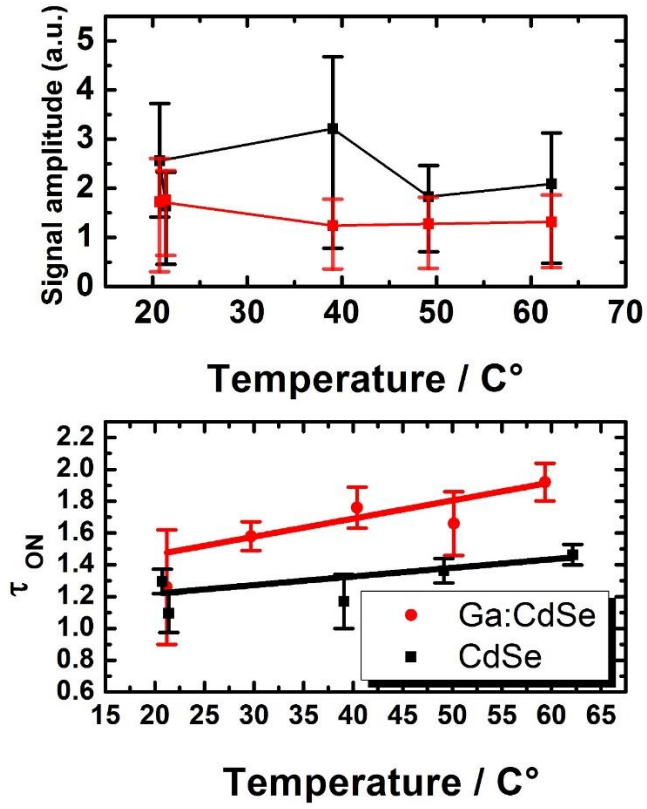

Figure 3.14 UPPER Amplitude of the fluorescence blinking of the gallium doped and undoped CdSe quantum dots at various temperatures. LOWER The change of the power law coefficient (τ_{ON}) of the blinking of the gallium doped and undoped CdSe/ZnS core shell structures as function of temperature. In both figures, the error bar represents the variation of the signal from particle to particle determined as standard deviation. (Reprinted with permission from ref. 110. Copyright © 2015 American Chemical Society.)

4. Conclusions

In this work, the preparation and characterization of gallium doped CdSe quantum dots are reported. The gallium induces important chemical, electrochemical and spectroscopic changes in the quantum dots that are consistent with n-type behavior of a semiconductor. The gallium doping of CdSe quantum dots might be an effective way to manipulate the electrical properties of quantum dot films and solar cells at near room temperature.

Chapter 4 - Indium and Gallium Doped CdSe Quantum Dot for Hybrid Solar Cell

1. Introduction

The so called 3rd generation solar cells have been the interest of the scientific community with a promise of providing cheap and efficient photovoltaic devices.[118] One of the 3rd generation solar cell concepts depends on a combination of inorganic and organic photosensitizers.[119] The inorganic components can consist of quantum confined semiconductor structures[118c, 120] (nanoparticle, nanorod, tetrapods) that are synthesized via colloidal route combined with conductive polymers such as P3HT.[121] Varying the composition, size and shape of the inorganic component these photovoltaic cells allows capturing and utilizing photons from different parts from the solar output. While these solar cells are proven to be functional, it is difficult to manufacture them with high overall power conversion efficiencies; therefore, research needs to focus on concepts that can identify components that are responsible for the lack of improvements.

Among the quantum dot (QD) materials, CdSe QDs received significant attention in this quest of producing efficient solar cells. Although CdSe is not a sustainable material, it provides a platform to study many different effects associated with the construction of polymer/inorganic solar cells.[118c] In addition, the bandgap of colloidal CdSe QDs (2.6-1.7 eV) overlaps reasonably well with the solar output to capture large portion of the sunlight's energy. There are several reports that show P3HT/CdSe QDs solar cells provide somewhat efficient power conversion efficiencies in the few percent range.[120, 122] Recently, Zhou *et al*. have reached 5.3% record power conversion efficiency in PCPDTBT: CdSe device as a result of removal of trap sites upon the ethanedithiol treatment.[123] Dixit el al. have shown that doping the CdSe/P3HT hybrid solar cell with carbon nantubes can lead to significant enhancement in power conversion efficiency. They have argued that the carbon nanotubes quickly transport the photo-generated electrons to the electrodes resulting in the power conversion efficiency of 5.4%.[124] Theory and experiments

suggests that at higher temperatures the charge transport is governed by space charge limited conduction influenced by traps.[125] Parisi *et al*.[122h] have found that amine modification of the surface of the CdSe QDs show significant impact on the solar cell performance. By attaching butylamine to the CdSe surface, they have achieved 2.0% power conversion efficiency. Mathur *et al*.[122b] have shown the surface of CdSe modified by addition of ZnS leading to 5.1% power conversion efficiency under non-standard illumination conditions. Parisi *et al*.[122n] even manipulated the ratio of Cd to Se resulting in variations in the conversion efficiencies of this type of solar cell. Their results have shown that excess amount of cadmium with respect to selenium could be favorable to produce efficient solar cells.

From these previous observations, it is clear that uncontrolled and controlled defects in CdSe influence solar energy performance significantly in the CdSe/P3HT photovoltaic device. Here, the effect of chemical doping (controlled introduction of defects) of CdSe QDs on the performance characteristics of bilayer CdSe/P3HT solar cells is investigated. In general, the process of doping has been instrumental in first generation solar cells to achieve the high efficiency of the silicon p-n junctions. Similar expectations can be raised towards doping QDs to improve the efficiency of these types of solar cells. Doping QDs during colloidal growth is difficult[90, 126] due to the limited understanding of the chemical steps involved during growth, self-purification of doped QDs[17] and the highly statistical nature of the doping process.[126a] CdSe has been doped successfully for the purpose of creating magnetic dilute semiconductors[126b, 127] or providing efficient energy transfer from QDs to dopant levels.[128] Early on, Guyot-Sionnest *et al*. have pointed out that the bottleneck of the widespread application of QDs is the improvement of their electrical conductivity. Their work addressed this via electrochemical doping of CdSe QDs.[82] Electrical doping of CdSe QDs through chemical means has also been investigated by introducing tin and indium into the CdSe QDs.[95] Photoluminescence quenching experiments show that the doped QDs exhibit increased temperature dependence due to the ionization of the dopant levels to the $1S_e$ level that turn the CdSe QD into a more n-type.[82] Here we expect to see that the doping will impact both the trap states in the composite solar cells and the mobility of the major and minority carriers. In agreement with the previous temperature dependent measurements, the photovoltaic devices constructed in this work show inverted behavior that potentially opens up ways to utilize the solar cells more efficiently combining them with solar concentrators.

2. Experimental Section

Chemicals: All chemicals are used as purchased with the exception of hexadecylamine, which is vacuum distilled at 2 torr. $InCl_3$, $SnCl_2$, $GaCl_3$, diethylzinc, hexamethyldisilithiane and tri-n-octyl phosphine (TOP) are all stored in an inert atmosphere/low water vapor concentration glovebox. Tri-n-octylphosphine oxide (TOPO) and 2-amino-propanol (APOL) are used as purchased and stored under ambient conditions.

Synthesis: Doped and undoped CdSe core particles are synthesized using the $Li_4[Cd_{10}Se_4(SPh)_{16}]$ single source precursor (SSP) prepared as reported by Cumberland[26] in hexadecylamine with metal chloride as the doping agent. Briefly, 50 g of distilled hexadecylamine and 0.6 g of the (SSP) are loaded into a three-neck flask and passed into a glovebox where the appropriate amount of metal chloride (gallium, tin, indium) is added. All dopant load percentages are based on the total cadmium content of the reaction. The reaction flask is purged on an Ar gas line for 20 minutes before being very slowly heated to 70 °C with careful attention made to minimize temperature overshoot, as the stability of the magic sized nanocluster is extremely sensitive to temperature. At this time the flask is then heated from 70 ^oC to 225 ^oC at the rate of 1 ^oC per minute. The flask is then cooled to 180 ^oC and annealed for 18 hours to decrease the size distribution.

Ligand exchange of undoped and doped CdSe QDs: Before being incorporated into P3HT polymer to form P3HT/CdSe hybrid blends, undoped and doped CdSe QDs with HDA capping ligands were treated by hexanoic acid-assisted washing procedure. Typically, 2 mL as-synthesized QDs were added to 10 mL hexanoic acid at 110 °C and stirred for 30 min. 20 mL anhydrous methanol was added and stirred to precipitate QDs, which were later recovered by the centrifugation. Then 1.5 mL chloroform and 4.5 mL methanol were added to precipitate the QDs again. After being recovered by centrifugation, QDs were finally dispersed into anhydrous 1,2-dichlorobenzene (1,2-DCB) at a concentration of about 30 mg/ml, showing a very good solubility.

Assembly and performance measurement of undoped and doped CdSe QD/P3HT photovoltaic devices: The whole photovoltaic device structure consists of the following sequence of films and thicknesses: ITO/poly(3,4-ethylenedioxythiophene):poly(styrenesulfonate) (PEDOT:PSS)(40 nm)/ P3HT: CdSe (120 nm)/Al (100 nm).[129] PEDOT:PSS (Baytron PVP CH 8000) is spin cast onto a 0.5 × 0.5 in2 glass substrate with pre-patterned ITO electrodes. The PEDOT: PSS is useful as a hole transport and smooths the surface of ITO. The P3HT in 1,2-DCB solution with different ratio concentrations were blended with undoped and doped CdSe QDs in

1,2-DCB solution. The blended solution is spun at 1000 rpm, dipped in 0.002 M EDT solution for 30 s, and exposed to solvent annealing overnight. The coated device was annealed at 175 °C for 10 min, and then quickly cooled to room temperature. The 10 nm thick Ca layer was evaporated at a rate of 0.1 nm/s as exciton blocking layer, which is followed by top contact Al layer. The top Al contact was evaporated through a shadow mask to generate an array of patterned electrodes. The final device area was defined by the overlap between the top and bottom electrodes. Current-voltage (J-V) characteristics of the finished devices are measured in a nitrogen atmosphere glovebox with a source-meter (Keithley 6487). The light response was measured under illumination from a 100mW/cm^2 AM1.5 solar simulator. Transmittance and absorbance spectra of the device active layer were measured with a Cary 5000 UV-Vis-NIR dual-beam spectrophotometer. Photoluminescence was performed on a Cary Eclipse fluorescence spectrometer equipped with a xenon flashlamp.

Structural characterization: A FEI FEG analytical electron microscope operated at 200 kV was used for transmission electron microscopy (TEM). Elemental mapping was performed using energy-dispersive X-ray spectroscopy (EDS) in conjunction with a TEM operating in STEM mode.

Structure and chemical characterization of doped CdSe QDs: The selective area electron diffraction pattern (SAED) and EDX spectra in Figure 4.1 obtained from Sn doped CdSe QDs confirmed the chemical composition and Sn dopants (40.0%). The EDX spectrum from the Ga-doped CdSe QDs (Figure 4.2b) shows Ga contents (5.5 at%), within the CdSe matrix. The EDX spectrum from the In-doped CdSe QDs (Figure 4.2d), shows a In composition (6.3 at%). The high concentration of the tin in the CdSe suggest alloy formation due to the preferential incorporation of the tin during syntheses. This has been observed previously with the same doping procedure. The dopant concentration affects the charge carrier density and mobility as shown in the discussion below.

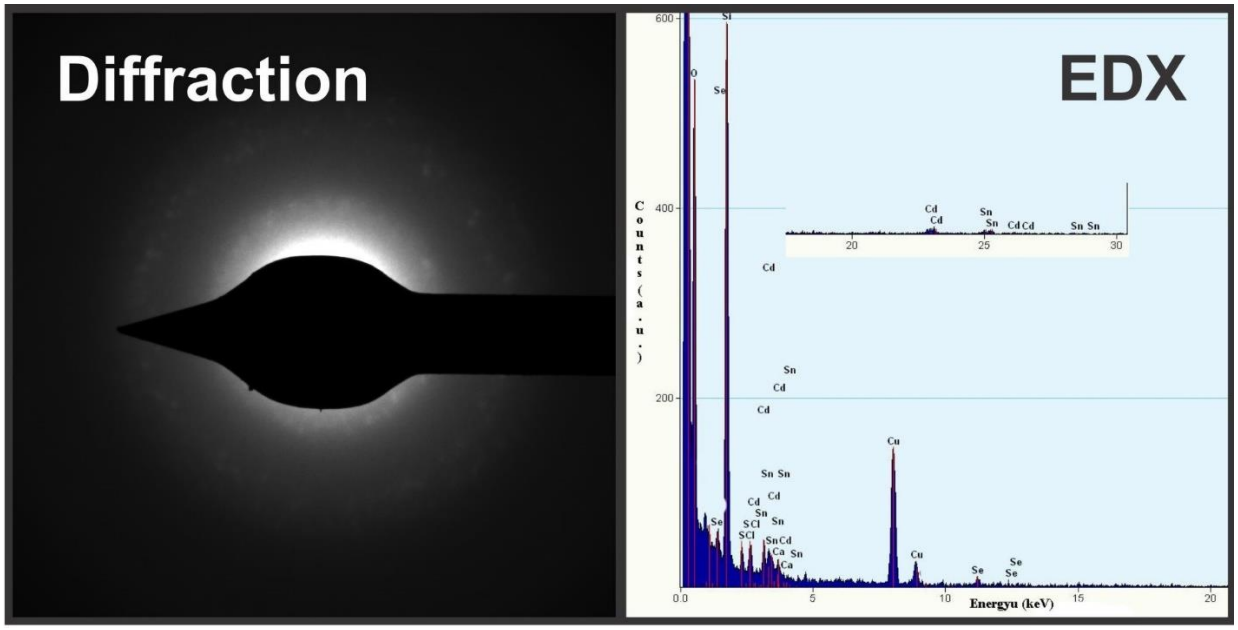

Figure 4.1[130] The selective area electron diffraction pattern (SAED) and EDX images of Sn doped CdSe QDs. (Reprinted with permission from ref. 131. Copyright © 2015 Electrochemical Society.)

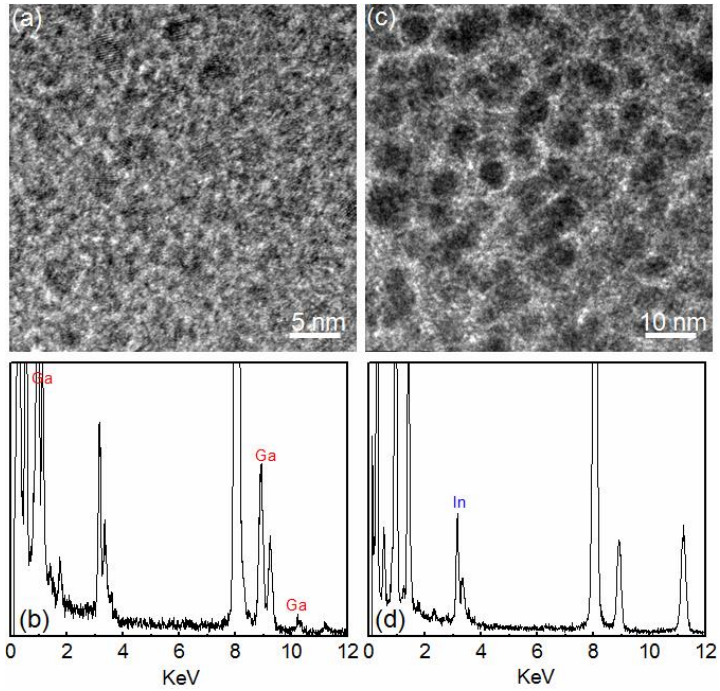

Figure 4.2 (a) and (b) TEM and EDX images of Ga doped CdSe QDs. (c) and (d) TEM and EDX images of In doped CdSe QDs. (Reprinted with permission from ref. 131. Copyright © 2015 Electrochemical Society.)

***J-V* Characterization of electron-only CdSe Schottky devices:** The effect of ligand exchange, Ga-, In- and Sn-dopants on the transport properties of doped CdSe films was demonstrated by the DC current density (*J*)–voltage (*V*) characteristics of the electron-only (Figure 4.3a) devices. The CdSe-based electron-only device consisted of Ag:self-assembled monolayer (SAM), CdSe, and Ag layers. The Ag:SAM layer blocks the hole injection to the CdSe. As shown in Figure 4.3a, the treated electron-only device shows a strong enhancement of electron transport over the untreated device. As shown in Figure 4.3a and Figure 4.3b, the treated device showed a decrease in *J* after EDT ligand exchange treatment. This result is again consistent with the fact that the ligand (EDT) exchange increases the electron transport in CdSe phase.

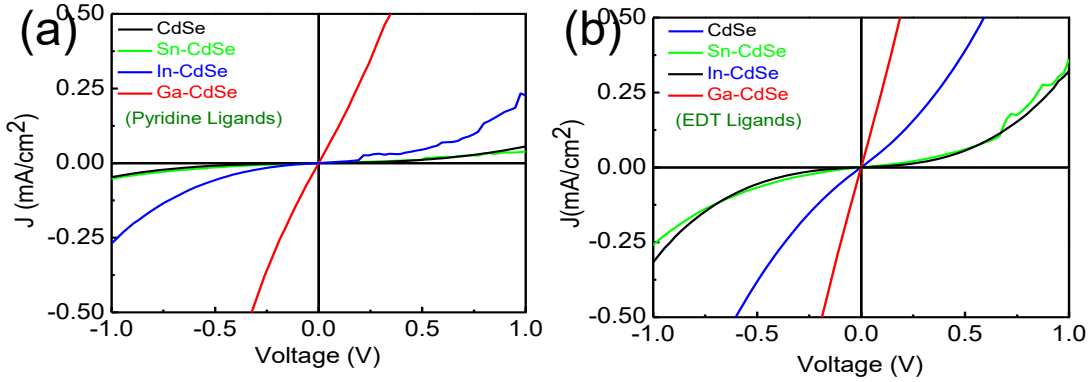

Figure 4.3 (a) J-V characteristicss of an electron only doped CdSe device measured with incident light intensities from 100 mW/cm^2 AM 1.5 solar simulator using pyridine ligand exchange treatment. (b) *J-V* characteristics of an electron only CdSe device measured with incident light intensities from 100 mW/cm^2 AM 1.5 solar simulator after EDT ligand exchange treatment. (Reprinted with permission from ref. 131. Copyright © 2015 Electrochemical Society.)

3. Results and Discussions

The QDs used to construct the photovoltaic cell consist of indium, tin and gallium doped crystalline CdSe. These dopants have been reported in the literature to increase the electrical conductivity of bulk CdSe.[131] Literature suggests that CdSe can be doped to increase the concentration of the electron carriers (n-type), however, recent reports by Norris *et al.* also show that CdSe QDs can be made p-type as well.[98] Here the purpose of doping CdSe QDs is to increase the n-type of carrier in hybrid CdSe/P3HT solar cell to achieve increased performance.

As a representative example, the low and high resolution transmission electron microscopy image shows narrow size distribution (<5%) and wurtzite structure of the gallium doped CdSe in Figure 4.4. The CdSe QDs are grown from a single precursor $Li_4[Cd_{10}Se_4(SPh)_{16}]$ developed by Yun *et al*.[26] The gallium, indium and tin dopant is introduced into the hexadecylamine solution prior to the growth of CdSe QDs. The quantum dots are grown via a temperature program from 70 ºC to 225 ºC at the rate of 1 ºC per minute followed by an annealing step at 180 °C for 18 hours.

The dopant atoms introduced into the growth solution are similar in size to the cadmium atoms except the gallium most likely resulting in a substitutional doping. Gallium (atomic radius=130 pm; ionic radius 76 pm) is significantly smaller than the cadmium (atomic radius=155pm; ionic radius=109pm), which suggest that the doping mechanism is either interstitial or facilitated by the lattice contraction in these nanoparticles. The concentration of the dopant probably follows the poissonian distribution and proportional to the volume of the particles.[12] For the doped QDs, the surface to volume ratio is relatively small; therefore, it is likely that the probability of finding the dopant atoms inside the QDs is greater than on the surface. Previous studies have shown that etching the surface of CdSe QDs from the single precursor synthesis did not change significantly the measured dopant concentration.[95b] Based on the elemental analysis (see supporting information), the tin doped QDs exhibit preferential incorporation of the dopant into the CdSe QDs forming an alloy of cadmium and tin with selenium.[95a] This can be due to the relatively large difference in the bind energy between cadmium selenide (310 kJ/mol) and tin selenide (410 kJ/mol) compared to indium selenide (247 kJ/mol).

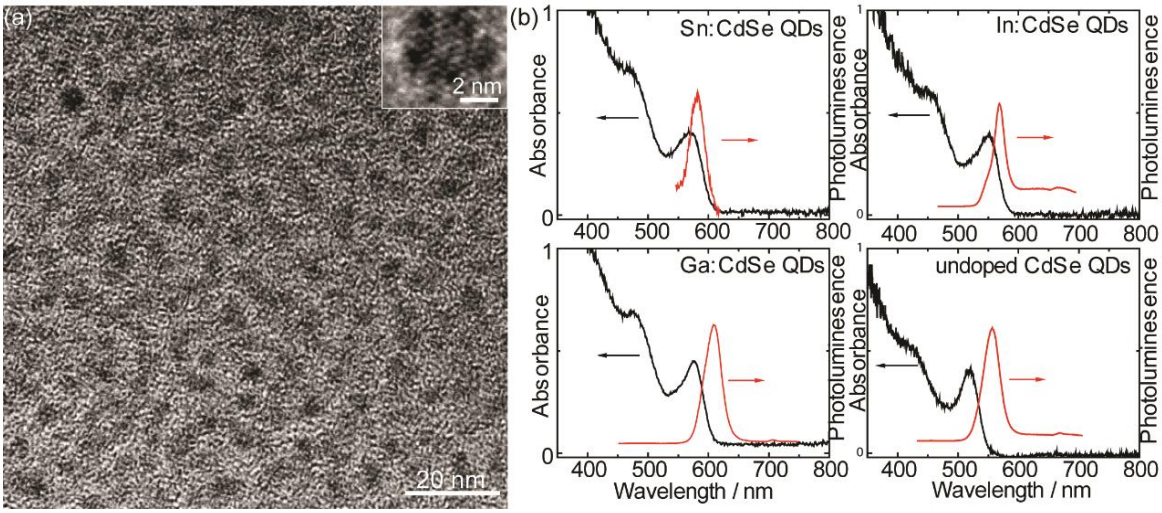

Figure 4.4 The TEM image of Ga-doped CdSe QDs. (b) The absorption and photoluminescence spectra of doped CdSe QDs. (Reprinted with permission from ref. 131. Copyright © 2015 Electrochemical Society.)

The construction of the P3HT/CdSe hybrid cell follows the preparation method described previously in the literature.[129] Figure 4.5a shows the schematic diagram of doped CdSe/P3HT hybrid solar cells discussed in this work. The ITO (indium tin-oxide) electrode is coated with PEDOT:PSS, which acts as the anode buffer layer. Different doped CdSe QDs are used in conjunction with P3HT to create the type-II heterojunction. Flat-band alignment of the prepared hybrid solar cell is shown in Figure 4.5b. The doped CdSe QDs do not interact with the P3HT in the dichlorobenzene solution, however when the solvent is evaporated the photoluminescence of the P3HT is strongly quenched. The corresponding excitation spectra of the luminescence at 400 nm of Ga-doped CdSe/P3HT in the solution and thin film form led to features that are in excellent agreement with the ground-state absorption features including a band gap onset at 600 nm (Ga-doped CdSe QDs), shown in Figure 4.5c. The underlying quenching mechanism is in line with the fact that now the charge transfer within the CdSe/P3HT hybrid system dominates.

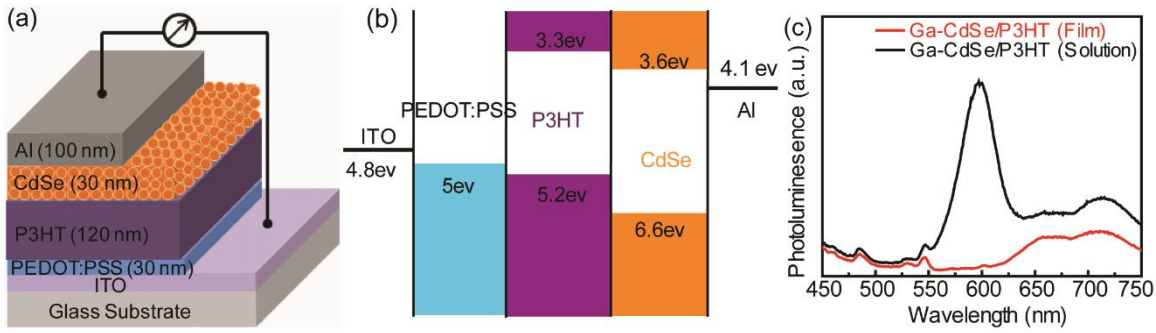

Figure 4.5 (a) The schematic image of doped CdSe/P3HT hybrid bi-layer solar cells. (b) The flat band diagram of type-II heterojunctions. (c) The photoluminescence spectra of Ga-doped CdSe/P3HT in solution and thin film form. (Reprinted with permission from ref. 131. Copyright © 2015 Electrochemical Society.)

As mentioned before, the electron mobility and charge carrier density depends on the dopant of the CdSe QDs. Therefore, the photovoltaic performance dependence on the doped CdSe is investigated. The current density/voltage characteristics of the photovoltaic cell are shown in Figure 4.6. Figure 4.6a shows the solar cell performance with different doped CdSe QDs layered with P3HT donor material. The current density of the cells significantly varies with doping. The lowest current density and open circuit voltage is observed in the case of photovoltaic cell constructed from undoped CdSe QDs. The cell constructed from tin-doped CdSe QDs exhibit very similar behavior to the undoped CdSe QDs. The performance of the gallium doped and indium doped samples exhibit appreciable performance increase in both open circuit voltage (Voc) and short circuit current density (Jsc). In case of Ga-doped CdSe/P3HT PV devices, the photocurrent increases from 1.6 mA/cm^2 to 6 mA/cm^2 compared to solar cells without dopant, which is about four fold increase. The Ga-doped CdSe/P3HT solar cell produces a power conversion efficiency of 1.2% under AM 1.5 (100 mW/cm^2) solar illumination, which is approximately six times more compared to that undoped CdSe/P3HT cells (0.2% power conversion efficiency). This demonstrates that the doped CdSe QDs induced mobility and charge carrier density enhancement in QD solar cells can be used to effectively improve the photocurrent and photovoltage. The photoabsorption of the doped samples is slightly red shifted, in comparison to undoped CdSe QDs. The calculated change (bandgap shift and absorption cross section change) accounts for a maximum factor of 1.5 fold increase in performance. The observed increase in solar cell performance is almost 10 fold, therefore the size effect is not likely the major component of the observed difference for the photovoltaic cells between the

doped and undoped CdSe QDs. To verify that the photocurrent is the result of the absorption of both the P3HT and the doped CdSe, the external quantum efficiency of the device is plotted against the absorption spectrum of the photovoltaic cell in Figure 4.6b. The photocurrent contribution is from the absorption of the P3HT and the CdSe QDs.

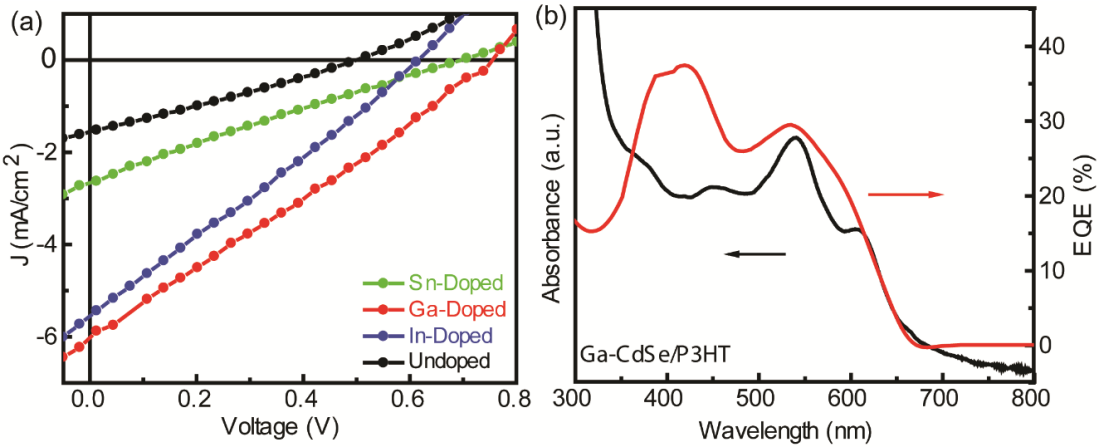

Figure 4.6 (a) The photovoltaic current density- voltage (J-V) characteristics of doped CdSe/P3HT hybrid bi-layer solar cells. (b) The photoabsorption (black curve) and external quantum efficiency (EQE, red curve) spectra of Ga-doped CdSe/P3HT bilayer solar cell. (Reprinted with permission from ref. 131. Copyright © 2015 Electrochemical Society.)

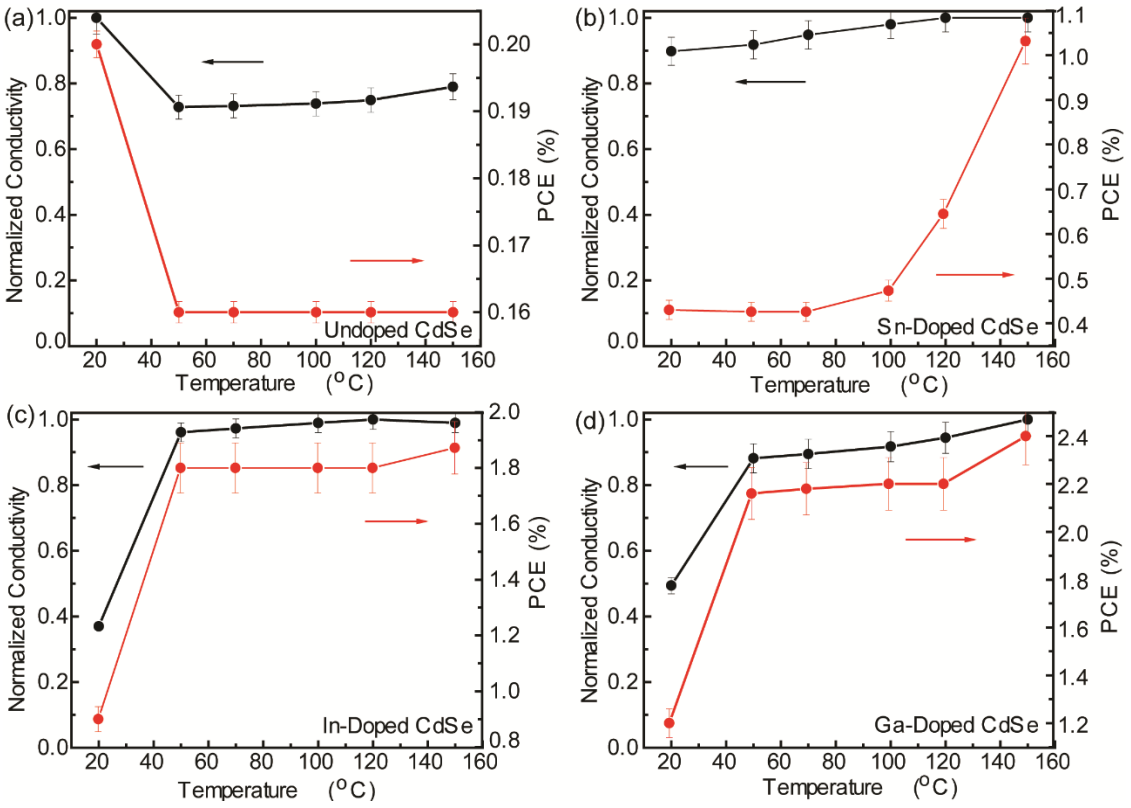

Figure 4.7 (a), (b), (c) and (d) The normalized electron conductivity of doped CdSe quantum dot (black curves) and doped CdSe/P3HT hybrid solar cell power conversion efficiency (PCE, red curves), undoped, Sn-doped, In-doped and Ga-doped CdSe shown respectively. Error bars represent the standard deviation. (Reprinted with permission from ref. 131. Copyright © 2015 Electrochemical Society.)

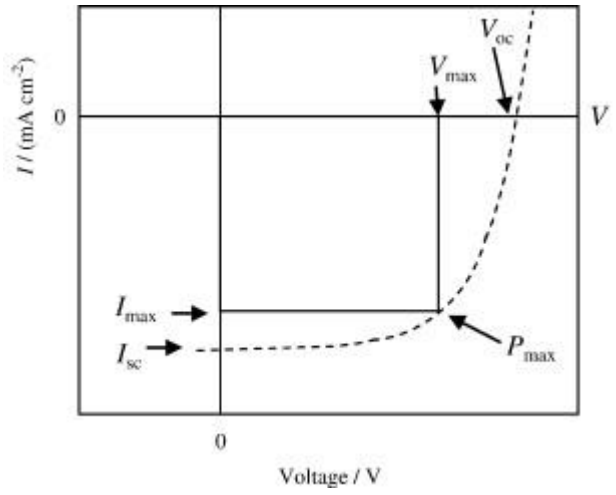

Figure 4.8[122j] Ideal current-voltage curve of a photovoltaic device. Max: maximum; oc: open circuit; sc: short circuit. (Reprinted with permission from ref. 123j. Copyright © 2008 Elsevier B.V.)

Although this study deals primarily with the effects of doping on the carrier density and conductivity, it is nevertheless important to discuss potential methods of optimization of its power conversion efficiency. As demonstrated in Figure 4.8, the power output of a photovoltaic device under illumination can be expressed as $P = IV$, where I is the current and V is the voltage. The power output is then represented as the area of the square formed by any point on the current-voltage curve and the x- and y-axis. Maximum power is achieved when this area is greatest, as noted by P_{max}. Our device showed acceptable open circuit and short circuit currents, which are important conditions for achieving high power output, but lacks in that the current-voltage curve is almost linear. Improvements and tuning could be made so that the curve is more square-like. Efforts such as identifying possible leakage of current at the edges of the device[122j], and direction of current flow through the layers of the device should be made to address this issue in further studies.

Upon doping, traditional bulk semiconductors exhibit strong temperature dependent photoconductivity and power conversion efficiency due to the mobility change and the ionization of the dopants. To characterize the changes in doped CdSe QD conductivity upon thermal annealing, Schottky devices are prepared. The photovoltaic cells that contain doped QDs exhibit this strong temperature dependent behavior in their photoconductivity (Figure 4.7) and power conversion efficiency (PCE). There is a strong correlation between the temperature dependent photoconductivity of the doped CdSe QDs and the temperature dependent PCE of the hybrid photovoltaic cells. The highest power conversion efficiency is reached within the photovoltaic cell that contains the gallium doped CdSe QDs. The power conversion efficiency under AM 1.5 illumination reaches 1.2% at room temperature and increases over 2% above 40 °C. The isolated ZnS coated gallium doped CdSe QDs exhibit significant photoluminescence quenching and shorter excitonic lifetime above room temperature range compared to the undoped CdSe dots due to Auger assisted recombination from the dopant ionization. The correlation between the photoluminescence quenching and the increase in efficiency suggests that the key reason of the efficiency increase may be the availability of electrons that can fill up some of the available trap sites. The current-voltage (I−V) characteristics of the cells at room temperature are ohmic for low voltages and turned to follow the dependence of I−Vu, with the exponent u less than 1. The power law dependence of I−V can be interpreted as a trap-controlled space charge-limited current. By adopting the model formulated by Lampert, the exponent u represents the trap

distribution, and less values of u correspond to a decreased number of traps.[132] The shape of the conductivity curve of Figure 4.7 under different annealing temperatures, suggesting that the decrease in electronic coupling energy is driven by the dopant incorporation that decreased CdSe QD surface traps. To gain further insight, the I−V measurement of doped CdSe QDs/P3HT hybrid solar cells under annealing is performed based on the bi-layer heterojunction structure, and this device geometry verified that the current transport followed the temperature dependent CdSe conductivity enhancement by the dopant incorporation. The PCE of hybrid PV devices show a consistent behavior as the temperature dependent conductivity of doped CdSe QDs. There are two outcomes of different doped CdSe QDs: (1) increasing conductivity, and (2) reducing surface traps, thereby increasing the carrier density of QDs. The first outcome enhances device charge mobility, and the second improves the charge carrier density. Thus, thermal annealing alone cannot lead to device-applicable quality for CdSe QDs. To attain high conductivity, carrier density as well as long carrier lifetime, the development of a controllable doping scheme coupled with temperature annealing is key. In addition, the inverted temperature behavior of the photovoltaic cell characteristics is expected for the cell made of doped materials with low ionization energies. This inverted characteristic could be efficiently utilized in solar concentrators where the photovoltaic cell is expected to operate at elevated temperatures.

4. Conclusions

A simple method to dope and control the photoconductivity and charge carriers of CdSe QDs is described, leading to an efficient hybrid solar cell. The chemical dopants (Ga, In and Sn) of CdSe QDs not only results in a controllable photoconductivity, but also a stronger electronic interaction at elevated temperatures. The high conductivity and stronger electronic coupling of doped CdSe QDs can largely enhance charge separation and transport efficiency, which are essential for hybrid inorganic-organic solar cells. The results shown here represent a potentially powerful tactic for increasing the efficiency of hybrid solar cells via enhancing the photoconductivity and controlling electronic interaction between the organic and inorganic materials.

Chapter 5 - Induction and Microwave Heating in Syntheses of CdSe Quantum Dots: A Comparative Study of Effects of Extreme High Heating Rate on Their Nucleation and Growth

1. Introduction

Semiconducting nanoparticles have a great variety of unique properties that are different from their bulk material because of the quantum size effect and large surface to volume ratio. These properties give them interesting application potential in solar cells[1], batteries, bio-imaging[2], catalysis[3] and data storage[4]. Due to the strong dependence of these properties on their crystalline size, controlling the size of these particles is crucial to tuning these characteristics[5]. CdSe quantum dots (QDs) have been studied extensively as a model system of such particles. The ability to manufacture mono-dispersed CdSe quantum dots in bulk is of critical interest since their photoelectronic properties are closely related to their size and low-cost fabrication make them desirable in application compared to conventional silicon-based solar cells. In order to study these properties with respect to the size variation, it is of great importance to be able to produce highly homogeneous, mono-dispersed nanoparticles in a bench-top synthetic route, with potential of scaling up to industrial production, which should also provide control over their surface chemistry, crystalline structure and shape[5].

Induction heating is a heating method that involves generating Eddy current in a conductor by applying rapidly alternating magnetic field, usually produced by an electromagnet, on the workpiece. The heat generated in the material through Joule heating is proportional to the resistance of the conductor. The increased temperature of the conductor results in increased resistance, which increases amount of heat generated, forming a positive feedback where the heating rate increases with time. In comparison, the heat generated by microwave heating, which is result of the thermal rotations of the dipoles in the workpiece, is linear with respect to time. Due to the different characteristics and mechanisms of the two heating method, it is reasonable to expect induction heating to be an interesting method to be applied to nanoparticle syntheses for its extremely high heating rate.

2. Experimental Section

Materials: $Cd(NO_3)_2 \cdot 4H_2O$ (99+%, ACROS), thiophenol (97%, Aldrich), triethylamine (≥99%, Sigma-Aldrich), lithium nitrate (Fisher), cadmium oxide (CdO) (≥99.0%, Fluka), tri-n-octylphosphine (TOP) (97%, Strem), Se powder (≥99.5%, Aldrich), oleylamine (≥98%, Aldrich), oleic acid (≥97%, Fisher), and dodecylamine (DDA) (98%, Aldrich), are used in this synthesis. All chemicals are used as purchased except dodecylamine, which is degassed prior to use.

Preparation of CdSe by $[Cd_{10}Se_4(SPh)_{16}]^{4-}$: The $Li_4[Cd_{10}Se_4(SPh)_{16}]$ single-source precursor (SSP) is prepared as reported by Cumberland.[26] $(Li)_2[Cd_4(SPh)_{10}]$ was first prepared by adding $Cd(NO_3)_2 \cdot 4H_2O$ into thiophenol and triethylamine, followed by addition of lithium nitrate. Selenium metal is then added to the product to produce $(Li)_4[Cd_{10}Se_4(SPh)_{16}]$. In a typical induction heating synthesis, 2.41 g of dodecylamine and 0.03 g of precursor are mixed at 45 °C in a glass container (Figure 5.1 Top Right). An optical temperature probe is inserted and immersed in the solution. 26.13 g of steel beads are added together with the mixture into the reaction vessel, which is then purged with argon for 5 min. Under argon flow, a current of 0 to 2.5A is applied for various durations. The temperature of the solution is then lowered to 45 °C and the samples are collected. The heating rate is controlled by the induction current. As shown on Figure 5.1 left, depending on the current used, induction heating rate can be as high as 110 °C/s. For microwave syntheses, the precursor solution was prepared by adding 0.3 g of $[Cd_{10}Se_4(SPh)_{16}]^{4-}$ into 25 mL of dodecylamine (DDA). The mixture is stirred and 3 mL of the mixture was taken to perform the synthesis. The synthesis is carried out in a microwave reactor (Anton Paar Monowave 300) at 850W (Figure 5.1 Mid Right). Temperature is measured with an IR probe outside the reaction vessel.

Preparation of CdSe by $Cd(OA)_2$: The CdSe is prepared using $Cd(OA)_2$, 1M TOPSe, TOP, and oleylamine. The $Cd(OA)_2$ is prepared using CdO and oleic acid at 1:5 mole ratio using the schlenk line. The CdO and oleic acid mixture is heated to 100 °C under vacuum for 2 hours and heated to 280 °C for 1 hour under N_2. The reaction is stopped after the color changed from red/brown to light yellow. 1M TOPSe is prepared by mixing 10 mL of TOP with 0.7896 g of Se powder. The mixture is sonicated until all Se powder has dissolved. Then 0.675 g of $Cd(OA)_2$, 5.5 mL of 1M TOPSe, 10 mL of TOP, and 2 mL of oleylamine are measured and stirred at 65 °C for 5 min in a 20 mL vial. For the microwave synthesis, 2 mL of the mixture is heated in an

Anton Paar Monowave 300 to prepare the CdSe nanocrystals. The same amount of mixture is used in the magnetic heating as well.

Characterization of CdSe Quantum Dots: For absorption and emission spectra measurements, the samples are diluted in toluene to equal concentrations. For Transmission Electron Microscopy, the imaging is done on Tecnai G2 Spirit BioTWIN. Samples are washed well in anhydrous methanol to remove excess ligands and then dispersed in toluene and dropped onto a Cu grid. The resolution of the instrument is 0.34 nm in TEM mode.

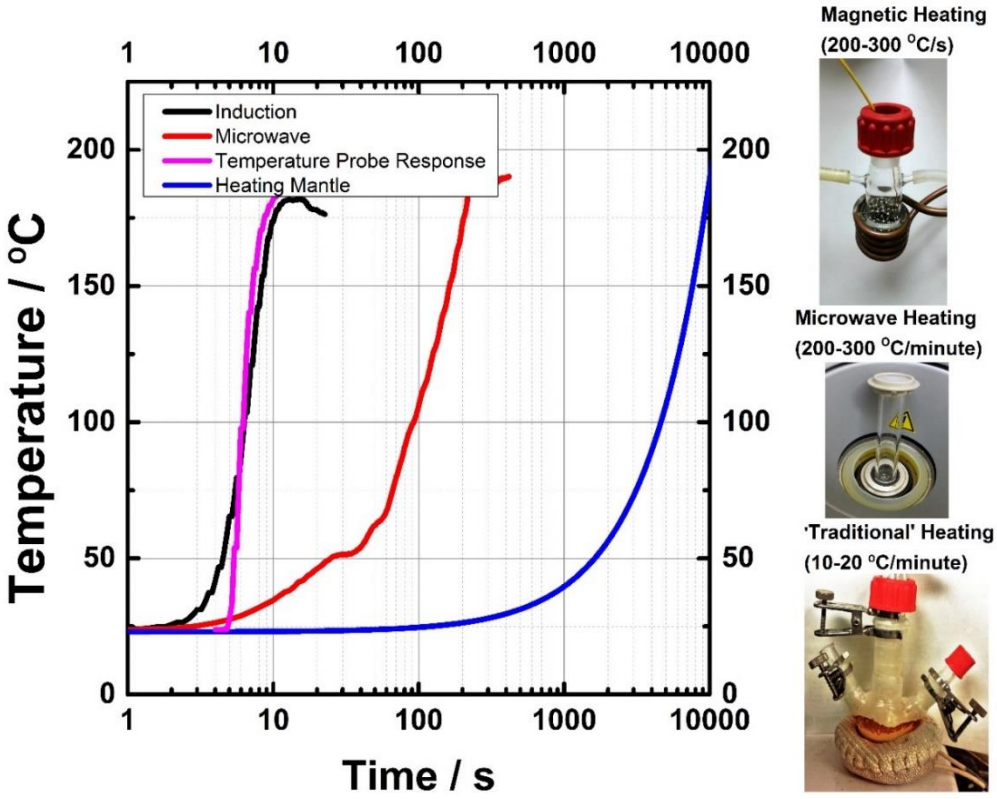

Figure 5.1[133] Left: Comparison of heating rate by induction heating, microwave, and heating mantle Right: Experimental setups. (Reprinted with permission from ref. 85. Copyright © 2016 Multidisciplinary Digital Publishing Institute.)

3. Results and Discussion

In nanoparticle synthesis, the rate of heating competes with the nucleation and growth rates that has important consequences for the final size and size distribution of the particles. With the experimental setup as shown here in Figure 5.1, the induction heating achieved a heating rate of 110 °C/s. Such rapid heating rate has allowed us to successfully synthesize sub 2nm ultra-small

CdSe QDs with only two seconds of heating, as shown in Figure 5.2. Absorption and photoluminescence spectra indicate that our particles have relative narrow size distribution, and have average size of 1.8nm based on a sizing curve reported in literature[73]. Through numerous experiments we've established that a minimum heating time, generally around 2 seconds with our setup, is needed. This is explained firstly by the non-linear relation between heating rate and time caused by increase of resistance in steel balls as temperature rises. It becomes increasingly less effective to reduce heating time by applying higher currents. Secondly, the heat transfer rate between steel balls, solvent, and precursor molecules stay constant regardless of the current applied. At certain point it is not surprising that heat transfer rate also becomes a bottleneck for achieving even faster synthesis. Due to the mechanism of induction heating explained above, it is expected that by using ferromagnetic materials for the synthesis the material can generate heat on itself thus eliminating the steel balls and the heat transfer process. Even faster heating rate could be achieved this way so that particles can be produced with <2s heating, which could be unprecedented and greatly attractive to industrial applications. Although particles continue to grow during the cooling process after heating, in streamlined "flow-through" industrial manufacturing such process will not hinder the efficiency of production as heated material can move through the heating "chamber" and continue to cool while new cold material moves in. We show in a later section that quenching has interesting effects on different properties and characters of the particles produced. Accelerated cooling can be implemented in our experimental setup and also easily in a potential industrial process accordingly to suit various needs. Figure 5.3 shows the quantum dots obtained demonstrate excellent white light emitting characteristics compared to commercial white light LEDs out of the box. The emission spectra can be further optimized to mimic the solar output.

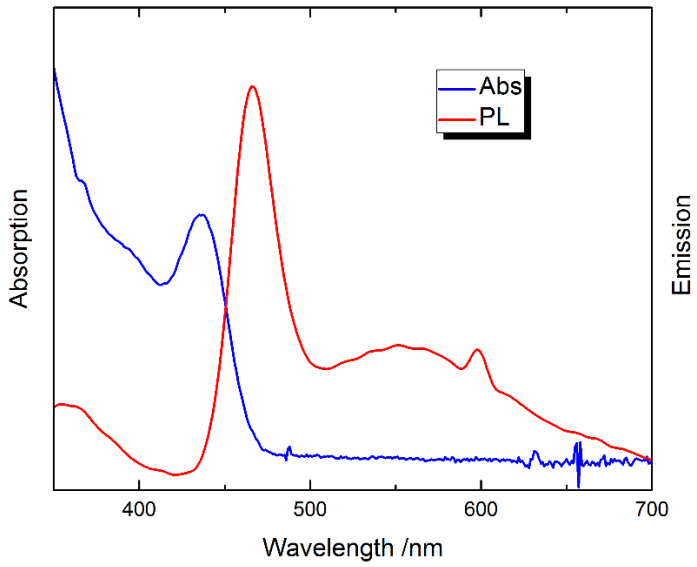

Figure 5.2 Photoluminescence and absorption spectra of 1.8 nm CdSe nanoparticles produced with magnetic heating.

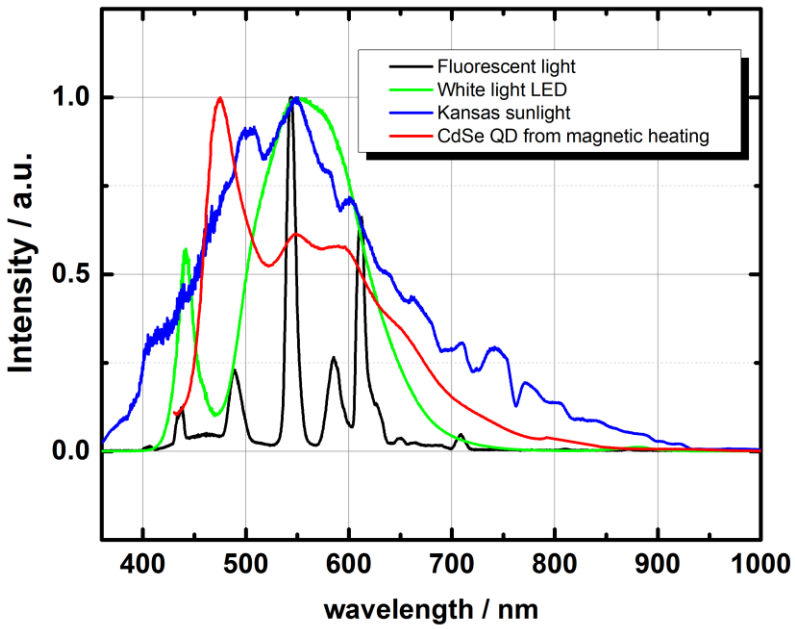

Figure 5.3 Emission spectra of obtained CdSe QDs compared with other light sources

To demonstrate the novel properties and advantages of rapid induction heating synthesis, we obtained a set of data comparing induction heating versus regular synthesis in a heating mantle, which typically runs at the heating rate of 1 °C /min (Figure 5.1). As shown in Figure 5.4, with 2

seconds of induction heating the smallest sized particles were produced with absorption peak at around 437nm. 2 hours of normal heating produced slightly larger particles and the 2 seconds induction heating followed by 2 hours normal heating resulted in the largest particles. The results agree with our hypothesis that fastest heating rate produced the smallest particles. However, by continuing heating the reaction mixture under normal heating condition after the 2 seconds rapid heating, we allowed the particles to grow larger, a process primarily dominated by the Ostwald ripening process. FWHMs of the 2s MH and 2s MH + 2hr NH show that the size distribution did not change after prolonged heating, which agrees with our expectation that the final size distribution is determined in the nucleation stage and that the growth stage merely changes the size of the ensemble uniformly. Such fact reveals that the nucleation stage is critical in controlling the size distribution of an ensemble of particles. Our rapid heating rate is key in quickly raising the monomer concentration in reaction mixture above the nucleation threshold, producing a large number of uniformly sized nuclei, and then quickly dropping the monomer concentration back below nucleation threshold again. A simple calculation shows that by having a higher heating rate, we increase the ratio of nucleation rate versus growth rate during the nucleation stage and thus decrease the initial size distribution of nuclei and particles. On the other hand, our 2-hour normal heating only data shows much larger size distribution, which is in accordance with our theoretical expectation.

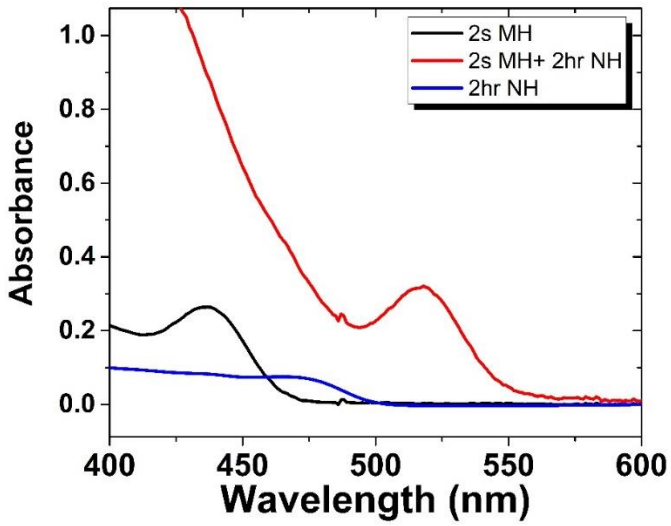

Figure 5.4 Comparison of absorption spectra of CdSe quantum dots synthesized with 2 seconds of magnetic heating (2s MH), 2 seconds magnetic heating followed by 2 hours normal heating (2s MH + 2hr NH), and 2 hours normal heating alone (2hr NH).

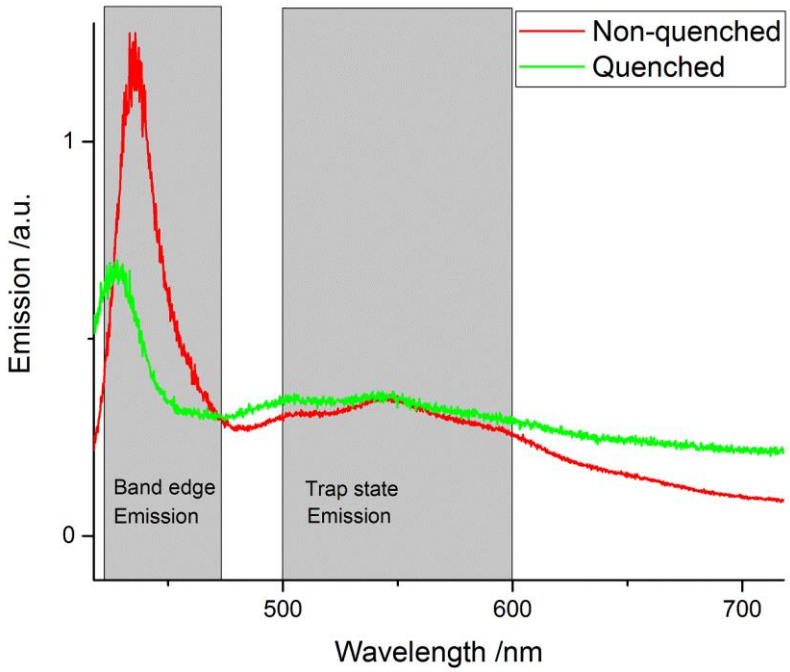

Figure 5.5 Comparison of photoluminescence of quenched and non-quenched CdSe quantum dots synthesized with magnetic heating

To further investigate the effect of rapid nucleation and growth, we obtained spectral data of samples synthesized with induction heating followed by rapid quenching in liquid nitrogen so that the reaction mixture is cooled to 40 °C in 60 seconds. (Figure 5.5) Looking at the band edge emission below 475nm of the quenched data compared with that of the non-quenched, we see that the quenched particles have slightly smaller sizes, which is explained by the fact that the cooling stopped growth early. Also, the non-quenched sample peak has overall higher intensity, indicating higher concentration of particles produced. This is not surprising since the non-quenched reaction mixture stayed at a high temperature for a while even after the heating source is shut off. This allowed for a larger number of nuclei to be formed, resulting in larger number of particles produced eventually. However, the peaks between 500-600 nm of the two samples appeared identical in position, with the quenched sample having slightly higher intensity. We think that such peak arises from the trap state emissions in the particles, primarily in the defect sites usually located on the surface and sometimes inside the particle as well. The energies of these trap states are independent of particle size, therefore resulting in an identical peak position and shape. On the other hand, the slower cooling of the non-quenched synthesis after the nucleation and growth serves as an annealing process, which removes some of the defects in the CdSe crystal structure. A faster cooling rate deters such process and as expected leaves more defect sites giving higher trap state

emission intensity. On the other hand, the formation of CdS with thiolate ligands on the surface of the particles[134] under different temperatures might also be a contributor to the difference of PL intensity, as CdS is also responsible for the trap state emissions.

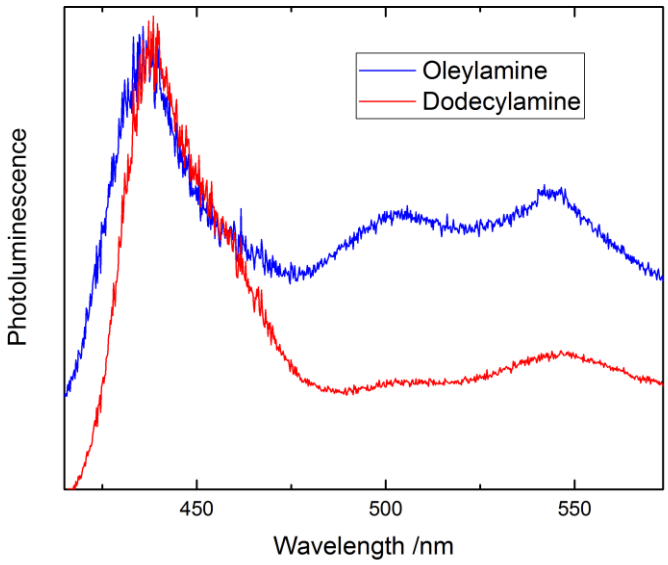

Figure 5.6 Comparison of photoluminescence spectra of CdSe quantum dots synthesized in oleylamine and dodecylamine with magnetic heating

We also performed comparative syntheses of CdSe QDs in oleylamine and dodecylamine. Previous studies suggest a correlation between the viscosity of solvent and the rate of nucleation, as it is related to the rate of diffusion of monomers. Therefore, solvents with lower viscosity would result in higher nucleation rate and narrower size distribution. However, contrary to this theory, our data (Figure 5.6) shows no significant difference under solvents with different viscosity. We think that it is because such theory is made under the assumption of normal heating and stirring conditions. With rapid induction heating, the effect of viscosity of solvent and stirring become negligible. When the usual nucleation process that normally lasts several tens of minutes is done in 2 seconds, along with the fast self-stirring of solvent caused by thermal diffusion and degasification, the difference in diffusion rate of monomers caused by viscosity and stirring becomes irrelevant in such dimension. The slightly larger size of dodecylamine sample is explained by the higher heat capacity of the solvent, which allowed the reaction mixture to stay at the temperature where the particles can continue to grow for several minutes longer. And the lower

trap state emission intensity corresponds to the slower cooling rate, as explained in the quenching section. It is also expected that different ligand-particle structures formed by the two solvents, whose electronic properties are unknown, could also contribute to different levels of trap state emissions. This result revealed one of the unusual effects of extreme high heating rate, which is not predicted under current theories. Future work will be done so that appropriate modification, among many other, is made to properly model the kinetics of nucleation and growth under such conditions.

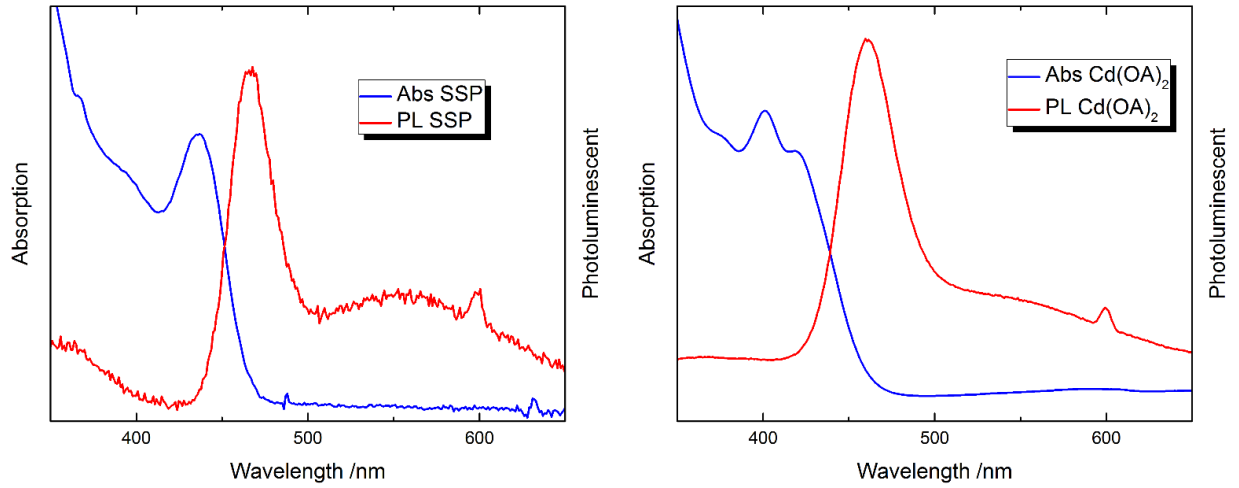

Figure 5.7 Comparison of absorption and photoluminescence spectra obtained from single-source precursor $(Li)_4[Cd_{10}Se_4(SPh)_{16}]$ and $Cd(OA)_2$ with magnetic heating

It is important to note that the induction heating syntheses were done in a preliminary way to explore the various effects of high heating rate from a thermodynamics point of view, and has not been optimized in any way. Various optimizations could be done to achieve certain characters or properties such as smallest size of particles possible, shortest reaction time, enhanced photoluminescence in certain wavelengths for light-emitting functions, etc. Here we show a simple example through comparison of CdSe QDs synthesized from single-source precursor and $Cd(OA)_2$ (Figure 5.7) under identical conditions. Shorter wavelength of the absorption peak corresponds to smaller sized particles that are produced with $Cd(OA)_2$ precursor compared to that of the SSP. A second peak of larger particles were also observed. The two distinct peaks are the result of the so-called sequential growth of such type of particles, where distinct sizes of particles co-exist at early stages of growth and then coalesce to form larger particles later. Combined with the fact that the shorter peak wavelength corresponds to smaller particles produce than that from SSP, it clear that

the $Cd(OA)_2$ precursor had slower reaction rate than SSP. Different reaction potentials of the precursor molecule can cause a difference in the nucleation rate, as it effects the rate at which monomers are provided. The $Cd(OA)_2$ precursor provides monomers through combination of two components, whereas the SSP does so through self-decomposition of the precursor molecule, a process whose mechanism is not yet fully known. Although it is difficult to determine the energies involved in both two reactions, we do qualitatively show such an effect as an example of potential optimizations available for industrial applications.

In this study, the effect of rapid quenching and different capping agents on the particles' growth is also explored. We think that quenching would stop the growth of the nanoclusters early and result in even smaller overall sizes, and that different capping agents would modify the chemical potential involved in nucleation and growth, and possibly even the decomposition of precursor molecules, thus changing the overall kinetics as well.

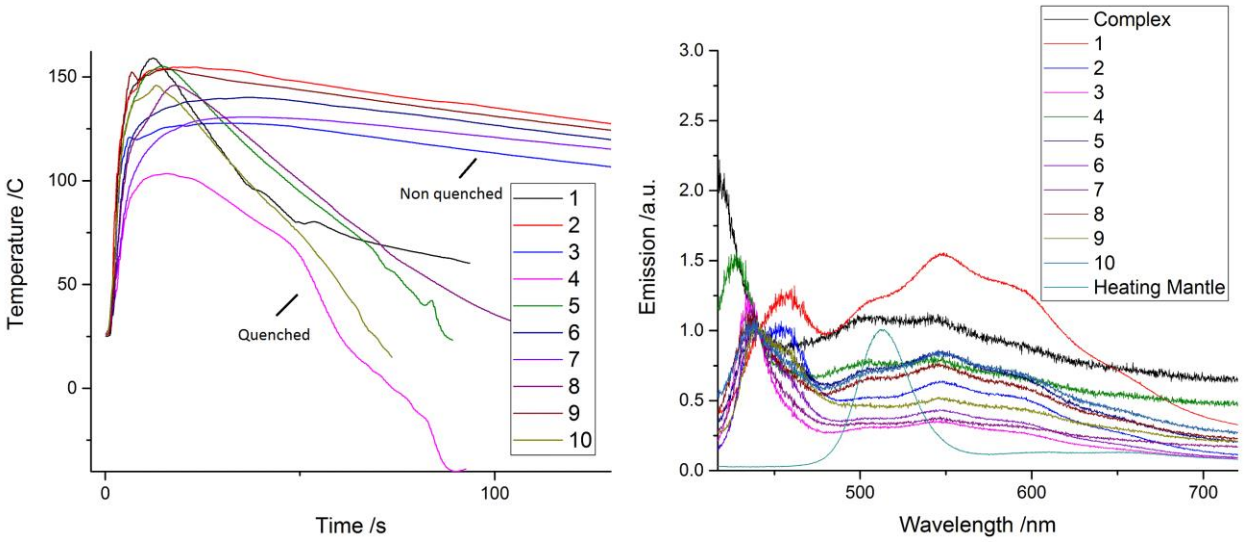

Figure 5.8 Heating temperatures (left) and PL (right) comparison of quenched, unquenched, and heating mantle synthesis

Table 5 Experimental parameters of the induction heating and quenching syntheses

	A	B	C	D	E	F
Comments	Parameters					
Units		A	g		s	
Long Name	#	Current	Steel balls	Complex	Duration	Quenched?
1	1	31.5	28.6	2.45	2	Yes
2	2	31.5	30.91	2.47	2	No
3	3	31.5	30	2.4	1.5	No
4	4	31.5	30.52	2.69	1.5	Yes
5	5	13.6	30.52	2.49	2	Yes
6	6	13.6	32.61	2.7	2	No
7	7	21.7	32.99	2.79	2	No
8	8	21.7	30.13	2.7	2	Yes
9	9	6.7	30.78	2.5	2	No
10	10	6.7	30.38	2.68	2	Yes

A set of experiments with varying parameters including induction heating current, heating time, and quenching were performed (Table 5). Emission spectra (Figure 5.8) taken of the sample indicate, for the quenched samples, that there's an increase in the ratio between the PL intensity of the trap state emission at 500 – 600 nm and the band edge emission at 420 – 470 nm, compared to the unquenched samples. We believe that it is plausible that such increase in trap state emission is caused by the larger number of particles. Such trap states emission arises from the surface interaction on the quantum dots, and is therefore independent of particle size. With rapid quenching, further growth and coalescence of particles were terminated at an early stage, leaving the solution with higher number of smaller particles. In addition, overall smaller sizes of particles also mean larger overall surface area for the same amount of particles, which contributes to the increased trap states emission. However, the increased intensity at 500 – 600 nm could also be caused by white light emission of the magic-sized quantum dots. To determine the actual size distribution of these particles, techniques such as TEM imaging or size-selective precipitation is needed. Quantum yield measurements could provide insights to this information as well.

We also see the band edge emission appear at a shorter wavelength for the quenched samples, which indicates smaller particle sizes. Interestingly, during tweaking of the experimental parameters, we discovered that there appears to be a minimum amount of heat needed to initiate growth. When the amount of heat applied is below such threshold, emission spectrum becomes identical to that of the complex, implying no significant growth was initiated. This could be understood by the fact that due to the heat capacity of the steel beads and solution,

and the heat transfer rate between interfaces, when heating time or current applied is below a certain value, there is not enough time or heat to effectively raise the temperature of the complex.

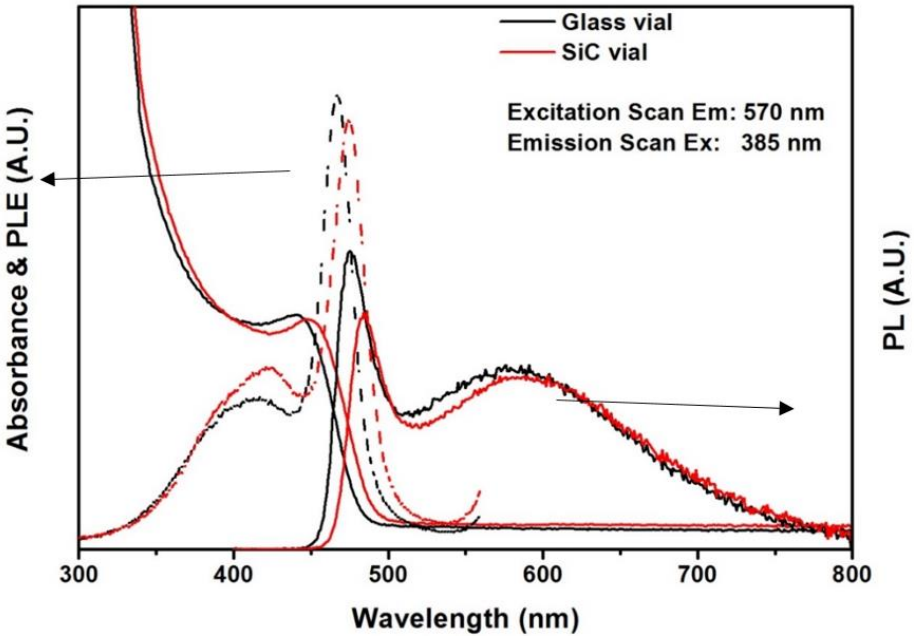

Figure 5.9 Room temperature absorption, photoluminescence, and photoluminescence excitation spectra of ultra-small CdSe nanocrystals synthesized using the single source precursor $Li_4[Cd_{10}Se_4(SPh)_{16}]$. The CdSe synthesis was carried out in both glass vial (Black) and silicon carbide (SiC) vial (Red) in the microwave reactor (Anton Paar Monowave 300) at 200 °C and 850 W. The photoluminescence (PL) was obtained using 385 nm excitation source while the photoluminescence excitation (PLE, dotted line) was obtained for the emission at 570 nm. The PLE shows the trap emission observed from the PL around 570 nm was from the nanocrystal.

In previous studies, microwave synthesis has shown a rapid heating rate in comparison to the traditional heating method (such as oil bath heating). Even though the heating rate of microwave synthesis is faster than conventional method, magnetic heating has the highest heating rate when compared. This rapid heating rate is achieved by using solutions that are polar or ionic, which the microwave radiation can interact directly with the molecules in the solution. For this comparative study, the synthesis of CdSe is studied using two different precursors. For the microwave synthesis, a Pyrex vial and a silicon carbide (SiC) vial were used to study the heating rate using the two precursors. The Pyrex vial transparent to microwave radiation which allows for direct interaction with the molecules, but SiC vial absorbs most of the microwave radiation and some pass through (depending on the thickness of the vial wall) which leads to a heat up method that is similar to traditional heating methods (such as oil bath) and allow for some direct heating

as well.[135] The UV-Vis absorption and PL spectra of the CdSe NCs synthesized using the single source precursor $Li_4[Cd_{10}Se_4(SPh)_{16}]$ in a Pyrex vial and SiC vial is shown in Figure 5.9. A red shift in both the absorption and emission peaks indicates a size increase of the CdSe NCs. The PL spectra show a band-edge emission peak centered at 475 nm (Pyrex vial) and 485 nm (SiC vial) and a trap emission peak around 570 nm. The PL spectra shows that the CdSe NCs have a narrow size distribution. The CdSe NCs were not washed after the synthesis because the emission goes away. The PLE spectra show a peak around 470 nm (570 nm detection), similar to the band-edge peak. This confirms the trap emission was from the NCs rather than impurities present in the solution. The small shift in the peak position of the PLE spectra from the absorbance is likely from ligands that are present in the solution.

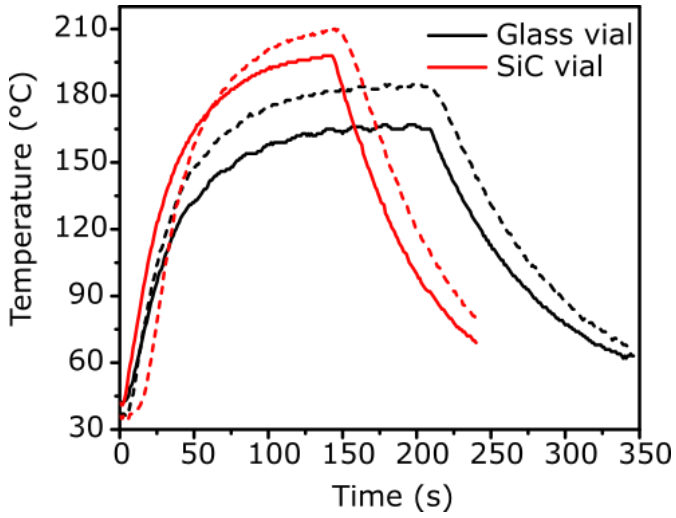

Figure 5.10 Temperature plot of the ultra-small CdSe nanocrystals synthesized using the single source precursor $Li_4[Cd_{10}Se_4(SPh)_{16}]$ in glass vial (black) and SiC vial (red). The internal temperature (dashed) was measured using fiber optic (FO) probe with ruby crystal while the external temperature (solid) was measured using infrared (IR) probe.

Overall, the CdSe NCs synthesized in the SiC vial were larger than those prepared in the Pyrex vessel. This is likely because the starting solution contains a non-microwave-absorbing material, which SiC vial can be used to solve the heating problem.[135] The temperature plot (Figure 5.10) shows the SiC vial having the shorter reaction time when compared to the Pyrex vial. The data collected from the heating profile of the two vials, the SiC vial had a faster heating rate. Also, it shows that the SiC vial temperature is much higher than the Pyrex vial. In previous studies, it has been found that increase in temperature leads to larger size NCs. The SiC vial absorbs some of the microwave radiation, which heats up the solution via convection method instead of a direct

heating method. For both vials, their internal temperature was recorded using fiber optic (FO) probe inserted into the solution with a glass tube and shows their internal temperature was much higher than the outside temperature, which was recorded using IR sensor. The outside temperature was used to control the reaction temperature. Based on the data collected, the larger sized CdSe was obtained from the SiC vial because of the higher heating rate and higher reaction temperature.

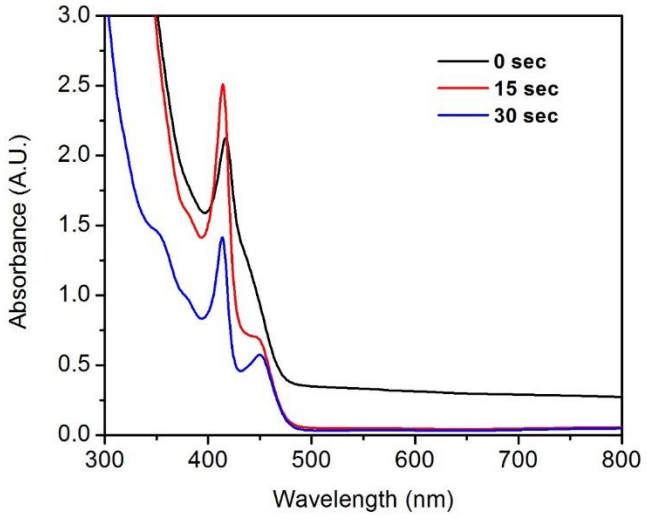

Figure 5.11 Room temperature UV-vis spectra of ultra-small CdSe nanocrystals synthesized using Cd(OA)2, 1M TOPSe, TOP, and Oleylamine in the microwave at 150 °C and 850 W with a hold time of 0 second (black), 15 second (red), and 30 second (blue).

In order to obtain the fastest heating rate when using the microwave synthesis, a better microwave absorbing material was used. The mixture contained $Cd(OA)_2$, 1M TOPSe, TOP, and oleylamine. As shown in the experimental section the mixture was then heated to 150 °C and 850 W with a hold time of 0, 15, and 30 seconds. Ultra-small CdSe NCs (below 2 nm)[135] were synthesized successfully. The UV-vis absorption shows a slight red shift with a new peak appearing around 450 nm as the hold time increases (Figure 5.11). The new peak around 450 nm is a result of the size increase of the CdSe NCs from the magic-size to ultra-small NCs. From the absorption peaks their relative size were found to be 1.67 nm (0 seconds), 1.69 and 1.93 nm (15 seconds), and 1.67 and 1.95 nm (30 seconds). Chikan *et al.* has shown that having tellurium-rich (selenium in this study) condition leads to the formation of magic-sized quantum dots.[136] The absorption shows the CdSe size increases from magic-sized to ultra-small NCs follows a homogenous growth.[67] One of the unique properties of ultra-small NCs is the presence of two emission peaks.[67] The PL spectra show a red shift as the hold time increases and it also shows a

trap emission (Figure 5.12). The peak shift observed from the PL spectra (Figure 5.12) was from 460 nm (0 seconds) to 472 nm (30 seconds). This proves that the CdSe NCs are increasing in size. Small sized nanocrystals are mostly dominated by trap emission due to the increase in the surface-to-volume ratio of the nanocrystals.[137] Therefore the trap emission observed from the PL spectra are from the NCs instead of impurities in the solution. To further investigate this, PLE spectra was recorded showing the trap emission seen from the PL spectra to be from the nanocrystal itself (Figure 5.12).

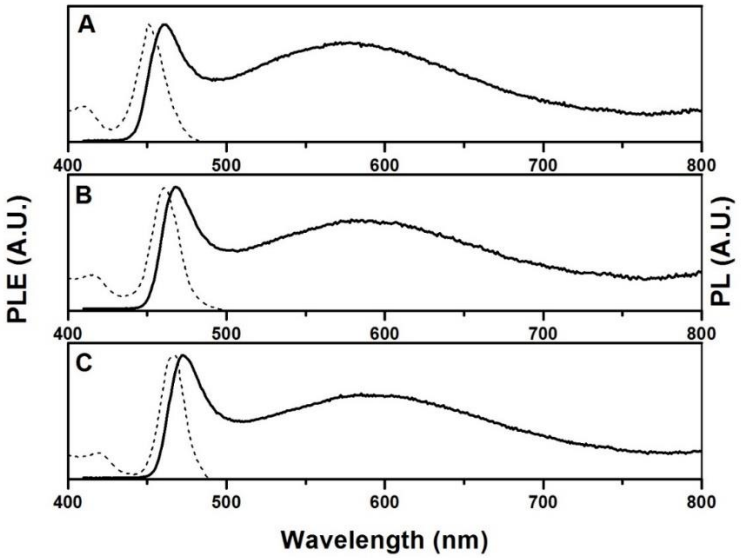

Figure 5.12 Room temperature photoluminescence (PL) and photoluminescence excitation (PLE) spectra of ultra-small CdSe nanocrystals synthesized using $Cd(OA)_2$, 1M TOPSe, TOP, and Oleylamine in the microwave at 150 °C and 850 W with a hold time of (A) 0 second, (B) 15 second, and (C) 30 second. The PL spectra was obtained using 405 nm excitation source and the PLE spectra was obtained for the emission at 575 nm. The synthesis was carried out using a glass vial in a microwave reactor (Anton Paar Monowave 300).

The temperature and power plots for the reaction are shown in Figure 5.13 and Figure 5.14 respectively. The temperature plot shows the internal temperature is higher than the external temperature. This result was as expected from our hypothesis. The solution mixture had TOP, which absorbs microwave radiation well, so the internal temperature would rise faster than the external temperature. For this reaction only Pyrex vial was used, since the mixture is better microwave-absorbing material the use of SiC vial will not be able to give us the fastest heating

rate. The heating profile recorded the heating rate is similar in all the reactions, which is seen on both the temperature plot and the power plot.

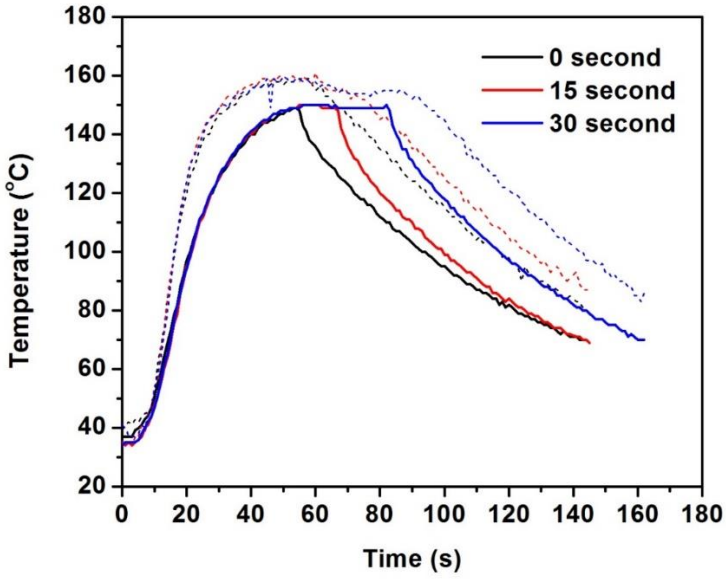

Figure 5.13 Temperature plot for the CdSe synthesis using $Cd(OA)_2$ in the microwave reactor that shows the internal temperature (dashed) and external temperature (solid) of the syntheses at 150 °C and 850 W.

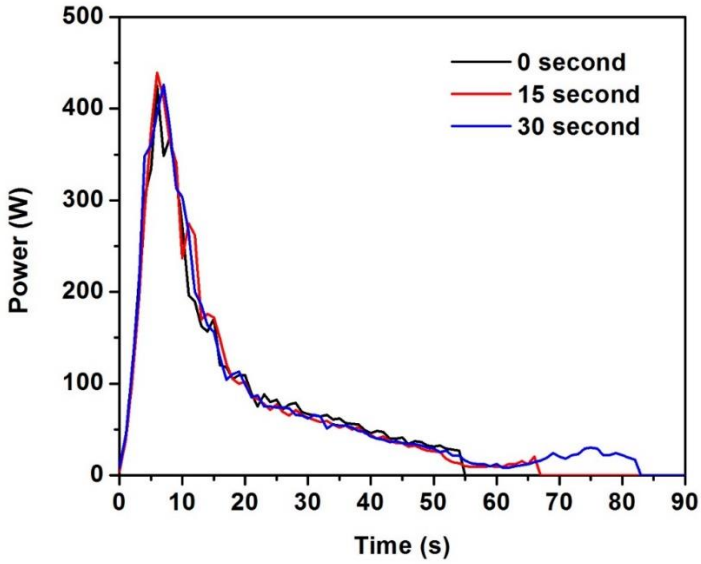

Figure 5.14 Power plot for the CdSe synthesis using $Cd(OA)_2$ in the microwave reactor set at 150 °C and 850 W with different hold times.

Although faster heating rates (more than observed with this experiment) can be achieved by using the microwave synthesis there are some limitations that will affect the heating rate. The power the instrument applies towards heating the reactions is not similar to the reaction set-power. This is to prevent arching and over-heating, which will lead to reaction vessel explosion due to pressure build up. The reaction set-power for Figure 5.14 was 850 W but the power maximum was only around 450 W. Further modification of the microwave reactor will be able to provide faster heating rate. In addition, the use of better microwave-absorbing materials (such as ionic liquids) will be able to provide faster heating rate.

4. Conclusions

This study demonstrated a novel heating method for the colloidal synthesis of nanoparticles. Sub 2 nm ultra-small CdSe quantum dots were prepared and showed significant agreement of its emission profile compared with that of natural sunlight. The results were also compared with those from microwave synthesis and proved to be an effective method for better control of size distribution of the particles prepared. Rapid quenching was discovered to lead to smaller particles and increased trap state/bandedge emission ratio and provides insights towards fine-tuning of the photoluminescence output of these materials.

Chapter 6 - Blinking Behavior of CdSe Nanorod in Gradient Film

1. Introduction

The blinking behaviors of semiconducting nanocrystals is an area of interest that could reveal important characters and light emitting mechanisms inside these materials. The development of single molecule spectroscopy in the past decades has enabled investigation into this phenomenon that was previously considered rather erratic. It was discovered that the period of time during which the emitters are fluorescent or stay dark, or the "on" "off" states, follow power law, and could range from just a few microseconds to several minutes[116]. Such behavior has excited widespread interests and attempts at explaining the underneath mechanism. So far, all known types of fluorophore studied exhibit fluorescence intermittency including single molecules, fluorescent proteins, polymer segments, and semiconductor nanocrystals such as quantum dots, nanorods and nanowires. Experimentally, the on-off periods are collected by detection of fluorescence with a CCD camera or photon counting as a function of time. Analysis could be made by constructing a time series of integrated intensity. Numerous measurements have been made to establish that[138] the off time follows:

$$P(t_{off}) = At_{off}^{-m_{off}}$$

and that the on time follows:

$$P(t_{on}) = At_{on}^{-m_{on}} e^{-t_{on}/\tau_{on}}$$

where τ_{on} is a variable dependent on parameters related to temperature, intensity and size of the nanocrystal, while the exponent m is dependent on the shape[139] of nanocrystal, wavelength[140] and intensity[141] of excitation light, and other environmental factors[142]. From the application point of view, the irregular fluorescence intermittency is unfavorable to development of NC-based lasers, light-emitting diodes, and efficient photovoltaics as the stability and lifetime of exciton are reflected by intensity and frequency of blinking. Therefore, understanding and controlling of the blinking behaviors of these emitters are crucial to its application in the above-mentioned areas. Many studies have been done for various nanocrystalline materials under different environments, but few explores those with the effects of polarity. In this study, focus is put on understanding how exciton lifetime of these fluorophores, in particular CdSe nanorods, is effected by polarity of its environment.

2. Experimental Section

Preparation of CdSe nanorods with polar ligands: CdSe nanorods are synthesized as described in literature[143]. In a typical synthesis, 50 mg of CdO, 4.1 g of trioctylphosphine oxide and 305 mg of tetradecyl phosphonic acid are mixed under argon and heated to 120 °C and then vacuumed for 1 hour to further remove water and oxygen. A selenium trioctylphosphine solution was prepared under nitrogen by mixing 4 mL of trioctylphosphine and 42.0 mg of Se powder, which was then sonicated for 30−45 s to completely dissolve the Se powder. The solution was then purged with nitrogen and vacuumed several times. Another weak vacuum was applied at 280 °C to the reaction mixture and stopped until its color changed to dark gold. 4.0 mL of the 0.16 M SeTOP was then injected at 270 °C to the solution, and afterwards the temperature decreased to 230 °C. The nanorods were grown at 260 °C for 5 min and then cooled to room temperature. The product is then washed with methanol by centrifuging five times to remove other organics to obtain the final dark red nanorods. (3-Aminopropyl)triethoxysilane could then be added to nanorods dissolved in toluene heated to 120 °C for 3 hours to obtain the amino-functionalized nanorods.

Preparation of Tetramethoxysilane (TMOS)/Phenyltrimethoxysilane (PTMOS) Gradient Film: The tetramethoxysilane/phenyltrimethoxysilane gradient films were prepared by the infusion withdrawal dip coating technique described in Chapter 2 - 5.

Collection of Blinking Image Series: The sample is observed with wide field microscope. As shown in Figure 6.1, a 532 nm laser is used for excitation of the samples. The laser source passes through a polarizer and onto a dichroic mirror and then shines on the objective of the microscope. The objective then focuses incoming light onto the observed sample. The emitted light from the sample is then passed through the dichroic mirror and reflected (M1) to pass through a notch filter and band pass filter to remove scattered laser light and select desired wavelength of fluorescence light to be measured by the CCD. The CCD takes a series of 300 images at 4 frames per second of the incoming light.

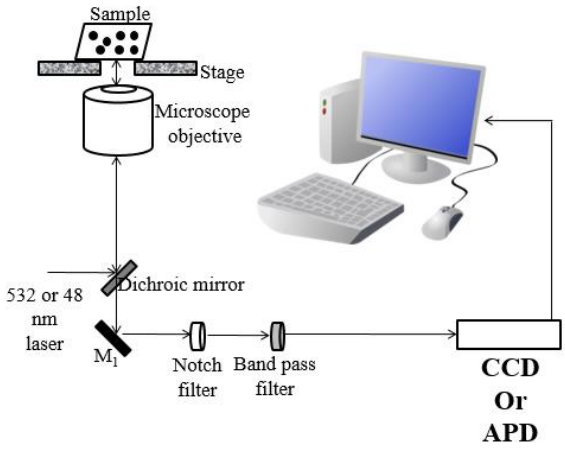

Figure 6.1 Schematic diagram showing the wide field microscope set up

3. Results and Discussion

Figure 6.2 shows the blinking data of NRs for comparison of in pure TMOS vs. PTMOS and when they are vertically (parallel to gradient direction) vs horizontally (perpendicular to gradient direction) oriented, and when they're bleached for 75s vs. unbleached. The combined statistics shows no significant difference in number of observed spots between samples in pure TMOS and pure PTMOS, and no significant difference between horizontal and vertically oriented NRs. There is however clearly lower number of spots observed for the bleached samples compared that with the unbleached. This result indicates that the excitation light induced certain types of chemical reaction of the NRs that permanently bleached the sample.

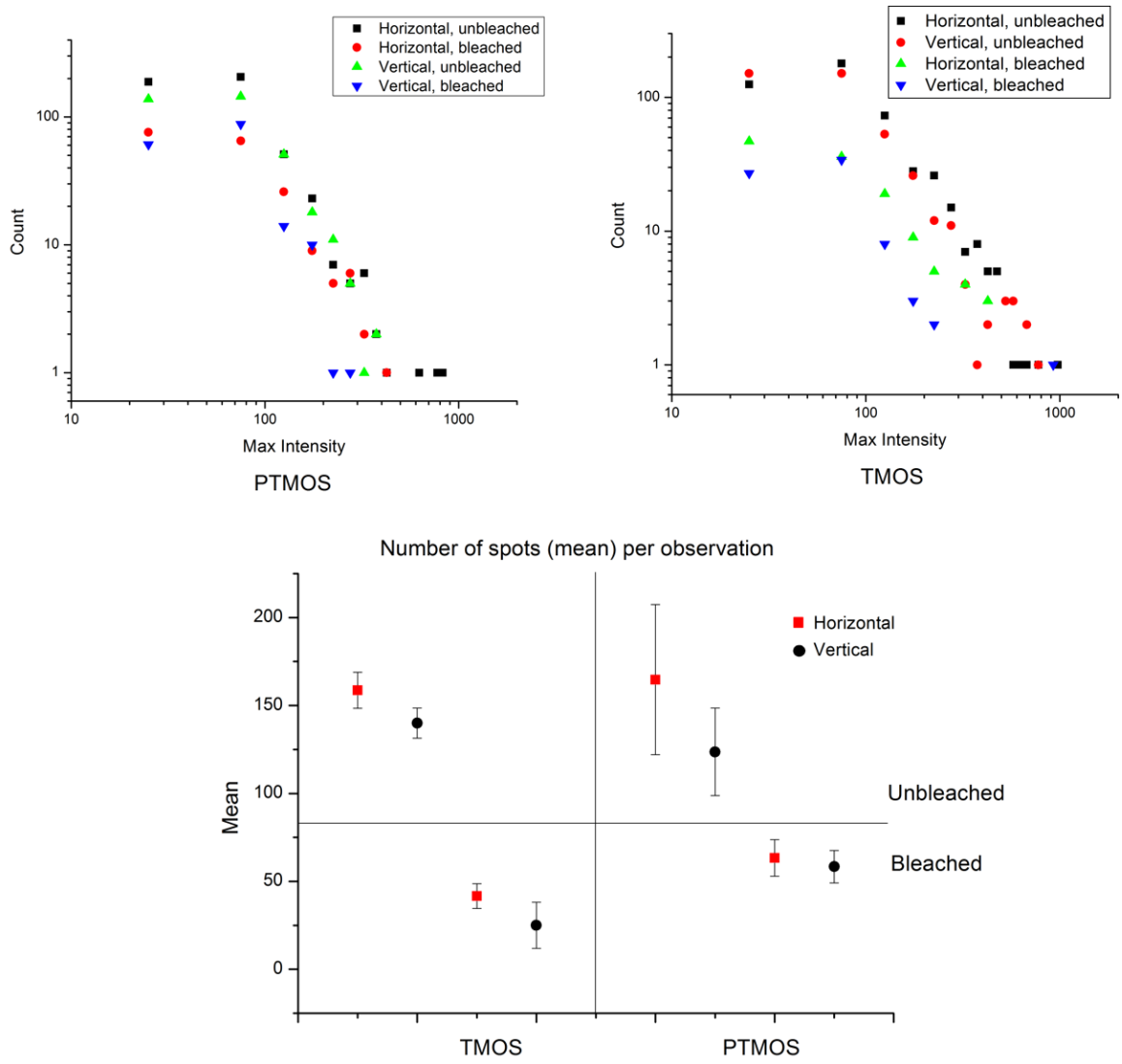

Figure 6.2 Fluorescence spot counts of NRs in different orientation and comparison of bleached vs. unbleached samples

On time and off time analysis was also performed by counting the total frames of a spot fluorescing and staying dark with the results plotted in Figure 6.4. Again, no significant difference between NRs vertically vs. horizontally oriented and in pure TMOS vs. pure PTMOS was observed. Agreeing with the above observed number of spots statistics, there is a jump in off time reaching the end of the 300-frame series for the unbleached samples, which indicates that a part of unbleached samples were permanently bleached after the first time being exposed to the laser light and do not fluoresce anymore. However, similar pattern was not observed in the

already bleached samples, indicating that the chemical reactions that caused permanent bleaching happened within the first 300 frames.

Since strong bleaching effect were observed, it is reasonable to postulate possible spectral shift corresponding to the chemical reactions involved. For this purpose, analyses of three randomly chosen spots on both TMOS and PTMOS films were made by plotting their spectral evolution over 300 frames, as shown in Figure 6.3. The spectra were recorded over 300 frames for the 6 spots and then plotted with color map indicating intensity in MATLAB. Aside from overall intensity differences of different spots which is expected, no significant intensity shift on the spectra of different wavelength were observed.

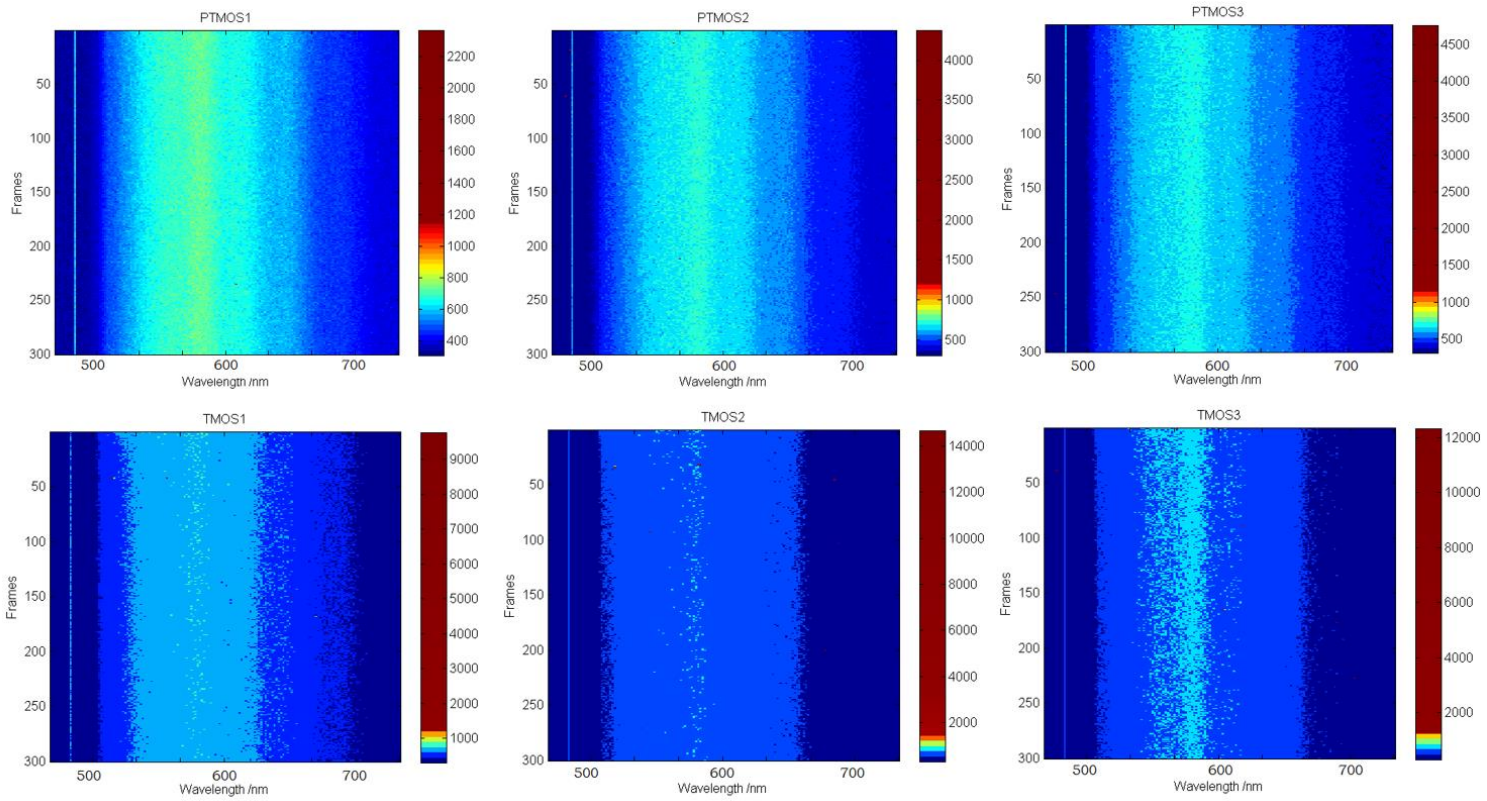

Figure 6.3 Spectral shift of 3 random spots on TMOS and PTMOS films

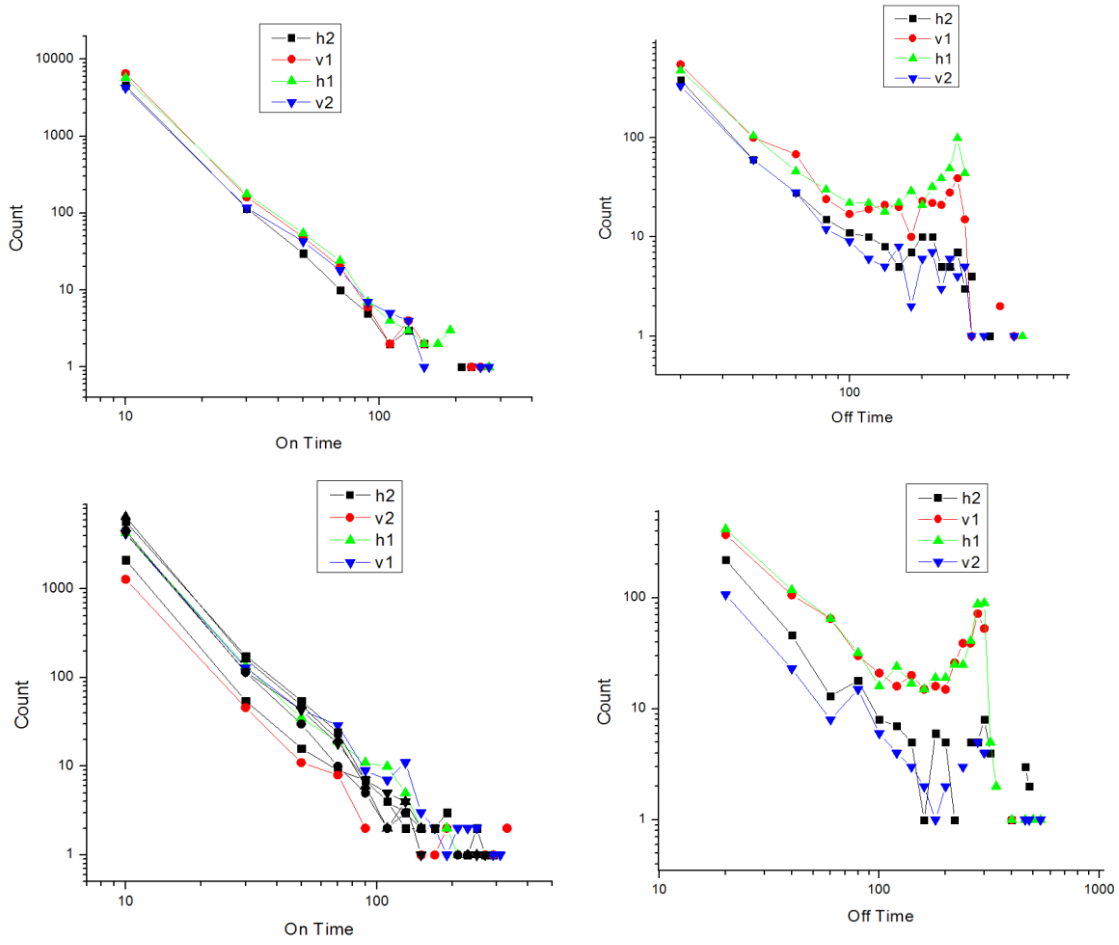

Figure 6.4 On time and off time analysis

TOP: PTMOS, BOTTOM: TMOS; "1": unbleached, "2": bleached; "v": vertical, "h": horizontal

Based on these results, it is conclusive that TMOS and PTMOS polar environment did not make any significant difference in the fluorescence intermittency of NRs oriented either vertically or horizontally. Then, analyses of fluorescence intensity were also done to 10 spots on a TMOS-PTMOS gradient film shown in Figure 6.5. The gradient of the film changes from TMOS from spot 1 to PTMOS to spot 10 and the max intensity distribution of the spots were plotted. Again, no significant pattern were observed of the gradual change of polar environment from TMOS to PTMOS for all 10 spots, a result in accordance with the pure TMOS and PTMOS comparison analyses above. Time sequence of mean fluorescence intensity change over 300 frames for the 10 spots were also plotted in Figure 6.6. No significant difference were observed for the gradual change of polar environment from TMOS to PTMOS for all 10 spots.

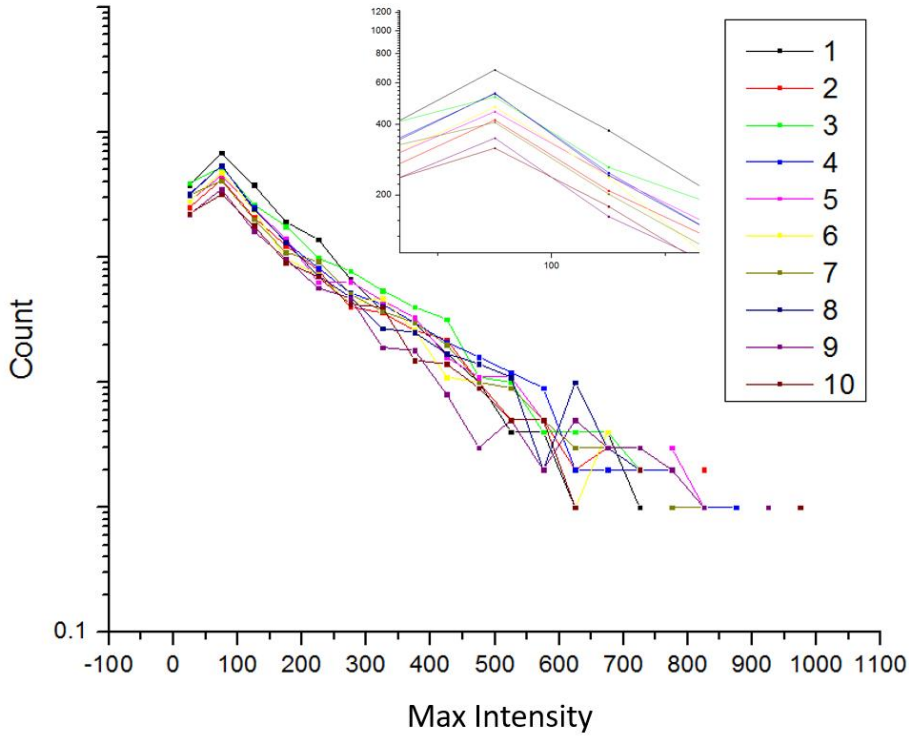

Figure 6.5 Fluorescence intensity analysis of 10 spots on the gradient film. From 1 (more TMOS) to 10 (more PTMOS).

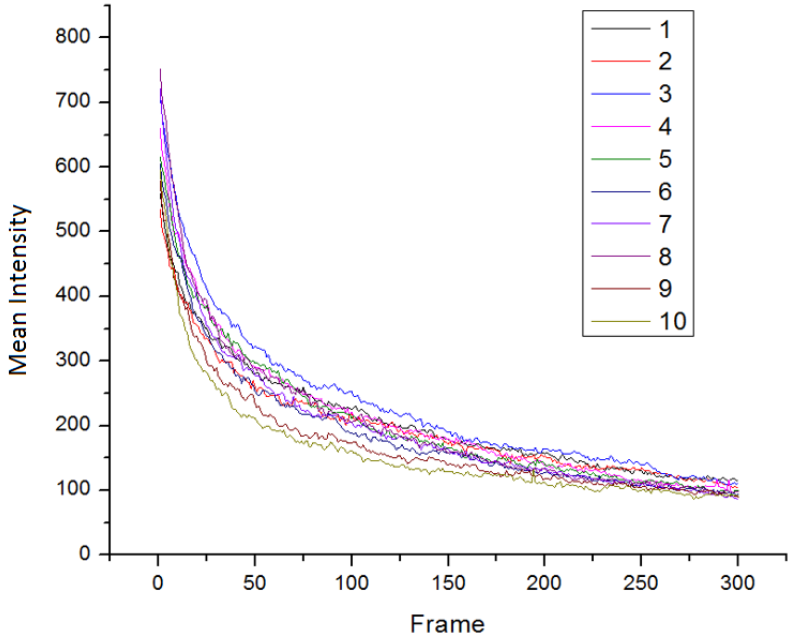

Figure 6.6 Mean intensity time sequence of 10 spots on the gradient film. From 1 (more TMOS) to 10 (more PTMOS).

4. Conclusions

This study investigated the blinking behavior of CdSe nanorods under different polar environments, specifically TMOS and PTMOS, with consideration of different orientation of the nanorods with respect to the gradient. Raw count of number of blinking spots did not show significant variation relating to the polar environment or NR orientation. Previously bleached NRs however show reduced number of blinking spots, indicating possible chemical bleaching induced by the exciting laser light. Such permanent bleaching is confirmed by on-off time analysis of unbleached samples which showed significantly increased off time at the end of the first exposure. However, no spectral shift was observed throughout the bleaching process for NRs in both TMOS and PTMOS films. Fluorescence intensity analyses of 10 spots from the TMOS end to PTMOS end on the gradient film was also performed, confirming that such variation of polar environment did not impact the blinking behaviors of CdSe NRs in any conclusive way. Nevertheless, this study demonstrated successfully the incorporation of infusion withdrawal dip coating technique to provide a platform of studying fluorescence behaviors of nanocrystals under polar gradient, and has proven to be an effective method that could be readily employed in similar studies of other nanocrystals as well.

Chapter 7 - Summary

In summary, this thesis presented investigations focusing on understanding and controlling defects in quantum confined systems, particularly CdSe quantum dots and nanorods.

Syntheses and characterization of gallium doped CdSe quantum dots are discussed, including the preparation of gallium doped CdSe quantum dots, as well as important chemical, electrochemical and spectroscopic changes in the quantum dots induced by gallium doping. It was discovered that gallium doping could be an effective way to manipulate the electrical properties of quantum dot films and solar cells at near room temperature.

Additionally indium and gallium doped CdSe quantum dot were studied for the purpose of manufacturing hybrid solar cells. A method to dope and control the photoconductivity and charge carriers of CdSe QDs is described. Strong evidences are presented that the chemical dopants (Ga, In and Sn) of CdSe QDs not only results in a controllable photoconductivity, but also a stronger electronic interaction at elevated temperatures, and that the high conductivity and stronger electronic coupling of doped CdSe QDs can largely enhance charge separation and transport efficiency, which are essential for hybrid inorganic-organic solar cells.

Then, induction and microwave heating syntheses of CdSe quantum dots are reported and the effects of extreme high heating rate on nucleation and growth of such nanocrystals are discussed. Experimental results and analyses show that induction heating not only has proven to be an effective way of achieving preparation of ultra-small sub-2 nm quantum dots, but could also provide a way of separating the nucleation and growth process, which could facilitate the development of a more accurate theory describing such processes.

Finally, a method of utilizing infusion withdrawal dip coating to prepare a polarity gradient film to study the blinking behaviors of CdSe nanorods were reported. Although through various analyses of data including count of number of blinking spots, spectral shift over time, on-off time frequency, spots intensity distribution and mean intensity time sequence, no conclusive variation was observed with respect to different polar environment and NR orientation, it did however point out a permanent bleaching process induced by the exciting light that resulted in significantly increased off time during the first exposure and reduced number of blinking spots during the second exposure.

References

1. Atwater, H. A.; Polman, A., Plasmonics for improved photovoltaic devices. *Nat Mater* **2010,** *9* (3), 205-213.

2. Pankhurst, Q. A.; Thanh, N. T. K.; Jones, S. K.; Dobson, J., Progress in applications of magnetic nanoparticles in biomedicine. *J Phys D Appl Phys* **2009,** *42* (22).

3. (a) Narayanan, R.; El-Sayed, M. A., Catalysis with transition metal nanoparticles in colloidal solution: Nanoparticle shape dependence and stability. *J Phys Chem B* **2005,** *109* (26), 12663-12676; (b) Astruc, D.; Lu, F.; Aranzaes, J. R., Nanoparticles as recyclable catalysts: The frontier between homogeneous and heterogeneous catalysis. *Angew Chem Int Edit* **2005,** *44* (48), 7852-7872.

4. Hyeon, T., Chemical synthesis of magnetic nanoparticles. *Chem Commun* **2003,** (8), 927-934.

5. Murray, C. B.; Kagan, C. R.; Bawendi, M. G., Synthesis and characterization of monodisperse nanocrystals and close-packed nanocrystal assemblies. *Annu Rev Mater Sci* **2000,** *30*, 545-610.

6. Alivisatos, A. P., Semiconductor clusters, nanocrystals, and quantum dots. *Science* **1996,** *271* (5251), 933-937.

7. Lee, Y. J.; Yao, Y. C.; Tsai, M. T.; Liu, A. F.; Yang, M. D.; Lai, J. T., Current matching using CdSe quantum dots to enhance the power conversion efficiency of InGaP/GaAs/Ge tandem solar cells. *Opt. Express* **2013,** *21* (22), A953-A963.

8. Yu, W. W.; Qu, L. H.; Guo, W. Z.; Peng, X. G., Experimental determination of the extinction coefficient of CdTe, CdSe, and CdS nanocrystals. *Chem Mater* **2003,** *15* (14), 2854-2860.

9. Klimov, V. I.; Ivanov, S. A.; Nanda, J.; Achermann, M.; Bezel, I.; McGuire, J. A.; Piryatinski, A., Single-exciton optical gain in semiconductor nanocrystals. *Nature* **2007,** *447* (7143), 441-446.

10. Wang, C. J.; Wehrenberg, B. L.; Woo, C. Y.; Guyot-Sionnest, P., Light emission and amplification in charged CdSe quantum dots. *J Phys Chem B* **2004,** *108* (26), 9027-9031.

11. Pradhan, N.; Goorskey, D.; Thessing, J.; Peng, X. G., An alternative of CdSe nanocrystal emitters: Pure and tunable impurity emissions in ZnSe nanocrystals. *J Am Chem Soc* **2005,** *127* (50), 17586-17587.

12. Tchebotareva, A. L.; de Dood, M. J. A.; Biteen, J. S.; Atwater, H. A.; Polman, A., Quenching of Si nanocrystal photoluminescence by doping with gold or phosphorous. *J Lumin* **2005,** *114* (2), 137-144.

13. Ihly, R.; Tolentino, J.; Liu, Y.; Gibbs, M.; Law, M., The Photothermal Stability of PbS Quantum Dot Solids. *Acs Nano* **2011,** *5* (10), 8175-8186.

14. Zherebetskyy, D.; Scheele, M.; Zhang, Y. J.; Bronstein, N.; Thompson, C.; Britt, D.; Salmeron, M.; Alivisatos, P.; Wang, L. W., Hydroxylation of the surface of PbS nanocrystals passivated with oleic acid. *Science* **2014,** *344* (6190), 1380-1384.

15. Stavrinadis, A.; Konstantatos, G., Strategies for the Controlled Electronic Doping of Colloidal Quantum Dot Solids. *Chemphyschem* **2016,** *17* (5), 632-644.

16. Norris, D. J.; Efros, A. L.; Erwin, S. C., Doped nanocrystals. *Science* **2008,** *319* (5871), 1776-1779.

17. Dalpian, G. M.; Chelikowsky, J. R., Self-purification in semiconductor nanocrystals. *Phys Rev Lett* **2006,** *96* (22).

18. Wu, P.; Yan, X. P., Doped quantum dots for chemo/biosensing and bioimaging. *Chem Soc Rev* **2013,** *42* (12), 5489-5521.

19. Yu, K.; Hu, M. Z.; Waing, R. B.; Le Piolet, M.; Frotey, M.; Zaman, M. B.; Wu, X. H.; Leek, D. M.; Tao, Y.; Wilkinson, D.; Li, C. S., Thermodynamic Equilibrium-Driven Formation of Single-Sized Nanocrystals: Reaction Media Tuning CdSe Magic-Sized versus Regular Quantum Dots. *J Phys Chem C* **2010,** *114* (8), 3329-3339.

20. Morris-Cohen, A. J.; Frederick, M. T.; Lilly, G. D.; McArthur, E. A.; Weiss, E. A., Organic Surfactant-Controlled Composition of the Surfaces of CdSe Quantum Dots. *J Phys Chem Lett* **2010,** *1* (7), 1078-1081.

21. Talapin, D. V.; Rogach, A. L.; Kornowski, A.; Haase, M.; Weller, H., Highly luminescent monodisperse CdSe and CdSe/ZnS nanocrystals synthesized in a hexadecylamine-trioctylphosphine oxide-trioctylphospine mixture. *Nano Lett* **2001,** *1* (4), 207-211.

22. Park, J.; An, K. J.; Hwang, Y. S.; Park, J. G.; Noh, H. J.; Kim, J. Y.; Park, J. H.; Hwang, N. M.; Hyeon, T., Ultra-large-scale syntheses of monodisperse nanocrystals. *Nat Mater* **2004,** *3* (12), 891-895.

23. Talapin, D. V.; Lee, J. S.; Kovalenko, M. V.; Shevchenko, E. V., Prospects of Colloidal Nanocrystals for Electronic and Optoelectronic Applications. *Chem Rev* **2010,** *110* (1), 389-458.

24. Murray, C. B.; Norris, D. J.; Bawendi, M. G., Synthesis and Characterization of Nearly Monodisperse Cde (E = S, Se, Te) Semiconductor Nanocrystallites. *J Am Chem Soc* **1993,** *115* (19), 8706-8715.

25. Brennan, J. G.; Siegrist, T.; Carroll, P. J.; Stuczynski, S. M.; Brus, L. E.; Steigerwald, M. L., The Preparation of Large Semiconductor Clusters Via the Pyrolysis of a Molecular Precursor. *J Am Chem Soc* **1989,** *111* (11), 4141-4143.

26. Cumberland, S. L.; Hanif, K. M.; Javier, A.; Khitrov, G. A.; Strouse, G. F.; Woessner, S. M.; Yun, C. S., Inorganic Clusters as Single-Source Precursors for Preparation of CdSe, ZnSe, and CdSe/ZnS Nanomaterials. *Chem Mater* **2002,** *14* (4), 1576-1584.

27. Gerbec, J. A.; Magana, D.; Washington, A.; Strouse, G. F., Microwave-enhanced reaction rates for nanoparticle synthesis. *J Am Chem Soc* **2005,** *127* (45), 15791-15800.

28. Coucouvanis, D., The Chemistry of the Dithioacid and 1, 1-Dithiolate Complexes, 1968–1977. In *Progress in Inorganic Chemistry*, John Wiley & Sons, Inc.: 2007; pp 301-469.

29. Banister, A. J.; Smith, N. R. M., Preparation of a conducting iodinated poly(sulphur nitride). *Journal of the Chemical Society, Dalton Transactions* **1980,** (6), 937-941.

30. Malik, M. A.; O'Brien, P., Organometallic and Metallo-Organic Precursors for Nanoparticles. In *Precursor Chemistry of Advanced Materials*, Fischer, R. A., Ed. Springer Berlin Heidelberg: Berlin, Heidelberg, 2005; pp 173-204.

31. Manna, L.; Scher, E. C.; Li, L. S.; Alivisatos, A. P., Epitaxial growth and photochemical annealing of graded CdS/ZnS shells on colloidal CdSe nanorods. *J Am Chem Soc* **2002,** *124* (24), 7136-7145.

32. Trindade, T.; OBrien, P., A single source approach to the synthesis of CdSe nanocrystallites. *Adv Mater* **1996,** *8* (2), 161-&.

33. Trindade, T.; OBrien, P., Synthesis of CdS and CdSe nanoparticles by thermolysis of diethyldithio- or diethyldiseleno-carbamates of cadmium. *J Mater Chem* **1996,** *6* (3), 343-347.

34. Revaprasadu, N.; Malik, M. A.; O'Brien, P.; Zulu, M. M.; Wakefield, G., Single-source molecular precursors for the deposition of zinc selenide quantum dots. *J Mater Chem* **1998,** *8* (8), 1885-1888.

35. Malik, M. A.; O'Brien, P.; Motevalli, M., Bis(μ-diethyldithiocarbamato)-1κS,1:2κ2S';2κS,1:2κ2S'-bis(ethylzinc). *Acta Crystallographica Section C* **1996,** *52* (8), 1931-1933.

36. Ludolph, B.; Malik, M. A.; O'Brien, P.; Revaprasadu, N., Novel single molecule precursor routes for the direct synthesis of highly monodispersed quantum dots of cadmium or zinc sulfide or selenide. *Chem Commun* **1998,** (17), 1849-1850.

37. Lazell, M.; O'Brien, P., A novel single source precursor route to self capping CdS quantum dots. *Chem Commun* **1999,** (20), 2041-2042.

38. Lazell, M.; O'Brien, P., Synthesis of CdS nanocrystals using cadmium dichloride and trioctylphosphine sulfide. *J Mater Chem* **1999,** *9* (7), 1381-1382.

39. Peng, Z. A.; Peng, X. G., Formation of high-quality CdTe, CdSe, and CdS nanocrystals using CdO as precursor. *J Am Chem Soc* **2001,** *123* (1), 183-184.

40. Lee, G. S. H.; Fisher, K. J.; Craig, D. C.; Scudder, M. L.; Dance, I. G., [Ecd8(E'ph)16]2- Cluster Chemistry (E, E' = S, Se, Te). *J Am Chem Soc* **1990,** *112* (17), 6435-6437.

41. Crouch, D. J.; O'Brien, P.; Malik, M. A.; Skabara, P. J.; Wright, S. P., A one-step synthesis of cadmium selenide quantum dots from a novel single source precursor. *Chem Commun* **2003,** (12), 1454-1455.

42. Sarigiannis, D.; Peck, J. D.; Kioseoglou, G.; Petrou, A.; Mountziaris, T. J., Characterization of vapor-phase-grown ZnSe nanoparticles. *Appl Phys Lett* **2002,** *80* (21), 4024-4026.

43. Abdelhady, A. L.; Afzaal, M.; Malik, M. A.; O'Brien, P., Flow reactor synthesis of CdSe, CdS, CdSe/CdS and CdSeS nanoparticles from single molecular precursor(s). *J Mater Chem* **2011,** *21* (46), 18768-18775.

44. Micic, O. I.; Ahrenkiel, S. P.; Bertram, D.; Nozik, A. J., Synthesis, structure, and optical properties of colloidal GaN quantum dots. *Appl Phys Lett* **1999,** *75* (4), 478-480.

45. Pan, G. Q.; Kordesch, M. E.; Van Patten, P. G., New pyrolysis route to GaN quantum dots. *Chem Mater* **2006,** *18* (17), 3915-3917.

46. Sardar, K.; Dan, M.; Schwenzer, B.; Rao, C. N. R., A simple single-source precursor route to the nanostructures of AIN, GaN and InN. *J Mater Chem* **2005,** *15* (22), 2175-2177.

47. Schofield, P. S.; Zhou, W. Z.; Wood, P.; Samuel, I. D. W.; Cole-Hamilton, D. J., Nanoparticles from the decomposition of the complex [InN3(CH2CH2CH2NMe2)(2)]. *J Mater Chem* **2004,** *14* (21), 3124-3126.

48. Zhou, Y. F.; Riehle, F. S.; Yuan, Y.; Schleiermacher, H. F.; Niggemann, M.; Urban, G. A.; Kruger, M., Improved efficiency of hybrid solar cells based on non-ligand-exchanged CdSe quantum dots and poly(3-hexylthiophene). *Appl Phys Lett* **2010,** *96* (1).

49. Choi, J.; Gillan, E. G., Low-temperature solvothermal synthesis of nanocrystalline indium nitride and Ga-In-N composites from the decomposition of metal azides. *J Mater Chem* **2006,** *16* (38), 3774-3784.

50. Schwenzer, B.; Meier, C.; Masala, O.; Seshadri, R.; DenBaars, S. P.; Mishra, U. K., Synthesis of luminescing (In, Ga)N nanoparticles from an inorganic ammonium fluoride precursor. *J Mater Chem* **2005,** *15* (19), 1891-1895.

51. Green, M.; O'Brien, P., The synthesis of III-V semiconductor nanoparticles using indium and gallium diorganophosphides as single-molecular precursors. *J Mater Chem* **2004,** *14* (4), 629-636.

52. Wells, R. L.; Self, M. F.; Mcphail, A. T.; Aubuchon, S. R.; Woudenberg, R. C.; Jasinski, J. P., Synthesis, Characterization, and Thermal-Decomposition of [Cl2gap(Sime3)2]2, a Potential Precursor to Gallium-Phosphide. *Organometallics* **1993,** *12* (7), 2832-2834.

53. Janik, J. F.; Wells, R. L.; Young, V. G.; Rheingold, A. L.; Guzei, I. A., New pnictinogallanes [H2GaE(SiMe3)(2)](3) (E = P, As) - Formation, structural characterization, and thermal decomposition to afford nanocrystalline GaP and GaAs. *J Am Chem Soc* **1998,** *120* (3), 532-537.

54. Malik, M. A.; O'Brien, P.; Helliwell, M., A new synthesis of InAs quantum dots from [(Bu2AsInEt2)-Bu-t](2). *J Mater Chem* **2005,** *15* (14), 1463-1467.

55. Malik, M. A.; Afzaal, M.; O'Brien, P.; Bangert, U.; Hamilton, B., Single molecular precursor for synthesis of GaAs nanoparticles. *Mater Sci Tech-Lond* **2004,** *20* (8), 959-963.

56. Dimitrijevic, N. M.; Kamat, P. V., Formation and Corrosion Processes of Colloidal In2se3. *Langmuir* **1987,** *3* (6), 1004-1009.

57. Kamat, P. V.; Dimitrijevic, N. M.; Fessenden, R. W., Photoelectrochemistry in Particulate Systems .7. Electron-Transfer Reactions of Indium Sulfide Semiconductor Colloids. *J. Phys. Chem.* **1988,** *92* (8), 2324-2329.

58. Stoll, S. L.; Gillan, E. G.; Barron, A. R., Chemical vapor deposition of gallium selenide and indium selenide nanoparticles. *Chem Vapor Depos* **1996,** *2* (5), 182-&.

59. Revaprasadu, N.; Malik, M. A.; Carstens, J.; O'Brien, P., Novel single-molecule precursor routes for the direct synthesis of InS and InSe quantum dots. *J Mater Chem* **1999,** *9* (11), 2885-2888.

60. Dutta, D. P.; Sharma, G.; Ghoshal, S.; Kushwah, N. P.; Jain, V. K., Synthesis and characterization of indium xanthates and their use for the preparation of beta-In2S3 nanoparticles. *J Nanosci Nanotechno* **2006,** *6* (1), 235-240.

61. Trindade, T.; O'Brien, P.; Zhang, X.-m.; Motevalli, M., Synthesis of PbS nanocrystallites using a novel single molecule precursors approach: X-ray single-crystal structure of Pb(S2CNEtPri)2. *J Mater Chem* **1997,** *7* (6), 1011-1016.

62. Lee, S. M.; Jun, Y. W.; Cho, S. N.; Cheon, J., Single-crystalline star-shaped nanocrystals and their evolution: Programming the geometry of nano-building blocks. *J Am Chem Soc* **2002,** *124* (38), 11244-11245.

63. Zhang, Z. H.; Lee, S. H.; Vittal, J. J.; Chin, W. S., A simple way to prepare PbS nanocrystals with morphology tuning at room temperature. *J Phys Chem B* **2006,** *110* (13), 6649-6654.

64. Lee, S. M.; Cho, S. N.; Cheon, J., Anisotropic shape control of colloidal inorganic nanocrystals. *Adv Mater* **2003,** *15* (5), 441-444.

65. Koktysh, D. S.; McBride, J. R.; Rosenthal, S. J., Synthesis of SnS nanocrystals by the solvothermal decomposition of a single source precursor. *Nanoscale Res Lett* **2007,** *2* (3), 144-148.

66. Kudera, S.; Zanella, M.; Giannini, C.; Rizzo, A.; Li, Y. Q.; Gigli, G.; Cingolani, R.; Ciccarella, G.; Spahl, W.; Parak, W. J.; Manna, L., Sequential growth of magic-size CdSe nanocrystals. *Adv Mater* **2007,** *19* (4), 548-+.

67. Harrell, S. M.; McBride, J. R.; Rosenthal, S. J., Synthesis of Ultrasmall and Magic-Sized CdSe Nanocrystals. *Chem Mater* **2013,** *25* (8), 1199-1210.

68. Anikeeva, P. O.; Halpert, J. E.; Bawendi, M. G.; Bulovic, V., Electroluminescence from a mixed red-green-blue colloidal quantum dot monolayer. *Nano Lett* **2007,** *7* (8), 2196-2200.

69. Alivisatos, P., The use of nanocrystals in biological detection. *Nat Biotechnol* **2004,** *22* (1), 47-52.

70. Finney, E. E.; Finke, R. G., Nanocluster nucleation and growth kinetic and mechanistic studies: A review emphasizing transition-metal nanoclusters. *J Colloid Interf Sci* **2008,** *317* (2), 351-374.

71. Talapin, D. V.; Rogach, A. L.; Haase, M.; Weller, H., Evolution of an ensemble of nanoparticles in a colloidal solution: Theoretical study. *J Phys Chem B* **2001,** *105* (49), 12278-12285.

72. Lamer, V. K.; Dinegar, R. H., Theory, Production and Mechanism of Formation of Monodispersed Hydrosols. *J Am Chem Soc* **1950,** *72* (11), 4847-4854.

73. Jasieniak, J.; Smith, L.; van Embden, J.; Mulvaney, P.; Califano, M., Re-examination of the Size-Dependent Absorption Properties of CdSe Quantum Dots. *J Phys Chem C* **2009,** *113* (45), 19468-19474.

74. Zheng, H. M.; Smith, R. K.; Jun, Y. W.; Kisielowski, C.; Dahmen, U.; Alivisatos, A. P., Observation of Single Colloidal Platinum Nanocrystal Growth Trajectories. *Science* **2009,** *324* (5932), 1309-1312.

75. Qu, L. H.; Yu, W. W.; Peng, X. P., In situ observation of the nucleation and growth of CdSe nanocrystals. *Nano Lett* **2004,** *4* (3), 465-469.

76. Kamat, P. V., Meeting the clean energy demand: Nanostructure architectures for solar energy conversion. *J Phys Chem C* **2007,** *111* (7), 2834-2860.

77. Henglein, A., Small-Particle Research - Physicochemical Properties of Extremely Small Colloidal Metal and Semiconductor Particles. *Chem Rev* **1989,** *89* (8), 1861-1873.

78. Nirmal, M.; Brus, L., Luminescence photophysics in semiconductor nanocrystals. *Accounts Chem Res* **1999,** *32* (5), 407-414.

79. Drndic, M.; Jarosz, M. V.; Morgan, N. Y.; Kastner, M. A.; Bawendi, M. G., Transport properties of annealed CdSe colloidal nanocrystal solids. *J Appl Phys* **2002,** *92* (12), 7498-7503.

80. Yang, L.; McCue, C.; Zhang, Q. F.; Uchaker, E.; Mai, Y. H.; Cao, G. Z., Highly efficient quantum dot-sensitized TiO2 solar cells based on multilayered semiconductors (ZnSe/CdS/CdSe). *Nanoscale* **2015,** *7* (7), 3173-3180.

81. Firdaus, Y.; Vandenplas, E.; Justo, Y.; Gehlhaar, R.; Cheyns, D.; Hens, Z.; Van der Auweraer, M., Enhancement of the photovoltaic performance in P3HT: PbS hybrid solar cells using small size PbS quantum dots. *J Appl Phys* **2014,** *116* (9).

82. Yu, D.; Wang, C. J.; Guyot-Sionnest, P., n-type conducting CdSe nanocrystal solids. *Science* **2003,** *300* (5623), 1277-1280.

83. Dance, I. G.; Choy, A.; Scudder, M. L., Syntheses, properties, and molecular and crystal structures of (Me4N)4[E4M10(SPh)16] (E = sulfur or selenium; M = zinc or cadmium): molecular supertetrahedral fragments of the cubic metal chalcogenide lattice. *J Am Chem Soc* **1984,** *106* (21), 6285-6295.

84. Luo, H. F.; Tuinenga, C.; Guidez, E. B.; Lewis, C.; Shipman, J.; Roy, S.; Aikens, C. M.; Chikan, V., Synthesis and Characterization of Gallium-Doped CdSe Quantum Dots. *J Phys Chem C* **2015,** *119* (19), 10749-10757.

85. Ye, F. M.; Cui, C. C.; Kirkeminde, A.; Dong, D.; Collinson, M. M.; Higgins, D. A., Fluorescence Spectroscopy Studies of Silica Film Polarity Gradients Prepared by Infusion-Withdrawal Dip-Coating. *Chem Mater* **2010,** *22* (9), 2970-2977.

86. (a) Murphy, C. J., Sustainability as an emerging design criterion in nanoparticle synthesis and applications. *Journal of Materials Chemistry* **2008,** *18* (19), 2173-2176; (b) Hillhouse, H. W.; Beard, M. C., Solar cells from colloidal nanocrystals: Fundamentals, materials, devices, and economics. *Current Opinion in Colloid & Interface Science* **2009,** *14* (4), 245-259.

87. (a) Peng, Z. A.; Peng, X. G., Nearly monodisperse and shape-controlled CdSe nanocrystals via alternative routes: Nucleation and growth. *Journal of the American Chemical Society* **2002,** *124* (13), 3343-3353; (b) Peng, X. G.; Manna, L.; Yang, W. D.; Wickham, J.; Scher, E.; Kadavanich, A.; Alivisatos, A. P., Shape control of CdSe nanocrystals. *Nature* **2000,** *404* (6773), 59-61.

88. Werlin, R.; Priester, J. H.; Mielke, R. E.; Kramer, S.; Jackson, S.; Stoimenov, P. K.; Stucky, G. D.; Cherr, G. N.; Orias, E.; Holden, P. A., Biomagnification of cadmium selenide quantum dots in a simple experimental microbial food chain. *Nature Nanotechnology* **2011,** *6* (1), 65-71.

89. Reiss, P.; Protiere, M.; Li, L., Core/Shell Semiconductor Nanocrystals. *Small* **2009,** *5* (2), 154-168.

90. Galli, G., Solid-state physics - Doping the undopable. *Nature* **2005,** *436* (7047), 32-33.

91. Wills, A. W.; Kang, M. S.; Wentz, K. M.; Hayes, S. E.; Sahu, A.; Gladfelter, W. L.; Norris, D. J., Synthesis and characterization of Al- and In-doped CdSe nanocrystals. *Journal of Materials Chemistry* **2012,** *22* (13), 6335-6342.

92. Sorokina, I. T., Cr2+-doped II-VI materials for lasers and nonlinear optics. *Optical Materials* **2004,** *26* (4), 395-412.

93. Bryan, J. D.; Schwartz, D. A.; Gamelin, D. R., The influence of dopants on the nucleation of semiconductor nanocrystals from homogeneous solution. *Journal of Nanoscience and Nanotechnology* **2005,** *5* (9), 1472-1479.

94. Meulenberg, R. W.; van Buuren, T.; Hanif, K. M.; Willey, T. M.; Strouse, G. F.; Terminello, L. J., Structure and composition of Cu-doped CdSe nanocrystals using soft X-ray absorption spectroscopy. *Nano Letters* **2004,** *4* (11), 2277-2285.

95. (a) Roy, S.; Tuinenga, C.; Fungura, F.; Dagtepe, P.; Chikan, V.; Jasinski, J., Progress toward Producing n-Type CdSe Quantum Dots: Tin and Indium Doped CdSe Quantum Dots. *J. Phys. Chem. C* **2009,** *113* (30), 13008-13015; (b) Tuinenga, C.; Jasinski, J.; Iwamoto, T.; Chikan, V., In situ observation of heterogeneous growth of CdSe quantum dots: Effect of indium doping on the growth kinetics. *Acs Nano* **2008,** *2* (7), 1411-1421.

96. Ladizhansky, V.; Lyahovitskaya, V.; Vega, S., Cd-113 NMR study of transferred hyperfine interactions in the dilute magnetic semiconductors Cd1-xCoxS and Cd1-xFexS and impurity distribution in Cd0.994Co0.006S. *Physical Review B* **1999,** *60* (11), 8097-8104.

97. (a) Norris, D. J.; Yao, N.; Charnock, F. T.; Kennedy, T. A., High-quality manganese-doped ZnSe nanocrystals. *Nano Letters* **2001,** *1* (1), 3-7; (b) Magana, D.; Perera, S. C.; Harter, A. G.; Dalal, N. S.; Strouse, G. F., Switching-on superparamagnetism in Mn/CdSe quantum dots. *Journal of the American Chemical Society* **2006,** *128* (9), 2931-2939.

98. Sahu, A.; Kang, M. S.; Kompch, A.; Notthoff, C.; Wills, A. W.; Deng, D.; Winterer, M.; Frisbie, C. D.; Norris, D. J., Electronic Impurity Doping in CdSe Nanocrystals. *Nano Lett* **2012,** *12* (5), 2587-94.

99. Perna, G.; Capozzi, V.; Minafra, A.; Pallara, M.; Ambrico, M., Effects of the indium doping on structural and optical properties of CdSe thin films deposited by laser ablation technique. *European Physical Journal B* **2003,** *32* (3), 339-344.

100. He, Z. B.; Jie, J. S.; Zhang, W. J.; Zhang, W. F.; Luo, L. B.; Fan, X.; Yuan, G. D.; Bello, I.; Lee, S. T., Tuning Electrical and Photoelectrical Properties of CdSe Nanowires via Indium Doping. *Small* **2009,** *5* (3), 345-350.

101. Knox, C. K.; Fillmore, S. D.; Call, D. M.; Allen, D. G.; Hess, B. C.; Davis, R. C.; Evenson, W. E.; Harrison, R. G., Synthesis and characterization of photoluminescent In-doped CdSe nanoparticles. *Journal of Colloid and Interface Science* **2006,** *300* (2), 591-596.

102. Lott, K.; Nirk, T.; Volobujeva, O.; Shinkarenko, S.; Turn, L.; Kallavus, U.; Grebennik, A.; Vishnjakov, A., High-temperature investigation of ZnS : Ga and CdSe : Ga. *Physica B-Condensed Matter* **2006,** *376*, 764-766.

103. Hines, M. A.; Guyot-Sionnest, P., Synthesis and characterization of strongly luminescing ZnS-Capped CdSe nanocrystals. *J. Phys. Chem.* **1996,** *100* (2), 468-471.

104. Cui, C. C.; Kirkeminde, A.; Kannan, B.; Collinson, M. M.; Higgins, D. A., Spatiotemporal Evolution of Fixed and Mobile Dopant Populations in Silica Thin-Film Gradients as Revealed by Single Molecule Tracking. *J. Phys. Chem. C 115* (3), 728-735.

105. te Velde, G.; Bickelhaupt, F. M.; Baerends, E. J.; Fonseca Guerra, C.; van Gisbergen, S. J. A.; Snijders, J. G.; Ziegler, T., Chemistry with ADF. *J. Comput. Chem.* **2001,** *22* (9), 931-967.

106. Perdew, J. P.; Burke, K.; Ernzerhof, M., Generalized Gradient Approximation Made Simple. *Phys. Rev. Lett.* **1996,** *77* (18), 3865-3868.

107. (a) van Lenthe, E.; Baerends, E. J.; Snijders, J. G., Relativistic total energy using regular approximations. *J. Chem. Phys.* **1994,** *101* (11), 9783-9792; (b) van Lenthe, E.; Ehlers, A.; Baerends, E.-J., Geometry optimizations in the zero order regular approximation for relativistic effects. *J. Chem. Phys.* **1999,** *110* (18), 8943-8953.

108. (a) Pye, C. C.; Ziegler, T., An implementation of the conductor-like screening model of solvation within the Amsterdam density functional package. *Theor. Chem. Acc.* **1999,** *101* (6), 396-408; (b) Klamt, A.; Schuurmann, G., COSMO: a new approach to dielectric screening in solvents with explicit expressions for the screening energy and its gradient. *Journal of the Chemical Society, Perkin Transactions 2* **1993,** (5), 799-805.

109. Luo, H.; Tuinenga, C.; Guidez, E. B.; Lewis, C.; Shipman, J.; Roy, S.; Aikens, C. M.; Chikan, V., Synthesis and Characterization of Gallium-Doped CdSe Quantum Dots. *The Journal of Physical Chemistry C* **2015,** *119* (19), 10749-10757.

110. Chandrasekhar, V.; Goura, J.; Duthie, A., Molecular Indium(III) Phosphonates Possessing Ring and Cage Structures. Synthesis and Structural Characterization of In-2(t-BuPO3H)(4)(phen)(2)Cl-2 and In-3(C5H9PO3)(2)(C5H9PO3H)(4)(phen)(3) center dot NO3 center dot 3.5H(2)O. *Inorg. Chem.* **2013,** *52* (9), 4819-4824.

111. Hagen, K. S.; Stephan, D. W.; Holm, R. H., METAL-ION EXCHANGE-REACTIONS IN CAGE MOLECULES - THE SYSTEMS M4-ETAM'ETA(SC6H5)10 2- (M, M' = FE(II), CO(II), ZN(II), CD(II)) WITH ADAMANTANE-LIKE STEREOCHEMISTRY AND THE STRUCTURE OF FE4(SC6H5)10 2. *Inorg. Chem.* **1982,** *21* (11), 3928-3936.

112. Inamdar, S. N.; Ingole, P. P.; Haram, S. K., Determination of Band Structure Parameters and the Quasi-Particle Gap of CdSe Quantum Dots by Cyclic Voltammetry. *Chemphyschem* **2008,** *9* (17), 2574-2579.

113. Kucur, E.; Riegler, J.; Urban, G. A.; Nann, T., Determination of quantum confinement in CdSe nanocrystals by cyclic voltammetry. *Journal of Chemical Physics* **2003,** *119* (4), 2333-2337.

114. Shim, M.; Guyot-Sionnest, P., N-type colloidal semiconductor nanocrystals. *Nature* **2000,** *407* (6807), 981-983.

115. Li, R. F.; Lee, J.; Yang, B. C.; Horspool, D. N.; Aindow, M.; Papadimitrakopoulos, F., Amine-assisted facetted etching of CdSe nanocrystals. *Journal of the American Chemical Society* **2005,** *127* (8), 2524-2532.

116. Kuno, M.; Fromm, D. P.; Hamann, H. F.; Gallagher, A.; Nesbitt, D. J., Nonexponential "blinking" kinetics of single CdSe quantum dots: A universal power law behavior. *J Chem Phys* **2000,** *112* (7), 3117-3120.

117. Nirmal, M.; Norris, D. J.; Kuno, M.; Bawendi, M. G.; Efros, A. L.; Rosen, M., OBSERVATION OF THE DARK EXCITON IN CDSE QUANTUM DOTS. *Physical Review Letters* **1995,** *75* (20), 3728-3731.

118. (a) Ginley, D.; Green, M. A.; Collins, R., Solar energy conversion toward 1 terawatt. *Mrs Bull* **2008,** *33* (4), 355-364; (b) Yamaguchi, M.; Takamoto, T.; Araki, K.; Ekins-Daukes, N., Multi-junction III-V solar cells: current status and future potential. *Solar Energy* **2005,** *79* (1), 78-85; (c) Huynh, W. U.; Dittmer, J. J.; Alivisatos, A. P., Hybrid nanorod-polymer solar cells. *Science* **2002,** *295* (5564), 2425-2427; (d) Kamat, P. V., Quantum Dot Solar Cells. Semiconductor Nanocrystals as Light Harvesters. *J Phys Chem C* **2008,** *112* (48), 18737-18753.

119. (a) Plass, R.; Pelet, S.; Krueger, J.; Gratzel, M.; Bach, U., Quantum dot sensitization of organic-inorganic hybrid solar cells. *J Phys Chem B* **2002,** *106* (31), 7578-7580; (b) Ren, S.; Bernardi, M.; Lunt, R. R.; Bulovic, V.; Grossman, J. C.; Gradecak, S., Toward Efficient Carbon Nanotube/P3HT Solar Cells: Active Layer Morphology, Electrical, and Optical Properties. *Nano Lett* **2011,** *11* (12), 5316-5321; (c) Ren, S.; Chang, L.-Y.; Lim, S.-K.; Zhao, J.; Smith, M.; Zhao, N.; Bulovic, V.; Bawendi, M.; Gradecak, S., Inorganic-Organic Hybrid Solar Cell: Bridging Quantum Dots to Conjugated Polymer Nanowires. *Nano Lett* **2011,** *11* (9), 3998-4002; (d) Ren, S.; Zhao, N.; Crawford, S. C.; Tambe, M.; Bulovic, V.; Gradecak, S., Heterojunction Photovoltaics Using GaAs Nanowires and Conjugated Polymers. *Nano Lett* **2011,** *11* (2), 408-413.

120. Dayal, S.; Reese, M. O.; Ferguson, A. J.; Ginley, D. S.; Rumbles, G.; Kopidakis, N., The Effect of Nanoparticle Shape on the Photocarrier Dynamics and Photovoltaic Device Performance of Poly(3-hexylthiophene):CdSe Nanoparticle Bulk Heterojunction Solar Cells. *Advanced Functional Materials* **2010,** *20* (16), 2629-2635.

121. (a) Sanchez, C.; Julian, B.; Belleville, P.; Popall, M., Applications of hybrid organic-inorganic nanocomposites. *J Mater Chem* **2005,** *15* (35-36), 3559-3592; (b) Beek, W. J. E.; Wienk, M. M.; Janssen, R. A. J., Efficient hybrid solar cells from zinc oxide nanoparticles and a conjugated polymer. *Adv Mater* **2004,** *16* (12), 1009-+.

122. (a) Brandenburg, J. E.; Jin, X.; Kruszynska, M.; Ohland, J.; Kolny-Olesiak, J.; Riedel, I.; Borchert, H.; Parisi, J., Influence of particle size in hybrid solar cells composed of CdSe nanocrystals and poly(3-hexylthiophene). *J Appl Phys* **2011,** *110* (6), 064509-9; (b) Dixit, S. K.; Madan, S.; Madhwal, D.; Kumar, J.; Singh, I.; Bhatia, C. S.; Bhatnagar, P. K.; Mathur, P. C., Bulk heterojunction formation with induced concentration gradient from a bilayer structure of P3HT:CdSe/ZnS quantum dots using inter-diffusion process for developing high efficiency solar

cell. *Org. Electron.* **2012,** *13* (4), 710-714; (c) Fu, H.; Choi, M.; Luan, W.; Kim, Y.-S.; Tu, S.-T., Hybrid solar cells with an inverted structure: Nanodots incorporated ternary system. *Solid State Electron* **2012,** *69* (0), 50-54; (d) Fu, H. H.; Choi, M. J.; Luan, W. L.; Kim, Y. S.; Tu, S. T., Hybrid solar cells with an inverted structure: Nanodots incorporated ternary system. *Solid State Electron* **2012,** *69*, 50-54; (e) Lili, H.; Donghuan, Q.; Xi, J.; Yanshan, L.; Li, W.; Junwu, C.; Yong, C., Synthesis of high quality zinc-blende CdSe nanocrystals and their application in hybrid solar cells. *Nanotechnology* **2006,** *17* (18), 4736; (f) Noone, K. M.; Subramaniyan, S.; Zhang, Q.; Cao, G.; Jenekhe, S. A.; Ginger, D. S., Photoinduced Charge Transfer and Polaron Dynamics in Polymer and Hybrid Photovoltaic Thin Films: Organic vs Inorganic Acceptors. *The Journal of Physical Chemistry C* **2011,** *115* (49), 24403-24410; (g) Olson, J. D.; Gray, G. P.; Carter, S. A., Optimizing hybrid photovoltaics through annealing and ligand choice. *Sol Energ Mat Sol C* **2009,** *93* (4), 519-523; (h) Radychev, N.; Lokteva, I.; Witt, F.; Kolny-Olesiak, J.; Borchert, H.; Parisi, J., Physical Origin of the Impact of Different Nanocrystal Surface Modifications on the Performance of CdSe/P3HT Hybrid Solar Cells. *J Phys Chem C* **2011,** *115* (29), 14111-14122; (i) Ren, S. Q.; Chang, L. Y.; Lim, S. K.; Zhao, J.; Smith, M.; Zhao, N.; Bulovic, V.; Bawendi, M.; Gradecak, S., Inorganic-Organic Hybrid Solar Cell: Bridging Quantum Dots to Conjugated Polymer Nanowires. *Nano Lett* **2011,** *11* (9), 3998-4002; (j) Saunders, B. R.; Turner, M. L., Nanoparticle–polymer photovoltaic cells. *Adv. Colloid Interface Sci.* **2008,** *138* (1), 1-23; (k) Yang, J. H.; Tang, A. W.; Zhou, R. J.; Xue, J. G., Effects of nanocrystal size and device aging on performance of hybrid poly(3-hexylthiophene):CdSe nanocrystal solar cells. *Sol Energ Mat Sol C* **2011,** *95* (2), 476-482; (l) Zhang, Q. L.; Russell, T. P.; Emrick, T., Synthesis and characterization of CdSe nanorods functionalized with regioregular poly(3-hexylthiophene). *Chem Mater* **2007,** *19* (15), 3712-3716; (m) Zhong, M.; Yang, D.; Zhang, J.; Shi, J.; Wang, X.; Li, C., Improving the performance of CdS/P3HT hybrid inverted solar cells by interfacial modification. *Sol Energ Mat Sol C* **2012,** *96* (0), 160-165; (n) Zutz, F.; Lokteva, I.; Radychev, N.; Kolny-Olesiak, J.; Riedel, I.; Borchert, H.; Parisi, J., Study of the influence of the Cd:Se precursor ratio during the synthesis of CdSe nanocrystals on the performance of CdSe/P3HT hybrid solar cells. *Phys. Status Solidi A-Appl. Mat.* **2009,** *206* (12), 2700-2708.

123. Zhou, R. J.; Stalder, R.; Xie, D. P.; Cao, W. R.; Zheng, Y.; Yang, Y. X.; Plaisant, M.; Holloway, P. H.; Schanze, K. S.; Reynolds, J. R.; Xue, J. G., Enhancing the Efficiency of Solution-Processed Polymer:Colloidal Nanocrystal Hybrid Photovoltaic Cells Using Ethanedithiol Treatment. *Acs Nano* **2013,** *7* (6), 4846-4854.

124. Dixit, S. K.; Madan, S.; Kaur, A.; Madhwal, D.; Singh, I.; Bhatnagar, P. K.; Mathur, P. C.; Bhatia, C. S., Enhancement of efficiency of a conducting polymer P3HT:CdSe/ZnS quantum dots hybrid solar cell by adding single walled carbon nanotube for transporting photogenerated electrons. *J. Renew. Sustain. Energy* **2013,** *5* (3).

125. Kumar, V.; Jain, S. C.; Kapoor, A. K.; Geens, W.; Aernauts, T.; Poortmans, J.; Mertens, R., Carrier transport in conducting polymers with field dependent trap occupancy. *J Appl Phys* **2002,** *92* (12), 7325-7329.

126. (a) Chikan, V., Challenges and Prospects of Electronic Doping of Colloidal Quantum Dots: Case Study of CdSe. *J Phys Chem Lett* **2011,** *2* (21), 2783-2789; (b) Erwin, S. C.; Zu, L. J.; Haftel, M. I.; Efros, A. L.; Kennedy, T. A.; Norris, D. J., Doping semiconductor nanocrystals. *Nature* **2005,** *436* (7047), 91-94.

127. Mikulec, F. V.; Kuno, M.; Bennati, M.; Hall, D. A.; Griffin, R. G.; Bawendi, M. G., Organometallic synthesis and spectroscopic characterization of manganese-doped CdSe nanocrystals. *J Am Chem Soc* **2000,** *122* (11), 2532-2540.

128. Archer, P. I.; Santangelo, S. A.; Gamelin, D. R., Direct observation of sp-d exchange interactions in colloidal Mn2+- and Co2+-doped CdSe quantum dots. *Nano Lett* **2007,** *7* (4), 1037-1043.

129. Zhou, Y.; Riehle, F. S.; Yuan, Y.; Schleiermacher, H.-F.; Niggemann, M.; Urban, G. A.; Krueger, M., Improved efficiency of hybrid solar cells based on non-ligand-exchanged CdSe quantum dots and poly(3-hexylthiophene). *Appl Phys Lett* **2010,** *96* (1).

130. Scott, R.; Kirkeminde, A.; Gong, M.; Totleben, J.; Ren, S.; Tuinenga, C.; Lewis, C.; Luo, H.; Higgins, D.; Chikan, V., (Invited) Impact of Indiumand Gallium Doping on the Photovoltaic Performance of CdSe Quantum Dot Hybrid Solar Cells. *ECS Transactions* **2015,** *66* (15), 1-8.

131. (a) Lott, K.; Volobujeva, O.; Öpik, A.; Nirk, T.; Türn, L.; Nõges, M., High temperature electrical conductivity in donor-doped II–VI compounds. *physica status solidi (c)* **2003,** *0* (2), 618-621; (b) Gonzalez, A. M. P.; Arreola, I. V., Effects of indium doping on the structural and optical properties of CdSe thin films deposited by chemical bath. *Rev. Mex. Fis.* **2009,** *55* (1), 51-54.

132. Baik, S. J.; Kim, K.; Lim, K. S.; Jung, S.; Park, Y.-C.; Han, D. G.; Lim, S.; Yoo, S.; Jeong, S., Low-Temperature Annealing for Highly Conductive Lead Chalcogenide Quantum Dot Solids. *J Phys Chem C* **2011,** *115* (3), 607-612.

133. Chikan, V.; McLaurin, E., Rapid Nanoparticle Synthesis by Magnetic and Microwave Heating. *Nanomaterials-Basel* **2016,** *6* (5), 85.

134. Razgoniaeva, N.; Carrillo, L.; Burchfield, D.; Moroz, P.; Adhikari, P.; Yadav, P.; Khon, D.; Zamkov, M., Colloidal Synthesis of Monodisperse Semiconductor Nanocrystals through Saturated Ionic Layer Adsorption. *Chem Mater* **2016,** *28* (8), 2823-2833.

135. Ashley, B.; Lovingood, D. D.; Chiu, Y. C.; Gao, H. W.; Owens, J.; Strouse, G. F., Specific effects in microwave chemistry explored through reactor vessel design, theory, and spectroscopy. *Phys Chem Chem Phys* **2015,** *17* (41), 27317-27327.

136. Dagtepe, P.; Chikan, V., Effect of Cd/Te ratio on the formation of CdTe magic-sized quantum dots during aggregation. *J Phys Chem A* **2008,** *112* (39), 9304-9311.

137. McBride, J. R.; Dukes, A. D.; Schreuder, M. A.; Rosenthal, S. J., On ultrasmall nanocrystals. *Chem Phys Lett* **2010,** *498* (1-3), 1-9.

138. Chung, I. H.; Bawendi, M. G., Relationship between single quantum-dot intermittency and fluorescence intensity decays from collections of dots. *Phys Rev B* **2004,** *70* (16).

139. Wang, S.; Querner, C.; Emmons, T.; Drndic, M.; Crouch, C. H., Fluorescence blinking statistics from CdSe core and core/shell nanorods. *J Phys Chem B* **2006,** *110* (46), 23221-23227.

140. Peterson, J. J.; Nesbitt, D. J., Modified Power Law Behavior in Quantum Dot Blinking: A Novel Role for Biexcitons and Auger Ionization. *Nano Lett* **2009,** *9* (1), 338-345.

141. Stefani, F. D.; Knoll, W.; Kreiter, M.; Zhong, X.; Han, M. Y., Quantification of photoinduced and spontaneous quantum-dot luminescence blinking. *Phys Rev B* **2005,** *72* (12).

142. Lee, D. H.; Yuan, C. T.; Tachiya, M.; Tang, J., Influence of bin time and excitation intensity on fluorescence lifetime distribution and blinking statistics of single quantum dots. *Appl Phys Lett* **2009,** *95* (16).

143. Knappenberger, K. L.; Wong, D. B.; Xu, W.; Schwartzberg, A. M.; Wolcott, A.; Zhang, J. Z.; Leone, S. R., Excitation-Wavelength Dependence of Fluorescence Intermittency in CdSe Nanorods. *Acs Nano* **2008,** *2* (10), 2143-2153.

Appendix A - List of Publications

- Lu, R. T.; Liu, J. W.; **Luo, H. F.**; Chikan, V.; Wu, J. Z., Graphene/GaSe-Nanosheet Hybrid: Towards High Gain and Fast Photoresponse. *Sci Rep-Uk* 2016, 6.

- **Luo, H.**; Tuinenga, C.; Guidez, E. B.; Lewis, C.; Shipman, J.; Roy, S.; Aikens, C. M.; Chikan, V., Synthesis and Characterization of Gallium-Doped CdSe Quantum Dots. The *Journal of Physical Chemistry C* 2015, 119 (19), 10749-10757.

- Scott, R.; Kirkeminde, A.; Gong, M.; Totleben, J.; Ren, S.; Tuinenga, C.; Lewis, C.; **Luo, H.**; Higgins, D.; Chikan, V., (Invited) Impact of Indium and Gallium Doping on the Photovoltaic Performance of CdSe Quantum Dot Hybrid Solar Cells. *ECS Transactions* 2015, 66 (15), 1-8.